Thermal hydraulic investigation of molten fuel relocation in a fast reactor during severe accident

By

Prasant Kumar Panigrahi

(Enrolment No: ENGG02201505018)

Indira Gandhi Centre for Atomic Research, Kalpakkam

A dissertation submitted to the
Board of Studies in Engineering Sciences

In partial fulfillment of requirements
for the Degree of

MASTER OF SCIENCE (Engineering)

of

HOMI BHABHA NATIONAL INSTITUTE

October 2018

Thermal hydraulic investigation of molten fuel relocation in a fast reactor during severe accident

By

Prasant Kumar Panigrahi

(Enrolment No: ENGG02201505018)

Indira Gandhi Centre for Atomic Research, Kalpakkam

A dissertation submitted to the
Board of Studies in Engineering Sciences

In partial fulfillment of requirements
for the Degree of

MASTER OF SCIENCE (Engineering)

of

HOMI BHABHA NATIONAL INSTITUTE

October 2018

Homi Bhabha National Institute

Recommendations of the Thesis Examining Committee

As members of the Thesis Examining Committee, we recommend that the thesis prepared by Mr. Prasant Kumar Panigrahi entitled "Thermal hydraulic investigation of molten fuel relocation in a fast reactor during severe accident" be accepted as fulfilling the thesis requirement for the Degree of Master of Science (Engineering).

	Name	Signature
Member 1	Dr. Anil Kumar Sharma	30/10/2018
Member 2	Dr. V. S. Srinivasan	30/10/2018
Member 3	Dr. Prasad Patnaik B.S.V.	
Guide/Convener	Dr. K. Velusamy	30/10/2018
Chairman	Dr. S. Murugan	30.10.2018

Final approval and acceptance of this thesis is contingent upon the candidate's submission of the final copies of the thesis to HBNI.

I hereby certify that I have read this thesis prepared under my direction and recommend that it may be accepted as fulfilling the thesis requirement.

Date: 31/10/2018

Place: Kalpakkam

Dr. K. Velusamy
(Guide)

DECLARATION

I, hereby declare that the investigation presented in the thesis has been carried out by me. The work is original and has not been submitted earlier as a whole or in part for a degree /diploma at this or any other Institution / University.

Prasant Kr. Panigrahi

Prasant Kumar Panigrahi

LIST OF PUBLICATIONS

JOURNAL

Panigrahi, P. K., Velusamy, K., A Robust Multi Phase Model to Investigate Molten Material Relocation due to Total Flow Blockage in SFR Fuel Subassembly, Nuclear Engineering and Technology, 2018 (To be communicated).

CONFERENCE PROCEEDINGS

Prasant Kumar Panigrahi, K. Velusamy, Development of Computational Model for Molten Fuel Relocation in a Fast Reactor during Severe Accident, *Proceedings of the 7th International and 45th National Conference on Fluid Mechanics and Fluid Power*, December 10-12, **2018**, IIT Bombay, Mumbai, India. (FMFP-2018/704)

To

My Beloved Parents

&

Diligent Guide

ACKNOWLEDGMENTS

First and foremost, I would like to convey my special appreciation and thanks to my advisor Dr. K. Velusamy, Associate Director, Nuclear Systems Analysis Group, Reactor Design Group (RDG), IGCAR for all his eternal patience, seemingly infinite knowledge, and strong guidance throughout my research. Besides my advisor, I am very grateful to the rest of my Doctoral Committee: Dr. S. Murugan, Dr. Anil Kumar Sharma, Dr. V. S. Srinivasan, Dr. Prasad Patnaik B.S.V., and Dr. K. Laha (former member) for their insightful comments and encouragement, which incented me to broaden my research from various perspectives.

I express my sincere thanks to Dr. G. Sasikala, former Dean of Engineering Sciences and our former Dean of Student Affairs Dr. M. Saibaba, for their constant academic support and care.

I would like to acknowledge Smt. R. Vijayashree, Mr. P.A. Sasidhran, and Mr. B. Madhavan for providing an excellent work environment and computational facility. Thanks are due to Mr. Dass and Mr. S. Jaisankar for their assistance in the thesis work.

Further thanks go out to all my fellow lab mates and beloved friends for making my days at Kalpakkam enlightening and colorful.

Lastly, I must express my very profound gratitude to my family for providing me with unfailing support and being with me always to reach this far.

CONTENTS

SYNOPSIS

Sodium-cooled Fast Reactor (SFR) features a fast-neutron spectrum, high burn up, large breeding capacity, and actinide transmutation ability. These potential merits are attributed to its closely-packed compact core. The wire wrapped long fuel pins are positioned in a tightly packed triangular array, housed inside a hexagonal wrapper forming a fuel subassembly (SA). These altogether yields a large number of narrow channels in between the fuel pins, termed as subchannels, available for the coolant flow. The tiny subchannels eventually make the fuel SA vulnerable to flow blockage. Therefore, the flow blockage accident is a practicable risk for the SFRs. In this domain, Total Instantaneous Blockage (TIB) at the foot of a fuel SA is a kind of upper bound of all the flow blockages. A postulated TIB accident scenario in a blocked fuel SA involves an inlet flow blockage, resulting in flow starvation leading to sodium boiling, followed by dry out of the fuel, clad melting, and subsequently fuel melting forming a melt pool. The molten fuel has the potential to relocate axially through the available subchannels in the downward direction. This fuel relocation towards the lower plenum is strongly influenced by the freezing of the molten fuel on the way, resulting in plugging of the coolant channels and restricting the axial fuel relocation. If the available subchannels are not blocked, the molten fuel escapes out of the core to reach the bottom end. The blockage formation, if it transpired, advances the accident progression, resulting in ablation of the hexcan and release out of fissile inventories attacking the neighbouring SAs leading to a severe accident. Thus, the accident progression is better described as a spectrum of event sequences, making TIB a very complex phenomenon.

A good deal of information on the dynamics of molten material relocation following severe accident is reported in open literature. Most of these studies investigate the fundamental freezing behaviour of molten material during penetration

into relatively simple structures. Experimental and theoretical studies on molten fuel relocation in reactor case scenario are still limited. Towards this, a transient enthalpy based computational model is developed to simulate the relocation of molten fuel in a blocked fuel SA under accident condition. The present model predicts the transient penetration length of the molten fuel in the subchannel before blockage and the plugging time required for the melt to form the blockage. Another and probably more important aspect of the present work is the assessment of molten fuel mass dispersed out of the core, which then evaluates the fuel inventories in the core and is directly connected to the core reactivity. The mathematical model comprises of two modules; a Fluid Dynamics module and a Heat Transfer module. The transient model considering single-material and multi-phase flow features adopt finite difference approximations of both implicit and explicit types employing a variable grid for boundary tracking. The model is validated against the published experimental and SIMMER III code results.

The developed mathematical model is applied to analyse the streaming, freezing, and blocking phenomena of the molten fuel in the subchannels of a blocked fuel SA. The melt relocation simulation results describe that the molten fuel is unable to cross the blanket zone of the blocked SA, resulting in damage propagation to the neighbouring SAs. Further, the influence of critical parameters on the melt relocation and freezing characteristics is carried out. The parametric study reveals that altering the fuel SA design, in particular length and diameter of fuel pin, notably enhances the material relocation characteristics of molten fuel and prevents the progression of the accident to the neighbouring SAs.

LIST OF FIGURES

LIST OF TABLES

CHAPTER 1

Introduction

1.1 FOREWORD

Growing population together with rapid industrialization necessitates a steady growth in the energy generation worldwide. Growing energy needs and concern for the environment drive the demand for large-scale and low impact energy sources. Towards this, nuclear energy undoubtedly plays a potential role. It is expected that the nuclear energy will supply huge amounts of energy and contribute significantly towards meeting the energy demands of both emerging and developed economies. In the worldwide energy scenario, the nuclear share is nominal, ~ 10.6% of overall electricity generation (IEA, 2017). In India, the present installed nuclear power capacity of ~ 6.8 GWe contributes to ~ 3% of overall electricity production (CEA, 2017). Societal acceptance of large-scale contributions delivered by nuclear energy will depend on the satisfaction of key drivers to enhance sustainability in terms of economy, safety, waste reduction and public acceptance. Fast reactors are a state of the art nuclear reactors that offer some key advantages over traditional thermal reactors in safety, sustainability and radioactive waste. Operating in a fully closed fuel cycle, they have the potential to

extract 60-70 times more energy from uranium than the thermal reactors and contribute to a significant reduction in radioactive waste. It is well-acknowledged that the fast reactors with recycling improve the sustainability indices significantly. Therefore, national and international research on fast reactor technology is increasing, primarily as breeders and, in recent years, also as high-level waste burners. Considering these, Dr. Homi Bhabha envisioned a three-stage nuclear power program to achieve India's long-term energy independence, through utilizing the modest uranium and abundant thorium resources available in the country (Venkataraman, 1994).

1.2 SODIUM COOLED FAST REACTOR

Sodium-cooled Fast Reactors (SFRs) are the Generation IV Nuclear Reactors (DOENE, 2002). In India, SFR stands as a potential workhorse for the second stage of the nuclear program. SFR features a fast-neutron spectrum, large breeding capacity, high burn up and a closed fuel cycle for efficient conversion of fertile uranium and better management of actinides. Despite numerous potential merits, the SFR design is very complex and challenging. Design of an SFR core is a trade-off between neutronics, materials, and thermal-hydraulic considerations. This demands a closely-packed compact core in order to maintain an optimum fast neutron population, which is necessary for breeding and transmuting actinides. Besides that, the large power density and specific power of SFR arise from its superior coolant properties. These were made achievable by the very high thermal conductivity of the liquid sodium coolant. The large thermal conductivity yields a large heat transfer coefficient for a typical Reynolds number of 1×10^5 dictated by the large density and modest viscosity values that offset the small hydraulic diameter (~3 mm) and related thermal hydraulic challenges, while still meeting clad temperature constraints (Todreas, 2009). Sodium with its high boiling

point (~1156 K) reduces the need for the high-pressure primary vessel unlike in the case of PHWR. But apart from this, handling sodium has other added challenges due to the reactive and opaque nature of sodium.

A typical pool type sodium-cooled fast reactor consists of three inter-linked circuits, viz., primary sodium circuit, secondary sodium circuit, steam-water circuit (Ref. Fig. 1.1). The primary sodium circuit which resides entirely inside the pool exchanges the heat carried away from the heat generating core to the secondary sodium circuit. The secondary sodium circuit is an intermediate loop connecting the primary sodium circuit to steam water circuit. This prevents any radioactivity release out of reactor containment, mainly to the turbine building during sodium leakage. The steam-water circuit generates steam to run the turbine which is connected to the generator building to produce electricity.

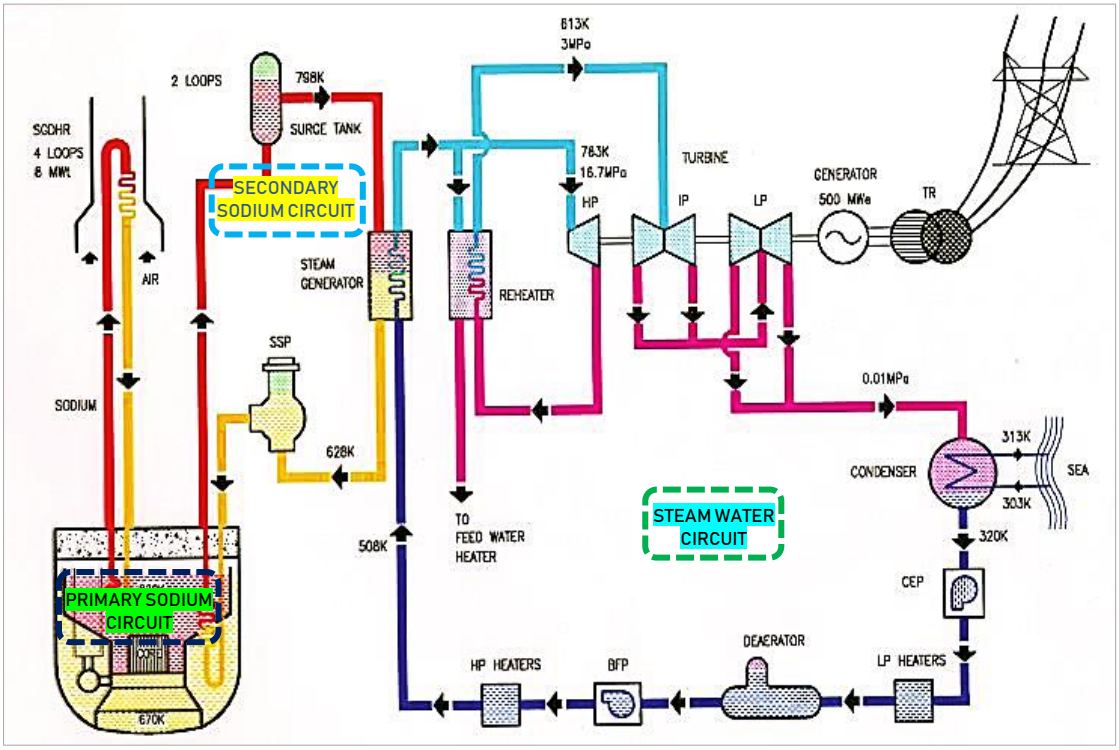

Fig. 1.1: Flow sheet of pool type sodium-cooled fast reactor.

In a pool type SFR, primary sodium circuit is submerged inside a large sodium pool. The components of the primary circuit of a pool type SFR can be seen in Fig. 1.2. All the components of the primary system are housed inside the main vessel which is surrounded by a safety vessel. The main vessel contains two primary sodium pools, viz., a hot pool (820 K) and a cold pool (670 K), separated by an inner vessel.

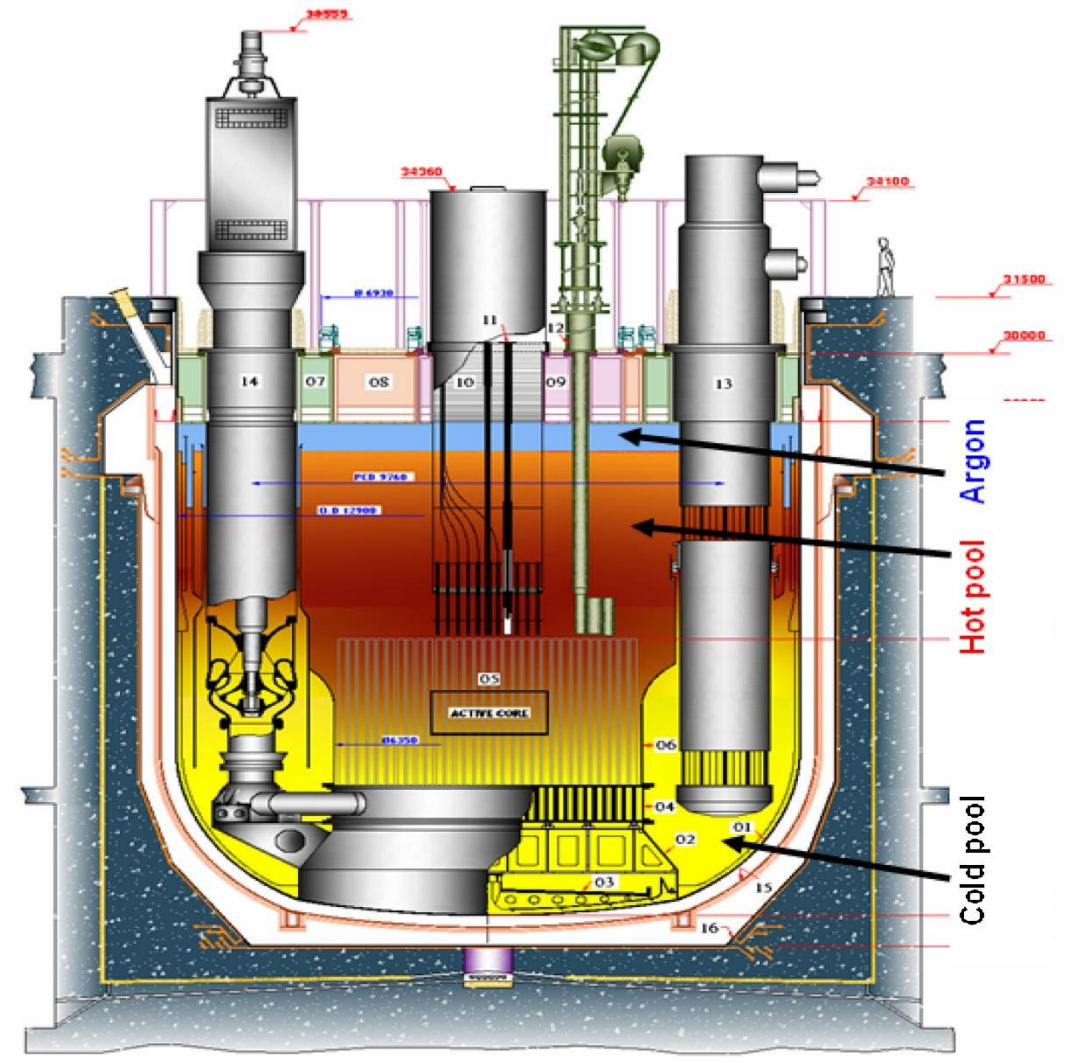

Fig. 1.2: Reactor assembly components of SFR

1.3 SFR CORE

A typical medium-sized SFR core consists of over 1700 subassemblies (SAs). These SAs are rested vertically on the grid plate. The fuel SA zone is the innermost zone of the core. The fuel SA are surrounded by blanket SAs. Typical core configuration of SFR is shown in Fig. 1.3. The fuel SA region consists of ~ 180 fuel SAs that generate ~ 8 MWt power per SA.

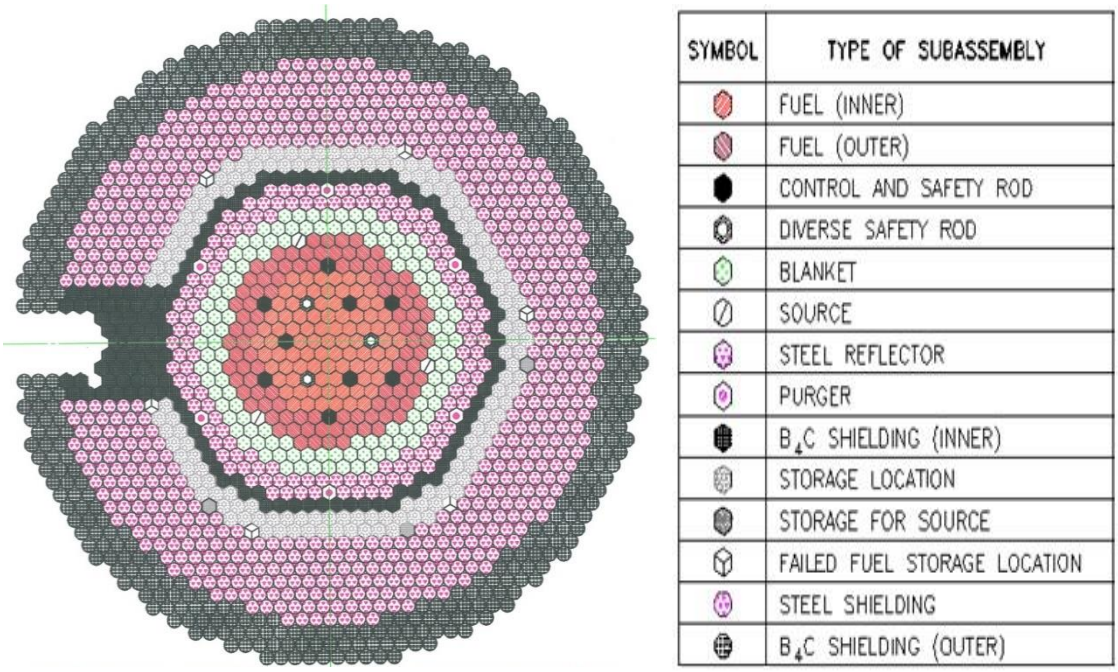

Fig. 1.3: SFR core configuration

The fuel pins are arranged in a closely packed triangular lattice, housed inside a hexagonal wrapper forming a fuel SA. A typical medium-sized SFR contains ~ 217 fuel pins per SA along with ~ 487 flow subchannels, the coolant flow space between the fuel pins (Chetal et al., 2006). Each of these fuel pins is wrapped with helical spacer wires to ensure proper spacing of the pins and promote transverse flow for better coolant

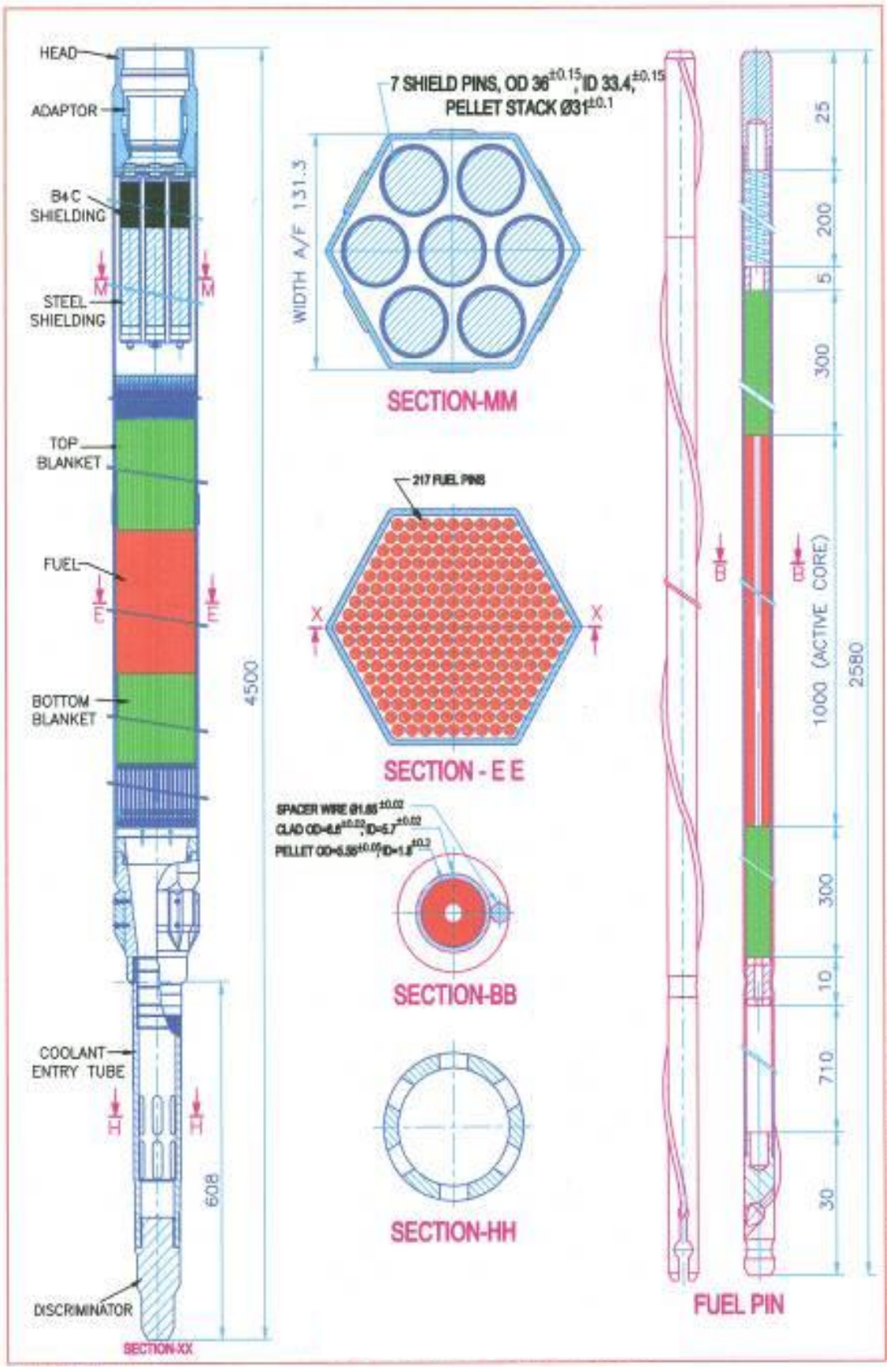

Fig. 1.4: Schematic of SFR fuel subassembly

mixing. A schematic of SFR fuel SA and fuel pin is shown in Fig. 1.4. Close spacing of fuel pins is required to increase the volume fraction of fuel in the core which reduces neutron leakage and fuel enrichment requirement. Due to the compact core and higher power density, continuous coolant (liquid sodium) flow in the SA is essential for the safe operation of the reactor. So, several challenges are there for SFR core cooling from safety point of view.

1.4 FLOW BLOCKAGE IN FUEL SUBASSEMBLY

The compact SFR core is not in most reactive configuration. The closely packed compact core together with a large number of tiny subchannels eventually makes the SFR fuel SA vulnerable to flow blockage. The helical wire wrap, intended for better flow distribution, appends the vulnerability index. The possible reasons for the flow blockage are deposition of corrosion products, fragments from failed fuel, fragments from spacer wire, irradiation swelling of fuel pins, loading of blocked subassembly, foreign materials left during construction, loose parts from structures, chemical product during operation (Roychowdhury et al., 1998; Yang, 1998). Any possible blockage would have an adverse impact on availability and safety of the reactor. In this domain, Total Instantaneous Blockage (TIB) at the foot of a fuel SA is a kind of upper bound of all the flow blockages.

TIB event can be described as an instantaneous blockage at the inlet of fuel SA, restricting the sodium coolant flow into the fuel SA, at nominal operating condition. Total instantaneous blockage in a fuel SA is a severe accident event in SFR due to its large power density and high burnup. Provisions of (i) multiple radial openings in the sleeves in grid plate and in the feet of all the core subassemblies to prevent total blockage at inlet of a SA and (ii) a blockage adaptor at the head with multiple radial

holes in the wrapper to ensure alternate path for flow through side gaps in case of a blockage occurring at the top (Ref. Fig. 1.5) make this event a Beyond Design Basis Event (BDBE). Analysis of the behaviour of the SFR following this accident is important in order to examine the potential for whole core severe accidents.

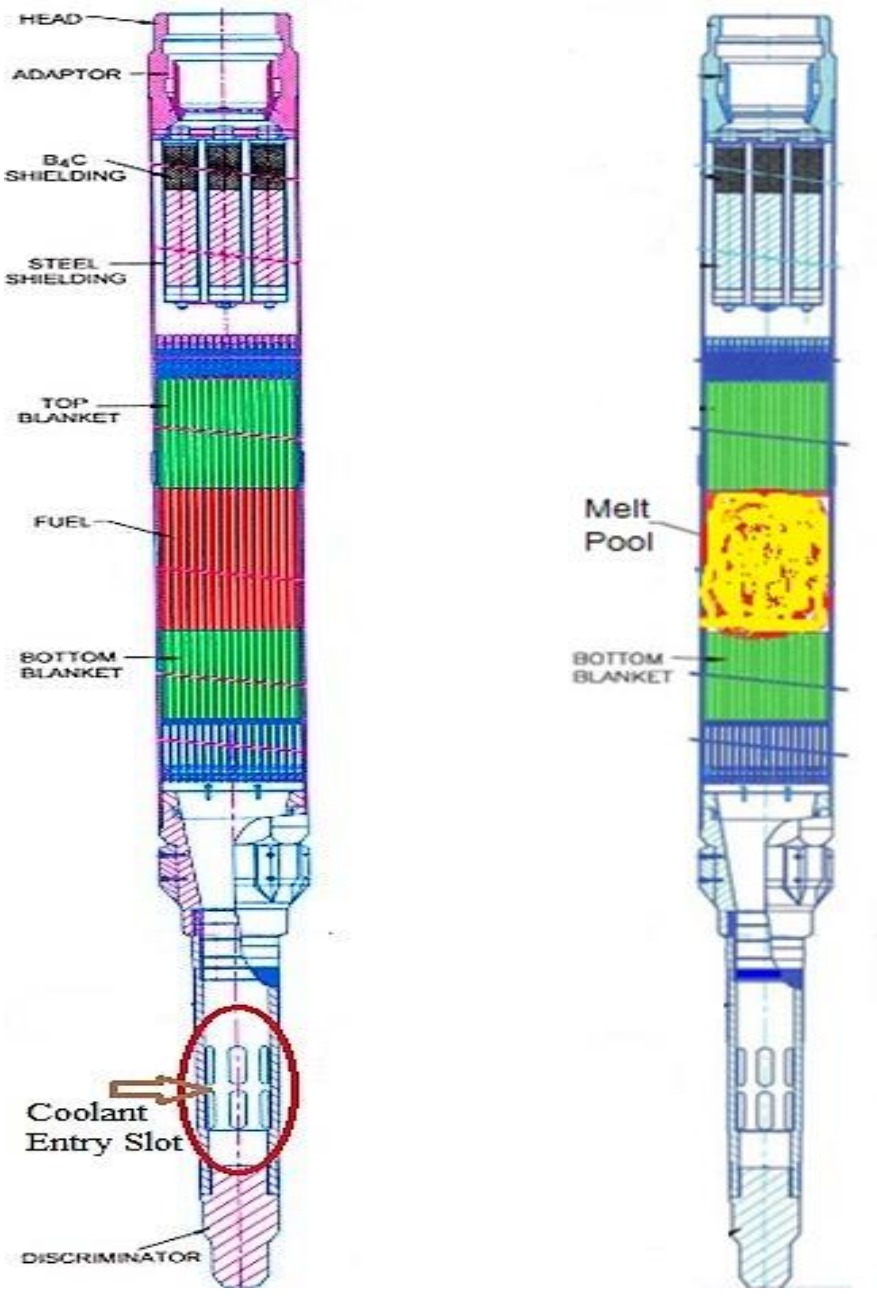

Fig. 1.5: (a) SFR fuel subassembly and (b) Melt pool formed during TIB accident

A postulated TIB accident scenario in a blocked fuel SA involves, an inlet flow blockage quickly leading to sodium boiling, followed by dry out of the fuel pin, thus resulting in a rapid increase in power due to reactivity insertion as a result of coolant void. This adds to further ingression of the accident. Clad melting eventuates due to unavailability of coolant in the subchannel. Fuel melting initiates in few seconds following clad melting forming a melt pool in the active core region as illustrated in Fig. 1.5. Subsequently, the molten material will disperse axially through the pin subchannels towards the core end in a downward direction. The mechanical force created by gravity plays an important role in relocating the fuel in a downward direction. The axial fuel relocation during severe accident in the pin subchannels away from the core region inserts negative reactivity that reduces the reactivity and power levels of the core. The extended axial fuel relocation from the core region to the bottom plug is strongly influenced by freezing of the molten fuel, leading to blocking of the pin subchannels and thus, restrains the axial fuel relocation. If coolant channels are not plugged, ejection of the molten material can occur within a few seconds. The plug formation, if it transpires, detains the axial fuel dispersal, offering sufficient time for the molten fuel to heat and ablate the wrapper walls, which eventually can be breached, allowing the fissile inventories to enter the inter subassembly space and eventually attacking some of the neighbouring subassemblies leading to a re-criticality event. Though the total instantaneous blockage of a single fuel SA is categorised as Beyond Design Basis Event, an internal core catcher is provided below the core support structure, as an engineered safety feature. This is designed for retention of core debris arising out of meltdown of 7 fuel SAs based on the SCARABEE tests (Kayser et al., 1998) which have indicated melt propagation at the most to the neighbouring six fuel SAs.

1.5 RATIONALE AND MOTIVATION BEHIND THE STUDY

Flow blockage accidents, specifically Total Instantaneous Blockage and Loss of Flow accident, have been of major concerns in the safety of SFRs because of the energetics potential resulting from a re-criticality event, eventually leading to a whole core accident. The foregoing section certainly delineates the accident scenario following a flow blockage incident. Specific interest lies in determining the possibility for either the formation of frozen plugs or, alternately, streaming without plugging under SFR conditions. It is strongly perceived from the preceding section that the blockage formation during the molten fuel relocation is dependent on both the fuel type and the core design, especially the length and diameter of the pin subchannels below the core and the thermophysical characteristics of the materials present in this region. The pin subchannel blocking will arrest the fuel escape from the core and eventually lead to melt through of wrapper, which marks the beginning of the transition phase. So, there is a need for the selection of subassembly designs that ensure complete relocation of molten material to the core catcher. Such design measures when integrated to the core, ensure quick drainage of molten fuel, rendering subcriticality that can evade the occurrence of the transition phase and provide an accident mitigation strategy. The melting and relocation of molten corium during TIB event is a very complex phenomenon involving multiphase and multi-materials. Several codes such as SIMMER, SAS4A, etc., have been reported for analysing the accident scenario. Such codes are very complex and are not commercially available. Thus, there is a need to develop a model for this material relocation phenomenon. Development of such a simple and lucid computational model to investigate the freezing characteristic of molten material during its downward

relocation through the coolant channel has acted as the driving rationale and propelling motivation behind present thesis work.

1.6 OBJECTIVES AND SCOPE OF THE STUDY

In the present study, the freezing characteristics of molten material during its axial penetration through the coolant channel is investigated. A transient, one-dimensional, single component, multiphase enthalpy based computational model has been developed to analyse the penetration and freezing behaviour of molten fuel during TIB at the inlet of an SFR fuel subassembly. In the context of the preceding discussions, the present study aims at the following objectives:

- Determination of transient penetration length of the melt front in the coolant channel before blockage following TIB in a fuel SA.
- Evaluation of freezing time (plugging time) required for the melt to form a blockage in the subchannel.
- Assessment of the percentage of molten fuel mass relocated out of core following TIB accident, necessary for evaluating core neutronics behaviour.
- Exploration of possible design measures that need to be considered for enhanced fuel relocation to ensure complete relocation of melt to the core catcher.

1.7 STRUCTURE OF THE THESIS

The present thesis is divided into four major parts. The first part includes the first two chapters, covering an introduction to the research problem and outlines the scope of the work in chapter-1 and a critical review of the literature in chapter-2. The second part comprises of next two chapters dealing with the development of a mathematical model in chapter-3 and validation of the mathematical model with

experimental result in chapter-4. The third part contains only one chapter, chapter-5, focusing the detailed simulation results of melt relocation in a prototype fuel subassembly. The final part of the thesis (chapter-6) highlights the summary of the major finding of the thesis and scope for future research.

CHAPTER 2

Literature Review

2.1 INTRODUCTION

Flow blockage accident is a practicable risk for SFRs in the domain of safety due to the energetics potential resulting from a re-criticality event, eventually leading to a whole core accident. Any possible blockage will have an adverse impact on the availability and safety of the fast reactor. The first reported flow blockage accident in a fuel subassembly of a fast reactor was in the Fermi-1 reactor at Michigan in 1966 (Alexanderson, 1979; Scott, 1971). The reactor was scrammed after the sounding of radiation alarms. The accident cause was characterized as “relatively trivial”. The accident was attributed to a loose crumpled Zircaloy plate, installed to direct the sodium coolant flow to the upward direction, which obstructed the coolant flow channel in the subassembly, resulting in flow starvation leading to a meltdown of two of the 105 fuel assemblies during the accident. This accident culminates a serious consideration on the analysis of internal and external blockage incident in a fuel subassembly. Towards this, several experimental and numerical studies have been carried out afterwards to understand and assess the severe accident scenario precisely. The present chapter

highlights some of the significant experimental and numerical investigations related to melt relocation dynamics and freezing characteristics in the aftermath of fuel meltdown during the subassembly flow blockage accident.

2.2 EXPERIMENTAL DATABASE

The dynamics of molten material movement during TIB and other Core Disruptive Accidents (CDAs) play a crucial role in determining the courses and consequences of accident progression in SFRs (Kondo, 1994). A number of in-pile and out-of-pile experimental programs have been conducted to improve phenomenological understandings on dynamics of melt relocation and freezing during a severe accident.

Worldwide various in-pile experiments, close to the reactor condition, were carried out to understand the accident behaviours. The SCARABEE-N (Livolant et al., 1990; Kayser et al., 1998) in-pile tests, consisting 14 tests with fresh fuel, were performed by the French CEA in the SURA facility of Cadarache. Their main objective was to study the consequences of a TIB at the inlet of an SFR subassembly at full power. Besides this main objective, the program assisted in understanding the physics of meltdown and propagation processes, which may be encountered during the transition phase after a TIB accident. The CABRI (Dadillon et al., 1979 and 1982) is an experimental facility developed at Cadarache under the international collaboration among CEA, JAEA, and other research organisations. This facility is used for SFR safety study, mainly focusing on the Unprotected Loss of Flow (ULOF) accident, using a single-pin geometry. The three-pin cluster CABRI tests (Onoda et al., 2011) simulating the ULOF accident were conducted focusing on post failure fuel relocation and freezing behaviour. These tests supplied complementary information to the existing CABRI tests with a single-pin geometry. Based on the results, it was concluded that the

axial fuel relocation and freezing are dominated by local fuel enthalpy and a fuel/steel mixture likely to create tight blockages near the axial ends of the relocating fuel during material movement. The Mol-7C is an experimental program (Schleisiek et al., 1998) carried out in the Belgian BR-2 reactor to investigate the consequences of local cooling disturbances in mixed oxide fuel subassemblies. In the test a 30 fuel-pin bundle was slowly melted by local cooling disturbances, leading to fuel and steel blockage. The in-pile tests in the United States include various experiments from small test capsules to seven-pin bundles in the test reactors of TREAT (Transient Reactor Test Facility) at INL and ACRR (Annular Core Research Reactor facility) at SNL. The TREAT-series tests (Doerner et al., 1992) include various fresh and pre-irradiated fuels subjected to power and coolant transients simulating the prototypical conditions under Unprotected Transient Overpower Accident (UTOPA) or Unprotected Loss of Flow Accident (ULOFA). The major objectives of these multi-pin tests were to measure post failure fuel motion and to determine the underlying dispersive mechanisms. In the SNL-ACRR reactor, the TRAN-series of in-pile fuel streaming and freezing experiments (Gauntt et al., 1987) addressed the melt freezing characteristics, where the molten fuel generated by nuclear heating was injected by gas pressure into various freezing channels; such as pipes, annular pipes, small pin bundles and flat plates simulating an inter-subassembly gap.

Several series of simulant and reactor-material out-of-pile experiments were undertaken extensively to study the separate effects of the key phenomena during severe accident. The European out-of-pile experiments were briefly summarized by Le Rigoleur et al. (1994). In the JRC-ISPRA, the fuel freezing and blockage was investigated using molten UO2 by Joule heating in the BLOKKER-II test section without sodium. This experimental program involved fuel freezing in circular

and rectangular channels to simulate melt flow in an inter-subassembly gap. Edwards et al. (1992) carried out Sodium Entry Series (SES) experiments using an UO_2 / Mo thermite mixture at Molten Fuel Test Facility (MFTF) in the UK to investigate the extent of penetration of molten fuel in test sections representing full-scale geometries of an SFR fuel SA. The study concluded that the presence of sodium has little effect on molten fuel penetration in initially intact SA geometries and no sign of any Molten Fuel Coolant Interaction (MFCI). In the French CEA, the SIGELCO experiments (Duret and Bonnard, 1988) was conducted to study freezing phenomena in various geometries (tube, pin bundle, etc.) using simulant materials (HITEC, Wood's metal and Tin). A series of experiments were also conducted using pure UO2 melt in the CEA-GEYSER facility to investigate freezing behaviour (Berthoud and Duret, 1989). In the German FZK, molten aluminium-iron oxide thermite mixture was injected into a tube, annular tube or seven-pin-bundle structure in the THEFIS experiments (Fieg et al., 1992). The SIMBATH experiments were carried out using a non-radioactive thermite (Al_2O_3 / Fe) in a single pin, 7-pin, or 37pin bundle geometry to investigate the meltdown and material relocation (Kaiser et al., 1994). Apart from that, a series of reactor-material experiments were conducted in the US-ANL using thermite generated molten fuel (UO2/Mo). The SHOTGUN fuel freezing experiments were performed in a simple pipe geometry for the purpose of investigating crust stability, crust growth and leading-edge penetration. A similar experiment was carried out by Peppler et al. (1988) in a freezing experiment with thermite melt injected into a colder annular channel. GAPFLOW tests simulated fuel ejection into the inter-subassembly gap (Spencer et al., 1985). Hossain et al. (2009) performed a series of simulant experiments using Wood's metal to determine the fundamental mechanisms of penetration and freezing behaviour of molten metal flowing through a seven-pin channel and to provide data for the

fundamental verification of the safety analysis code SIMMER-III. The transient penetration length and the solidified frozen metal in the flow channel were investigated in these experiments. These experimental results are considered as a standard benchmark data in the present research work for the verification and validation of the mathematical model, presented in next Chapter. A similar experimental analysis was carried out later by Soner et al. (2011), using low-melting-point alloy (viz., Bi-Sn-In alloy) and solid particles (of copper and bronze) mixtures as simulant mixed melts (molten-metal/ solid particle mixtures), to investigate the penetration and solidification behaviour of multi-component (liquid/solid-particles mixtures) melt in coolant subchannel during the course of Core Disruptive Accident (CDA). These in-pile and out-of-pile experiments have achieved major contribution to the improved understandings of key phenomena related to the severe accident and provide an experimental database for the validation and improvement of the models of fast reactor safety analysis codes.

2.3 THEORETICAL STUDIES

The experimental analyses carried out were either of small-scale or close to reactor-scale involving lone phenomenon, using either simulant/reactor material. But, the real behaviour of the reactor is much more complex involving multi-component, multi-phenomenon. No integral tests are possible to study the complete accident scenario of the reactor. However, the accumulated experimental findings and knowledge base are used for developing and validating the reactor safety analysis codes which comprehensively simulate the actual behaviour of the reactor during the course of the accident. Towards this, many experimental models and safety analysis codes have been developed for analysing the accident scenario. These computational models were

extensively validated against the experimental results. Some key mathematical models and safety codes pertaining to the present study are reported in this section.

SAS4A is an accident analysis code developed in the US at Argonne National Laboratory to analyse and assess the energetic potential of postulated SFR severe accidents (Tentner et al., 2010). The SAS4A code system models the events taking place in an SFR core during the initiating phase of postulated accidents such as UTOPA and ULOFA. The initiating phase events commence with initial insertion of sodium void reactivity, subsequent reactivity change due to fuel expansion, fuel and cladding relocation. SAS4A has a modular structure, with various modules describing specific phenomena relevant to the SFR accident scenario. It uses a multi-channel treatment approach (Fanning et al., 2017). Each channel represents a fuel pin, its associated coolant, and a fraction of the subassembly duct wall. The channel can be used to represent an average pin/hottest pin in a fuel subassembly or a group of similar subassemblies, a blanket assembly, a control-rod channel. Developed initially for the analysis of oxide-fuel SFRs, the code models have been later expanded to allow the simulation of postulated accident sequences in metal-fuelled SFRs as SAS4A-M (metal fuel) code. SAS4A code became the worldwide standard for the study of the initiating phase of postulated severe accidents in oxide fuelled SFRs.

An advanced safety analysis computer code, SIMMER, has been developed to investigate postulated core disruptive accidents in SFRs (Yamano et al., 2003;). It has undergone various stages of improvement, viz., SIMMER-I, SIMMER-II, SIMMER-III and SIMMER-IV. Further development of next-generation codes of SIMMER are being carried out by JNC (Japan) in collaboration with CEA (France) and FZK (Germany). SIMMER-III is a two-dimensional, three-velocity-field, multiphase,

multicomponent, Eulerian, fluid-dynamics code coupled with a space- and energy-dependent neutron kinetics model. The next edition, SIMMER-IV, is a three-dimensional code based on the SIMMER-III framework. The overall framework of both the codes consists of three elements: the fluid-dynamics model, the structure (fuel pin) model, and the neutronics model. The fluid-dynamics portion is interfaced with the structure model through heat and mass transfer at structure surfaces. The neutronics portion provides nuclear heat sources, based on the time-dependent neutron flux distribution in consistent with mass and energy distributions. The SIMMER code models the events taking place in an SFR core during the transition phase of postulated accidents in oxide fuelled reactor. The initial conditions for the SIMMER in analyses are provided by previous SAS4A analyses. Thus the interfacing between SIMMER and SAS4A becomes an important area in the domain of severe accident analysis.

Several theoretical studies have been carried out using various codes and models to analyse the sequence of events during TIB in SFRs. A TIB accident evaluation for Phenix reactor SA was carried out by Cadiou and Louvet (2006) using SIMMER code. It was found that the time interval between detection of TIB by delayed neutron detection (DND) system and onset of structure melting in the neighbouring SA is sufficient for safe shutdown of the reactor. Wang and Cao (2007) carried out an investigation of the TIB event in a fuel SA of the Chinese Experimental Fast Reactor (CEFR). An analogous approach has been followed by Ravi et al. (2013) to investigate the core damage due to TIB of an SFR fuel SA. He examined that complete melting of the blocked fuel SA occurs within ~20 s and the damage propagation is limited to neighbouring six SAs only.

Apart from that, several transient freezing models have been developed to study the dynamics of solidification of a flowing fluid. Cheung and Baker (1976) developed an analytical model for the transient freezing of liquids in tube flow. A two-dimensional transient freezing model in cylindrical geometry (El-Genk et al., 1978) is formulated to study the solidification of molten fuel through the lower shield plug of Clinch River Breeder Reactor (CRBR) subassembly. A similar mathematical model to investigate the material relocation dynamics is provided by Chun (1980). Gasser and Kazimi (1977) developed a two-dimensional transient freezing model to study the downward streaming of molten fuel through the coolant channels. The results of the model indicate that under post-accident conditions, a high potential exists for rapid relocation of significant quantities of core debris across the shield structure. Kamiyama et al. (2006) formulated a new mechanistic model for the freezing behaviour of the molten material and introduced into the fast reactor safety analysis code, SIMMER-III.

2.4 MITIGATION STRATEGY

The difficulty of accident termination in the Initiating phase (fuel pin disruption) was attributed to the high heat capacity rendered by the available top and bottom axial blankets, resulting in temporary freezing and blockage, thereby building a bottled up core, emanating rapid radial attack of SA structure, formation of melt pool and potential energetic recriticality events. Early benign termination of severe accident scenario in the Initiating phase eliminates potential concerns related to recriticality events and facilitates the potential for inherent in-vessel fuel debris coolability. Towards this, several innovative designs have been conceptualised/developed to mitigate/practically eliminate this type of accidents. One of the prospective concepts is Controlled Material Relocation (CMR) concept in which a portion of the fissile inventory is removed from

the traditional fuel SA/core to enhance the escape of molten fuel from the active core during the accident (Tentner et al., 2010). Several CMR approaches have been investigated; (i) Fuel Assembly Inner Duct System (FAIDUS) concept, (ii) Limited Blanket Removal (LBR) concept and (iii) Mitigation Tube (DCS-M-TT) concept.

2.4.1 Fuel Assembly Inner Duct System (FAIDUS)

The concept of a modified fuel assembly for enhanced fuel relocation has been developed at Japan Atomic Energy Agency (JAEA) for oxide-fueled cores. The Initial FAIDUS design (Fig. 2.1(a)) had a centrally located inner duct structure for fuel escape. During ULOFA, the thinner inner duct wall melts out, resulting downward fuel relocation through the extended inner duct, thereby preventing failure of the SA structure. This concept necessitates a higher failure potential for the inner duct wall than the companion SA structure. The above design concept renders a poor core performance and design complexity. These limitations have been addressed in the current reference design, the Modified-FAIDUS. The Modified-FAIDUS (Fig. 2.1(b)) includes a corner channel for fuel escape, with the fuel expected to relocate upwards to the upper plenum. The fuel discharge capability of the Initial FAIDUS and Modified-FAIDUS were investigated using the SIMMER-III code (Tobita et al., 1999). The analysis indicated that more than 60% of the initial fuel mass in the fuel SA is discharged from the core region by Initial FAIDUS and ~ 90 % of molten materials got expelled using Modified-FAIDUS. An extensive experimental program, the EAGLE (Experimental Acquisition of Generalized Logic to Eliminate re-criticalities) project, has been undertaken to confirm the capability of the fuel removal using the FAIDUS concept (Konishi et al., 2006).

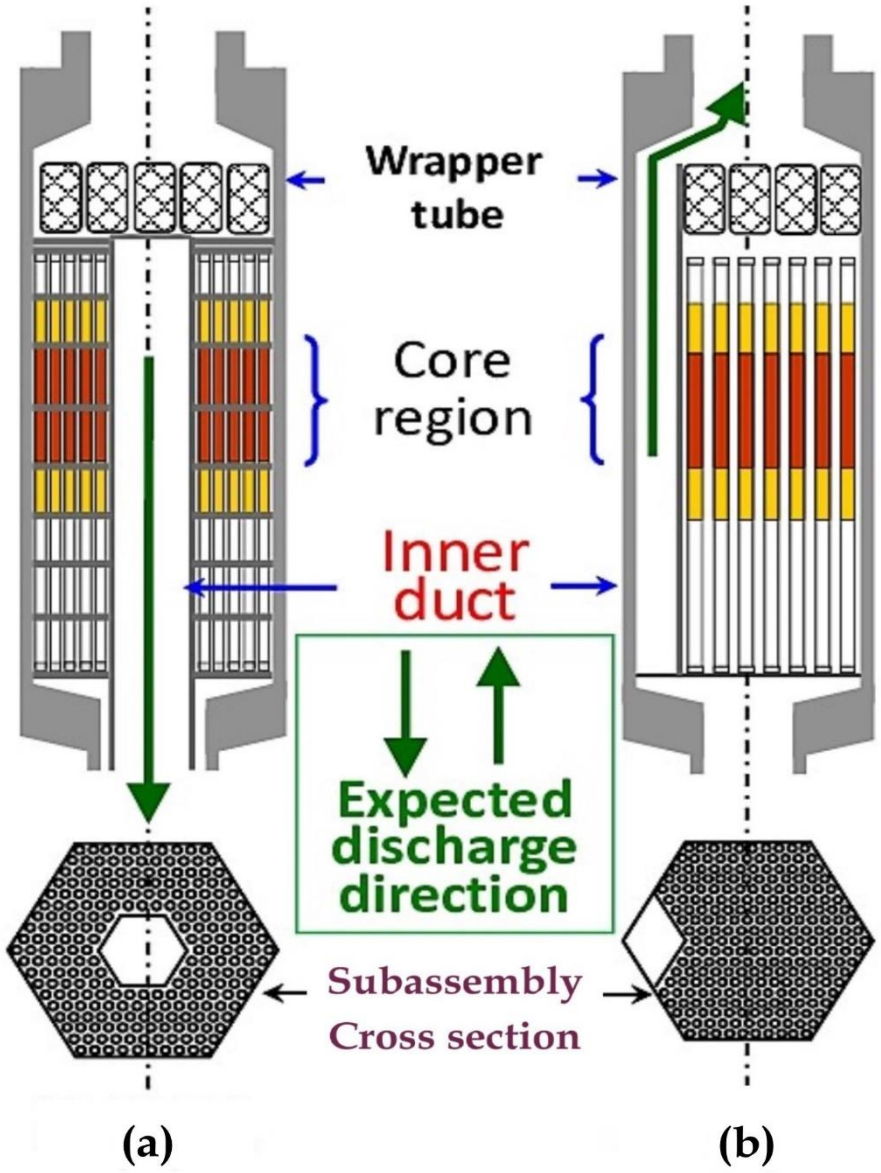

Fig. 2.1: a) Initial FAIDUS and b) Modified FAIDUS (Tentner et al., 2010).

2.4.2 Limited Blanket Removal (LBR)

LBR concept suggests that removal of a small fraction of the axial blanket regions can facilitate extended fuel relocation due to a reduction in heat capacity of the blankets in that region (Fig. 2.2). It remains to assess the potential for freezing and plugging as the fuel relocates through the empty fuel pin structures above and below the active fuel region (Fauske et al., 2002).

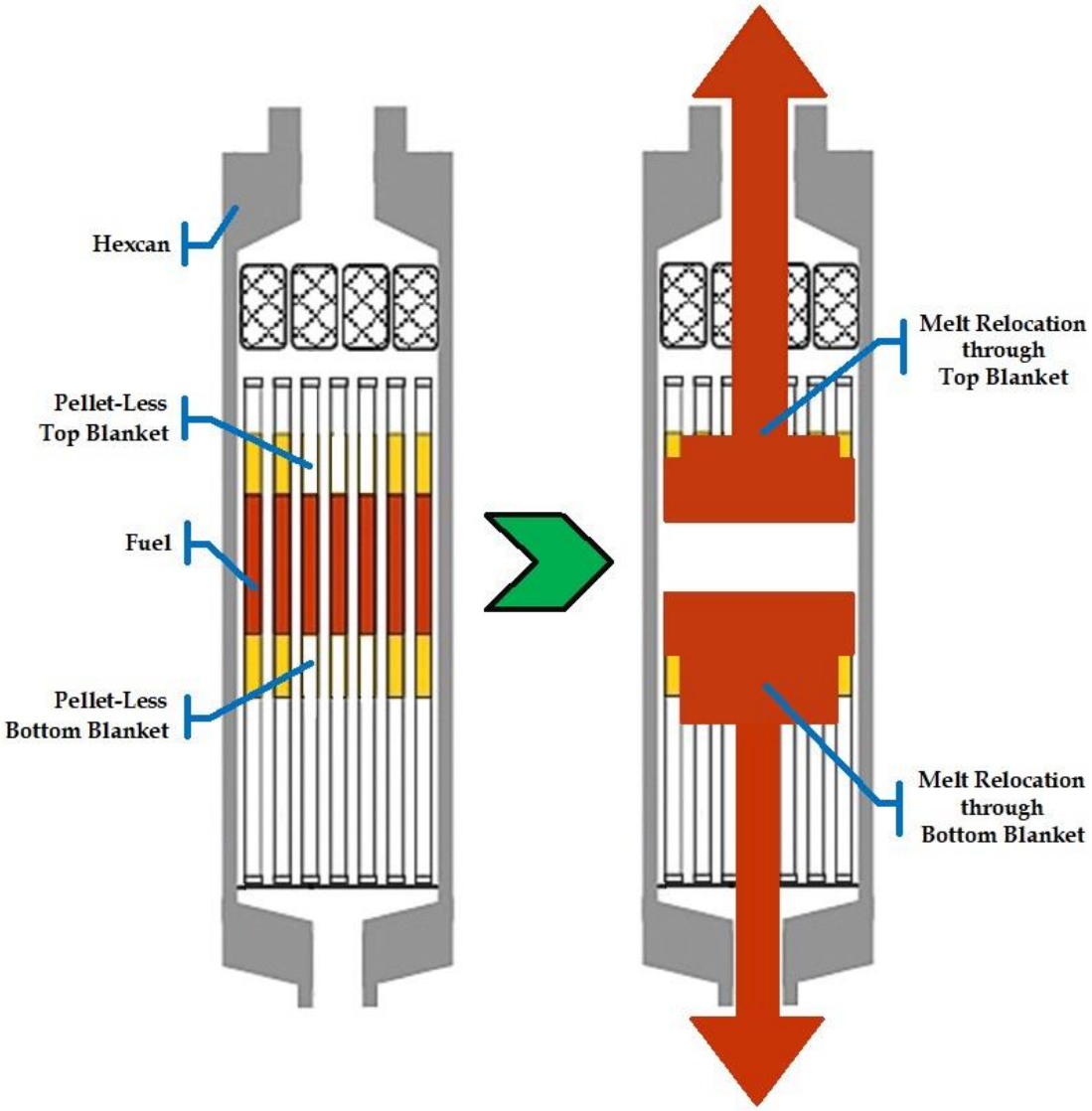

Fig. 2.2: LBR Concept - CMR through Axial Blanket

2.4.3 Mitigation Tube (DCS-M-TT)

ASTRID (Advanced Sodium Technological Reactor for Industrial Demonstration) reactor, developed by the French CEA, is an SFR prototype of Generation IV. Mitigation tubes (DCS-M-TT) are provided in the core as complementary safety devices to mitigate severe accidents (Bertrand et al., 2018). These transverse tubes are positioned within the core, inside and at the periphery (Fig. 2.3). These tubes run through the core support plate to the core catcher installed at

the reactor bottom. Their role is to favour the relocation of the molten corium to the core catcher. It is evident that the geometry of the mitigation tube should promote downstream material relocation to the core catcher as fast as possible. To achieve this, these tubes have a varying cross-section along the melt relocation path. The presence of the mitigation tube leads to a very large negative reactivity insertion as soon as the core becomes prompt-critical.

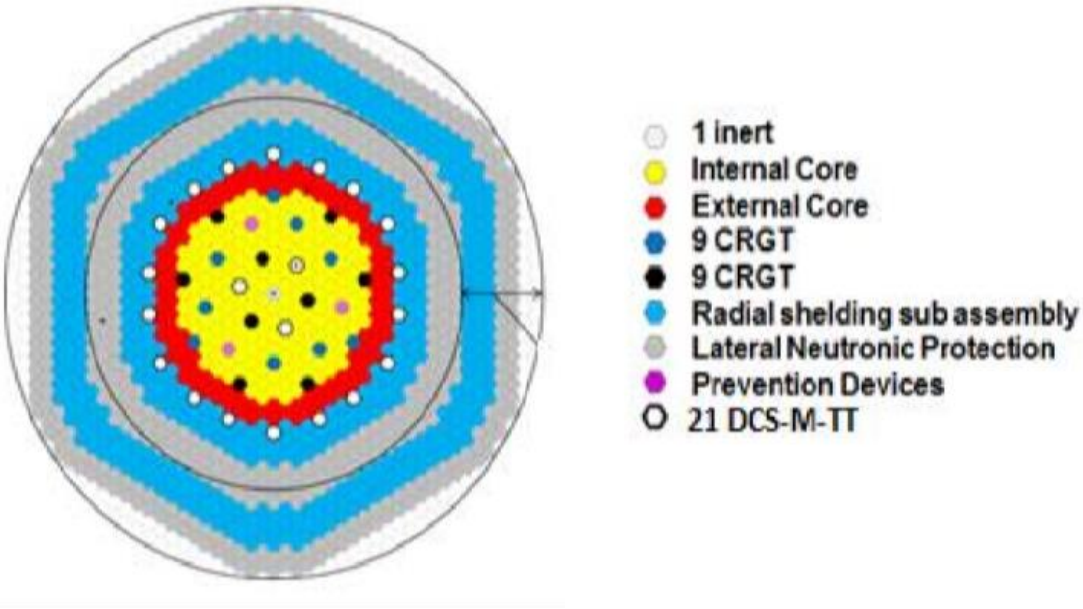

Fig. 2.3: DCS-M-TT Mitigation Tube in ASTRID Core (Bertrand et al., 2018).

2.5 CLOSURE

From the above literature survey, it is evident that there is a paucity of literature on the TIB study. In addition, most of the literature deals with experimental investigations or use complex numerical models such as SIMMER-III. There have been numerous studies to investigate the melt relocation dynamics and freezing characteristics. A closer look at these literature reveals that most of these studies investigate the fundamental freezing behaviour of molten metal during penetration into

relatively simple metal structures like pipes, annular channels and flat plates. Only a few works in the literature demonstrate the freezing behaviour of melt in the pin-bundle geometry. Most of these works are based on a series of simulant experiments and numerical simulation using complex models. Apparently, no robust computational model has been reported in open literature to analyse the penetration and freezing behaviour of molten fuel in the fuel subassembly following TIB event. Development of such a simple mathematical model to investigate the freezing characteristics of the molten material in the subassembly during its downward relocation form the motivation for the present research work. Further, the focus is on exploration of feasible design measures that favour complete relocation of melt to the core catcher.

CHAPTER 3

Mathematical Modelling

3.1 INTRODUCTION

As the present research work is intended towards analysing the penetration and freezing behaviour of molten fuel in a fuel SA, a mathematical model has been developed for this purpose. The model presented in this research work describes fuel freezing behaviour and predicts the penetration distance of fuel draining through the subchannel. Detailed discussion on the development of the mathematical model is presented in this chapter.

3.2 DEVELOPMENT OF 1-D MODEL

The melting and relocation of molten corium during TIB is a very complex phenomenon involving multiphase and multi-materials. In order to simulate the penetration of molten materials into, and their blockage formation in, a cold structure channel during TIB, a transient, one-dimensional, single-component, multiphase computational model has been developed.

The 1-D model comprises of two modules; a Fluid Dynamics module and a Heat Transfer module. Towards the development of the model, in the beginning, a heat generating melt pool is considered to be located at the top of the lower blanket region after the complete meltdown of fuel region of the blocked SA. This pool has the potential to slump down under its static pressure head through the available subchannels in that structure. During streaming down, the melt can freeze on cold structures as crusts or solidify as mobile particles. The streaming mechanism, therefore, must be considered in assessing the rate of melt relocation subsequent to a hypothetical severe accident. Considering the molten fuel solidification behaviour and depending on the flow conditions, fuel freezing in the coolant channels can occur in two distinct ways: Conduction-controlled freezing and Bulk freezing (Epstein et al., 1976).

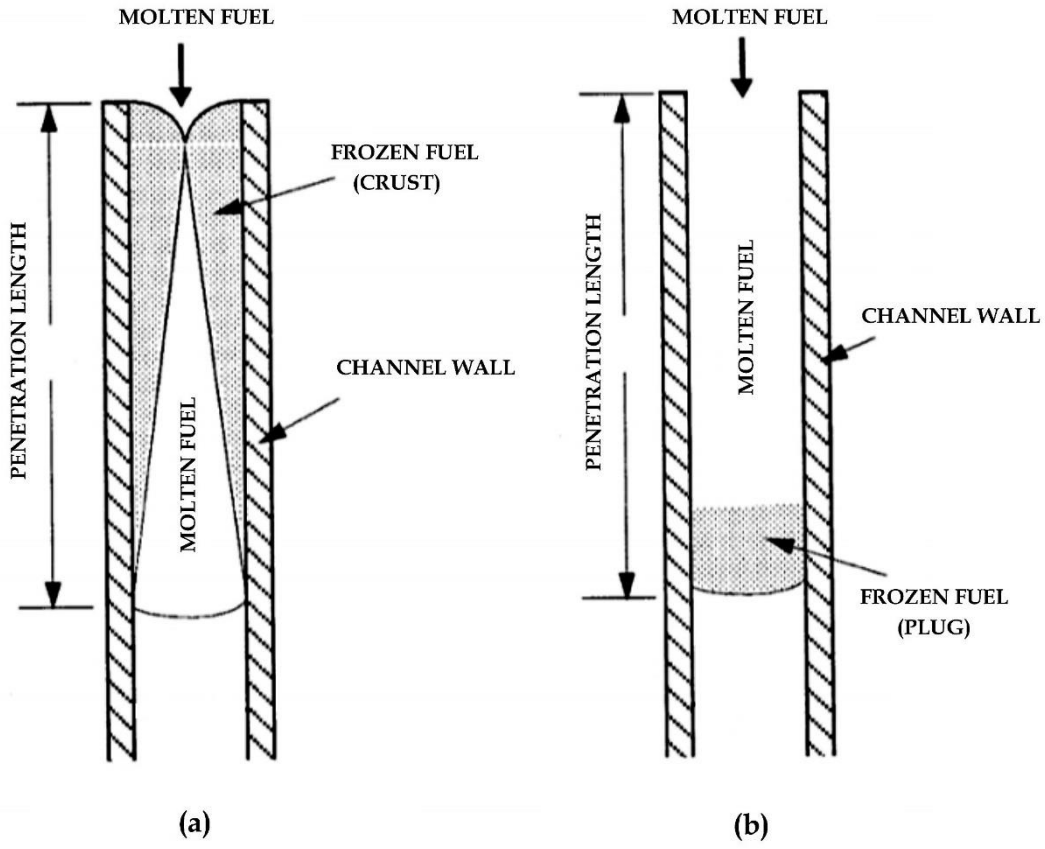

Fig. 3.1: a) Conduction-controlled freezing model and b) Bulk freezing model.

Conduction-controlled freezing, as illustrated in Fig. 3.1(a), is based on the notion that transient freezing is governed by heat conduction through a growing fuel crust at the channel wall. Plugging occurs near the channel inlet when the frozen fuel crust completely occludes the channel. In contrast to the Conduction-limited model, the Bulk freezing assumes that turbulence within the flowing fuel prevents the formation of a stable crust layer at the channel wall, but rather allows the formation of particles in the melt flow channel (Ref. Fig. 3.1(b)). Fuel penetration and freezing are controlled by turbulent heat transport from melt front to the exposed wall surface. Channel blockage is completed when the melt front loses its latent heat of fusion and freezes in bulk. It has been observed through experiments with UO_2 (Ostensen et al., 1974) that the molten fuel flow and freezing in a reactor subassembly structure agree quite well with the bulk freezing model and the same been adapted in the present work. In the present modelling, the molten fuel is assumed to freeze only on the flat surface of the hexcan wall and not on the convex surface of the fuel pin; the same assumption is considered in SIMMER III code too (Hossain et al., 2009). The behaviour of flow blockage formation in the subchannel due to bulk freezing is represented by particle formation due to heat interaction with cold structures in the flow path. This can be modelled by considering solid particles in the melt using the particle viscosity model, which was introduced to model the effective increase in fluid viscosity due to the existence of solid particles in the melt (Morita et al., 2009). In addition, the conditions imposed upon the structures and the molten fuel streaming through the coolant channel are stated as follows:

i. The molten fuel flow is incompressible, Newtonian, and axially symmetric.
ii. Temperature-dependent thermo-physical properties of molten fuel and structure are considered. But, the physical properties within each axial subdivision

(control volume) are assumed constant. The physical properties of the control volume are represented at the corresponding node point.

iii. The temperature of molten fuel and structure is taken to be constant in the radial direction and variable only in the direction of flow. The temperature is represented at the node point of the corresponding control volume.

iv. The velocity of molten fuel follows the plug flow condition.

v. A single pin heat transfer model is adapted to represent the entire pin bundle since similar temperature distribution is assumed to be experienced across all the fuel pins of the pin bundle during melt streaming. This is acceptable for the power reactors due to the presence of a large number of fuel pins (~ 217) in one SA.

vi. The effect of inter-wrapper sodium is minimal and is generally restricted to hexcan and fuel pins next to hexcan. It is not considered in the present model due to the presence of a large number of pins in a fuel SA.

vii. The heat exchange by radiation is not accounted in the present model since its fraction is noticed to be very insignificant compared to other modes of heat transfer.

viii. The fission gases emanated during the fuel meltdown is assumed to be escaped out through the available spaces. So the effect of fission gas pressure is not accounted for in the current analysis.

ix. In the present model variation in core reactivity during melt streaming is not accounted.

With the above assumptions, the mathematical model is formulated which is discussed broadly in the succeeding sections.

3.2.1 Fluid Dynamics Model

In order to simulate the streaming behaviour of molten fuel in the subchannel (Ref. Fig. 3.2(b)), it is essential to evaluate the forces experienced by flowing molten fuel during relocation to lower plenum. Therefore, the force balance on the molten fuel passing through subchannel in the bottom axial blanket gives the following equation:

$$\left(M \times g\right) - \left(\Delta P_{drag} \times A_c\right) - \left(\Delta P_{entry\,loss} \times A_c\right) = M \times \frac{dv}{dt} \tag{3.1}$$

where M is total mass of molten fuel, g is the acceleration due to gravity, A_c is the available subchannel cross-sectional area, ΔP_{drag} is the friction pressure loss, $\Delta P_{entry\,loss}$ is the pressure loss at the entrance of subchannel, v is the velocity of the streaming molten fuel, and t is the time.

The friction pressure loss is computed using the *Darcy-Weisbach equation* and can be expressed as follows:

$$\Delta P_{drag} = \frac{\rho_f F l}{2 D_h} v|v| \tag{3.2}$$

In the above expression ρ_f is the density of the molten fuel, l is the instantaneous penetration length of molten fuel in the subchannel, D_h is the hydraulic diameter of the available subchannel, v is the velocity of the streaming molten fuel, and F is Darcy friction factor. The value of F is generally a function of the Reynolds number (Re), and the Aspect ratio of the subassembly geometry, so that:

$$F = F(\mathrm{Re}, Aspect\,ratio) \tag{3.3}$$

The details of thermo-physical properties of the molten fuel is presented in Appendix A. The value of *F* is determined using Cheng and Todreas correlation (Chen et al., 2018), presented in Appendix B.

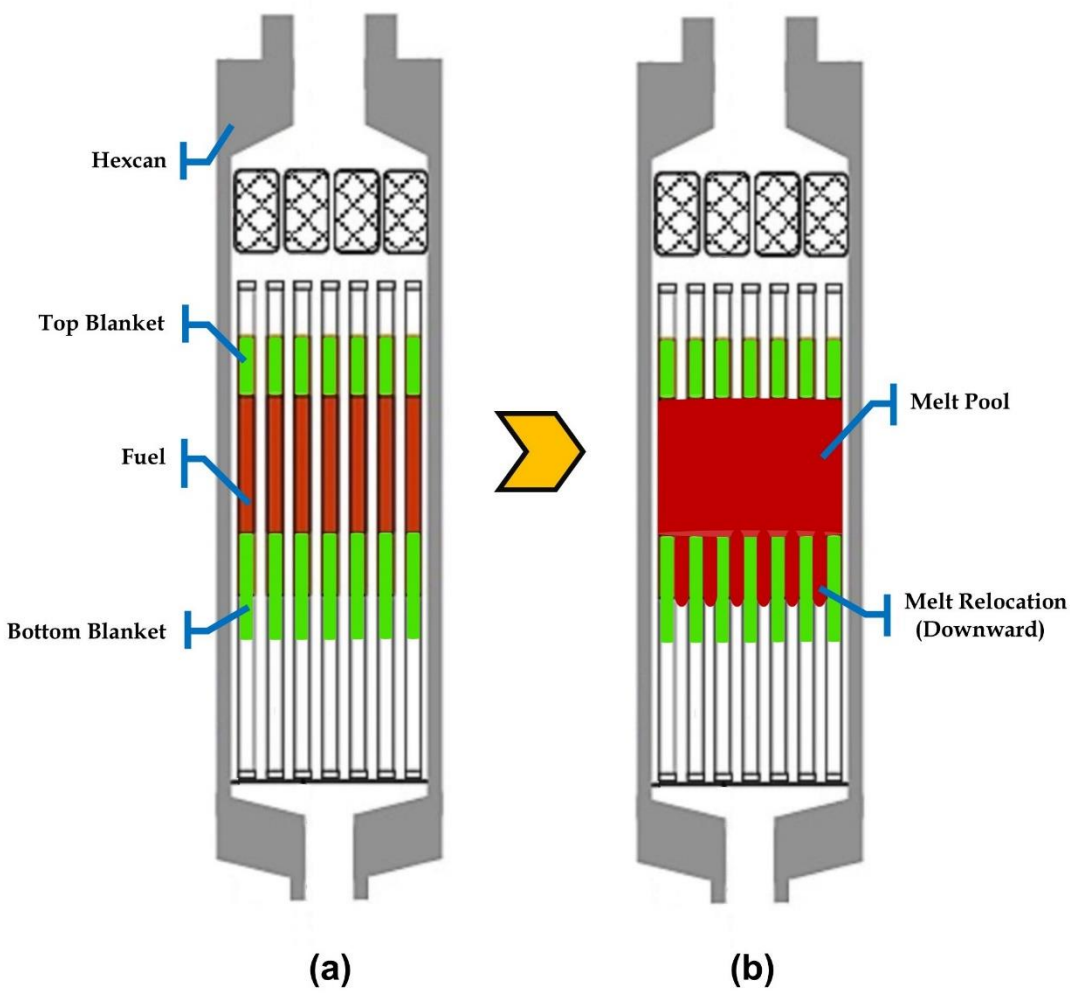

Fig. 3.2: Schematics of a) SFR fuel SA and b) Downward melt relocation phenomena.

The entrance pressure loss is due to abrupt change in flow geometry when the molten fuel is slumping down from the melt pool through the subchannel. The entrance pressure loss is, in practice, related to the kinetic pressure, so the pressure loss is given by:

$$\Delta P_{entry\,loss} = K_e \left(\frac{\rho_f}{2} v|v| \right) \tag{3.4}$$

where K_e is the entrance loss coefficient and K_e = 1 for the present geometry case, ρ_f is the density of the molten fuel, v is the velocity of the streaming molten fuel in the subchannel. The entry pressure loss is accounted in the model until the complete molten fuel is relocated from the melt pool to the subchannel.

Particle viscosity model

To model the flow blockage formation in the pin channel due to bulk freezing, it is necessary to consider the effect of the solid particle on the melt flow. Therefore, it is important to model the effective increase in fluid viscosity due to the existence of solid particles in the molten fuel. A particle viscosity model, adapted in the SIMMER III code, is used in the present study (Morita et al., 2009). As per this model, the fuel viscosity is calculated from:

$$\mu_{eff} = \mu_l \left\{ \frac{\alpha_l}{\alpha_l + \alpha_p} + \frac{f\,\alpha_{MP}\,\alpha_p}{\alpha_{MP}\left(\alpha_l + \alpha_p\right) - \alpha_p} \right\} \tag{3.5}$$

where μ_{eff} is the effective viscosity of continuous liquid phase, μ_l is the viscosity of liquid phase, α_p is particle volume fraction, α_l is the liquid volume fraction, α_{MP} is the maximum volume fraction of solid particles and f is the model parameter. In the present modelling, Eq. (3.5) is used with f = 8.0 and α_{MP} = 0.62 realizing the smooth change of effective viscosity over the wide range of particle volume fraction. With the application of Eq. (3.5) in the present modelling, μ_{eff} is used to substitute the conventional liquid viscosity appearing in the friction pressure loss term. The blockage formation is

simulated by increasing the effective viscosity sharply, owing to the mixing of generated solid particles with the melt, when the fraction of solid particles in the melt exceeds roughly 60%.

Therefore, the Eq. (3.1) can be written as:

$$\left(M \times g\right) - \left(\frac{\rho_f Fl}{2D_h} v|v| \times A_c\right) - \left(\frac{\rho_f}{2} v|v| \times A_c\right) = M \times \frac{dv}{dt}$$

which can be rearranged as:

$$\frac{dv}{dt} = g - \left(\frac{\rho_f Fl}{2D_h M} v|v| \times A_c\right) - \left(\frac{\rho_f}{2M} v|v| \times A_c\right) \tag{3.6}$$

The above equation forms the governing equation of the fluid dynamics model. After being integrated with the particle viscosity model, the fluid dynamics model simulates the dynamic penetrating behaviour of the molten fuel in the subchannel and subsequent blockage formation due to particle formation by freezing of the molten fuel in the flow path.

3.2.2 Heat Transfer Model

During relocation, the transient heat exchange between melt and structures results in freezing of melts and/or melting of the structures. Before proceeding, initially a control volume for the heat exchange analysis in the flow domain needs to be clearly specified. Since the molten fuel is streaming down through the subchannel along the pin bundle, consisting of a hexagonal array of pins, an equivalent annulus concept is adopted representing the basic heat transfer unit of the pin bundle (Ma et al., 2012; Rehme, 1972). Figure 3.3 illustrates a schematic of pin bundles arranged in a triangular

lattice and the hatched region is the basic heat transfer unit considered. The equivalent annulus of hexagonally arranged pin bundle is given by:

$$r_{eq} = \sqrt{\frac{\sqrt{3}}{2\pi}}\, P \tag{3.7}$$

where r_{eq} is the radius of the equivalent annulus, and P is the pitch of the pin bundle geometry.

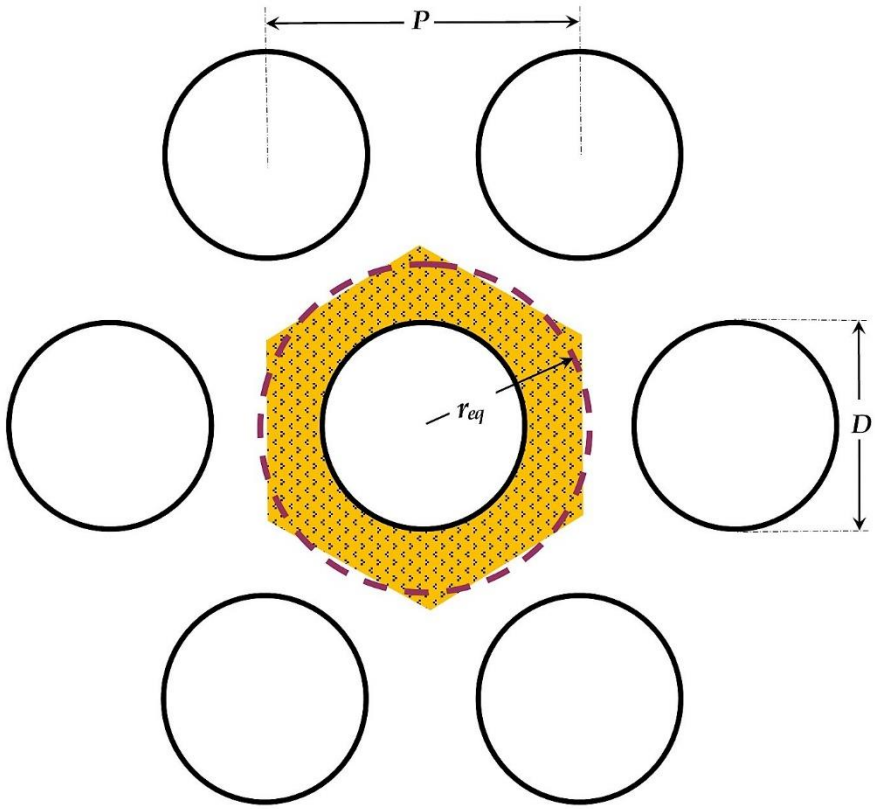

Fig. 3.3: Equivalent annulus in a triangular array pin bundle.

This annular zone concept is adopted for a single pin heat transfer model representing the entire pin bundle for carrying out the heat transfer analysis. In addition, this annular zone represents the molten fuel mass surrounding the fuel pin and is considered as the molten fuel control volume in the present model.

During streaming down along the pin bundle, the penetrating molten fuel exchanges heat with the clad. Eventually, the energy interaction takes place between the clad and the inside blanket through the gap, filled with Helium gas, by conduction phenomena. The energy interaction between the melt pool and the adjoining structures are accounted in the present model. In addition, both radial and axial heat exchanges are considered. The temperature-dependent thermo-physical properties of the molten fuel and the structural materials are included in the model and presented in Appendix A. Besides, transient decay heat generation in the molten fuel is considered in the model. A schematic diagram representing control volumes (CVs) of structure and surrounding molten fuel is shown in Fig. 3.4.

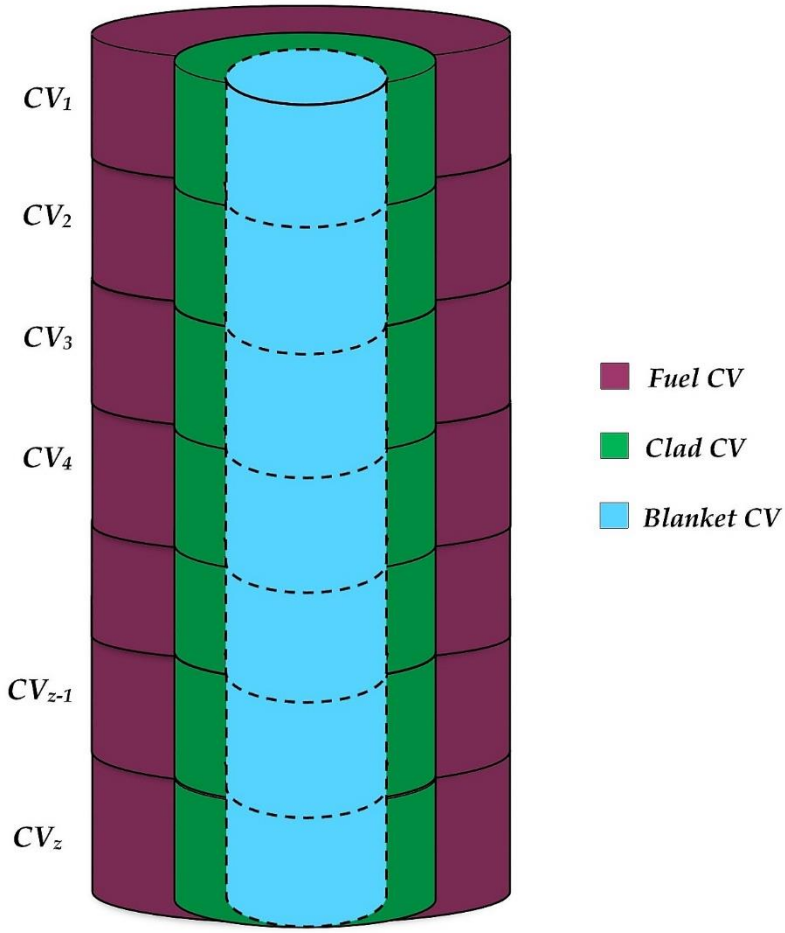

Fig. 3.4: Schematic of vertical cross section of control volumes of structure and fuel.

Of the many methods that have been proposed for dealing with phase change problems, the so-called enthalpy method is among the most popular (Voller, 1990). The major reason for this is that the method does not require explicit treatment of conditions on the phase change boundary. This means that a numerical treatment can be carried out on a fixed grid that is considered in the present modelling. Therefore, enthalpy based energy equations are adopted in the model. The transient enthalpy based heat balance equations for the melt pool, molten fuel inside the subchannel, clad, and blanket are:

Melt pool:

$$M_{pool} \times \frac{d}{dt}\left(H_{pool}\right) = M_{pool} \times \dot{Q}_g - G_{p-c}\left(T_{pool} - T_{dc}\right) - G_{p-b}\left(T_{pool} - T_{db}\right) \tag{3.8}$$

Fuel:

$$m_f \times \frac{d}{dt}\left(H_f\right) = \dot{m} \times H_f^o - \dot{m} \times H_f^n - G_{f-c}\left(T_f - T_c\right) + G_{f-f}\left(T_{uf} - T_f\right) - G_{f-f}\left(T_f - T_{df}\right) + m_f \times \dot{Q}_g \tag{3.9}$$

Clad:

$$m_c \times \frac{d}{dt}\left(H_c\right) = G_{f-c}\left(T_f - T_c\right) - G_{c-b}\left(T_c - T_b\right) + G_{c-c}\left(T_{uc} - T_c\right) - G_{c-c}\left(T_c - T_{dc}\right) \tag{3.10}$$

Blanket:

$$m_b \times \frac{d}{dt}\left(H_b\right) = G_{c-b}\left(T_c - T_b\right) + G_{b-b}\left(T_{ub} - T_b\right) - G_{b-b}\left(T_b - T_{db}\right) \tag{3.11}$$

In the above equations, M_{pool} is the remaining mass in the melt pool; m_f, m_c, and m_b are the masses of the fuel, clad, and blanket in a control volume respectively; $\dot{m}$ is the mass flow rate of the fuel across the control volume; H_{pool}, H_f, H_c, and H_b are the enthalpy

values of melt pool, fuel, clad, and blanket respectively; T_{pool} , T_f , T_c , and T_b are their respective temperatures. The subscripts *u* and *d* represent the adjacent upstream and downstream volumes of the control volume under analysis. H_f^o *and* H_f^n represent the initial and final enthalpy values of fuel while moving across the control volume. $\dot{Q}_g$ is the specific transient decay heat generation rate of molten fuel. *G* represents the effective thermal conductance, whereas the subscripts *p-c, p-b, f-c, f-f, c-b, c-c, and b-b* represent pool and clad, pool and blanket, fuel and clad, fuel and fuel, clad and blanket, clad and clad, blanket and blanket respectively.

Calculation of effective thermal conductance

The effective thermal conductance between the nodal points of the pool and adjoining downstream clad ($G_{p\text{-}c}$) for the axial heat exchange is mathematically expressed as:

$$G_{p-c} = \left[\frac{1}{G_p} + \frac{1}{G_c}\right]^{-1} = \left[\frac{\Delta z/2}{K_f a_c} + \frac{\Delta z/2}{K_c a_c}\right]^{-1} \tag{3.12}$$

Similarly, the overall thermal conductance between the nodal points of the pool and neighbouring downstream blanket ($G_{p\text{-}b}$) is expressed as:

$$G_{p-b} = \left[\frac{1}{G_p} + \frac{1}{G_b}\right]^{-1} = \left[\frac{\Delta z/2}{K_f a_b} + \frac{\Delta z/2}{K_b a_b}\right]^{-1} \tag{3.13}$$

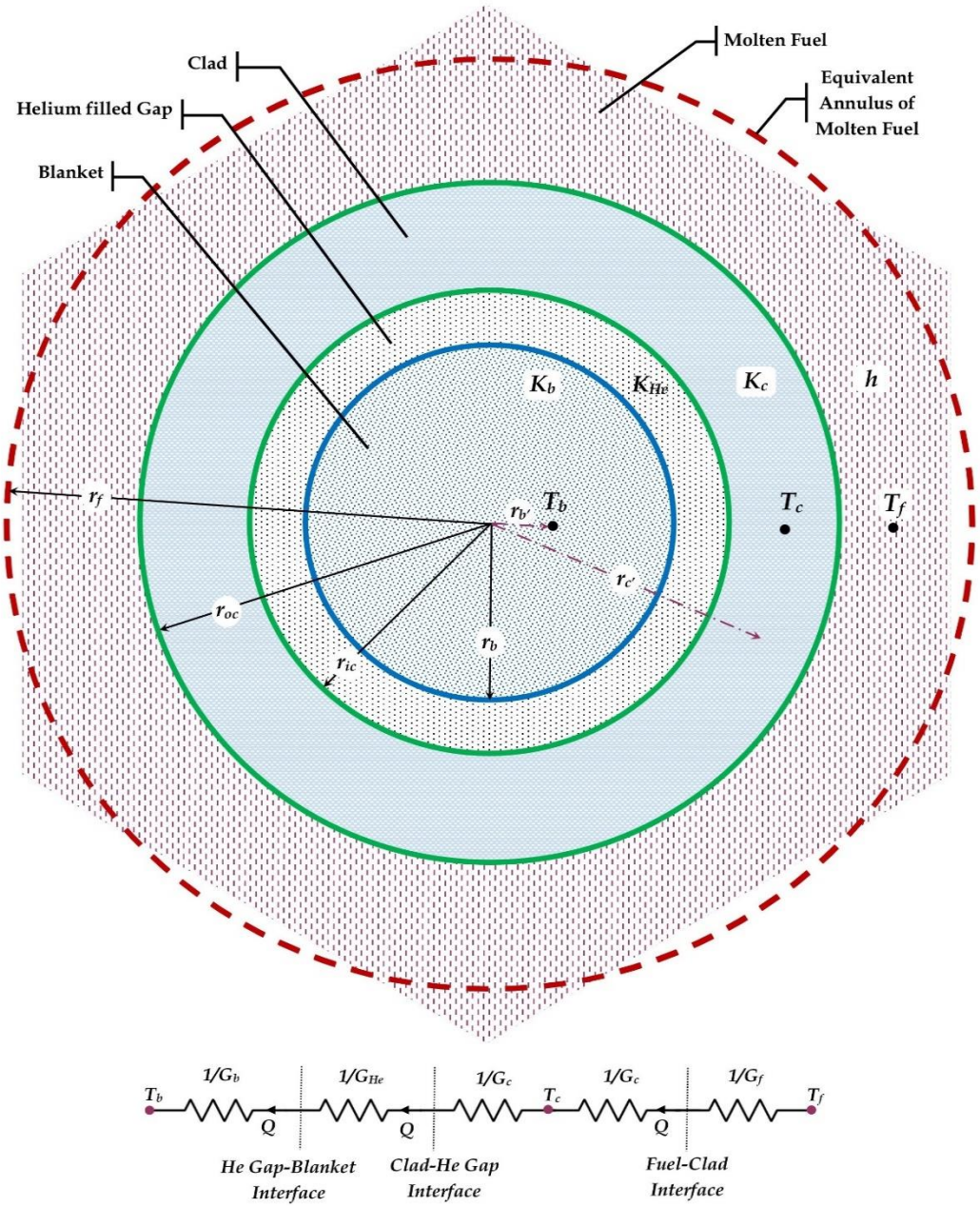

Fig. 3.5: Radial heat exchange between fuel, clad, and blanket control volumes.

Since the molten fuel flows over the clad, the effective thermal conductance between the molten fuel and clad ($G_{f\text{-}c}$) is evaluated by considering the surface convective resistance and the conductive resistance of clad thickness as (Ref. Fig. 3.5):

$$G_{f-c} = \left[\frac{1}{G_f} + \frac{1}{G_c}\right]^{-1} = \left[\frac{1}{hS_c} + \frac{\ln\left(r_{oc}/r_c'\right)}{2\pi K_c(\Delta z)}\right]^{-1} \tag{3.14}$$

The effective thermal conductance between the nodal points of molten fuel and adjacent upstream and/or downstream molten fuel ($G_{f\text{-}f}$) is expressed as (Ref. Fig. 3.6(a)):

$$G_{f-f} = \left[\frac{1}{G_f} + \frac{1}{G_f}\right]^{-1} = \left[\frac{\Delta z/2}{K_f a_f} + \frac{\Delta z/2}{K_f a_f}\right]^{-1} \tag{3.15}$$

The blanket is housed in the cylindrical cladding, both separated by a thin gap filled with inert Helium gas. So the effective conductance for the heat interaction between the clad and the blanket ($G_{c\text{-}b}$) is mathematically written as (Ref. Fig. 3.5):

$$G_{c-b} = \left[\frac{1}{G_c} + \frac{1}{G_{He}} + \frac{1}{G_b}\right]^{-1} = \left[\frac{\ln\left(r_c'/r_{ic}\right)}{2\pi K_c(\Delta z)} + \frac{\ln\left(r_{ic}/r_b\right)}{2\pi K_{He}(\Delta z)} + \frac{\ln\left(r_b/r_b'\right)}{2\pi K_b(\Delta z)}\right]^{-1} \tag{3.16}$$

The effective thermal conductance between the nodal points of clad and adjacent upstream and/or downstream clad ($G_{c\text{-}c}$) is expressed as (Ref. Fig. 3.6(b)):

$$G_{c-c} = \left[\frac{1}{G_c} + \frac{1}{G_c}\right]^{-1} = \left[\frac{\Delta z/2}{K_c a_c} + \frac{\Delta z/2}{K_c a_c}\right]^{-1} \tag{3.17}$$

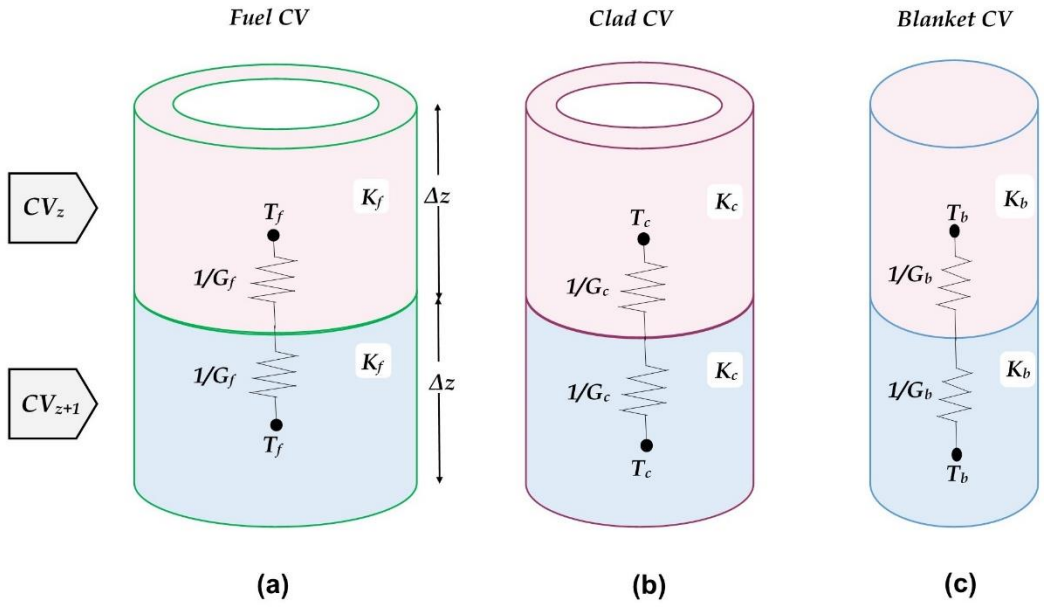

Fig. 3.6: Axial heat conductance among the control volumes.

Similarly, the effective thermal conductance between the nodal points of the blanket and adjacent upstream and/or downstream blanket ($G_{b\text{-}b}$) is expressed as (Ref. Fig. 3.6(c)):

$$G_{b-b} = \left[\frac{1}{G_b} + \frac{1}{G_b}\right]^{-1} = \left[\frac{\Delta z/2}{K_b a_b} + \frac{\Delta z/2}{K_b a_b}\right]^{-1} \tag{3.18}$$

In the above equations, K_f , K_c , K_{He} , and K_b are the thermal conductivity values of fuel, clad, He gas, and blanket respectively (Appendix A). a_f , a_c , and a_b are the cross-sectional area of the fuel, clad, blanket control volumes respectively. S_c represents the surface area of the clad being shared with fuel. Δz is the size of the control volume in the axial direction (Z - direction). r and r' are the corresponding radii of the control volumes in r- direction as represented in the above diagrams.

Typically the thickness of the molten fuel surrounding the pin is ~ 1mm and the diameter of the pin is ~ 6.6mm. Since the radial thickness to diameter ratio is small (~ 0.15mm), the flow can be considered to that between parallel plates. Besides, the parallel plates duct geometry is a limiting geometry for the family of concentric annular ducts. For most cases, it forms an upper bound for fluid friction and heat transfer for this duct class. The fully developed Nusselt number (Nu) for laminar flow between parallel plates is 8.235 (Shah and London, 1978). Therefore, the heat transfer coefficient on the surface of cladding due to forced molten fuel flow (h) is calculated using the correlation:

$$Nu = 8.235 \tag{3.19}$$

3.2.3 Discretization Method

The finite difference approximations of both the implicit and the explicit types have been used in various numerical techniques developed previously. Following this, the governing equations of the present mathematical formulation are discretized by the finite difference approximation method. One drawback with using a finite-difference based discretization method is that an implicit time integration scheme results in a set of nonlinear discretization equations. The efficiency of the method is hence limited by the efficiency of the techniques employed to solve the discretized equations. These limitations are carefully exercised in the present model. The discretization techniques are discussed in this section.

3.2.3.1 Fluid dynamics model discretization

To begin the numerical study, the governing equation of the fluid dynamic model (Eq. (3.6)) needs to be discretized. The governing equation is discretized

employing the finite difference discretization technique of implicit type and is stated as follows:

$$v^{(t+\Delta t)} = v^t + g \cdot \Delta t - \left(\frac{\rho_f Fl}{2D_h M} v^{(t+\Delta t)} \left| v^{(t+\Delta t)} \right| \times A_c \times dt \right) - \left(\frac{\rho_f}{2M} v^t \left| v^t \right| \times A_c \times \Delta t \right) \tag{3.20}$$

where Δt is the step size in the time domain.

The implicit type forward difference discretization technique results in a nonlinear discretization equation. So the relaxation method is incorporated to achieve a better convergence result. The relaxation approach is described below.

Let $\hat{v}^{(t+\Delta t)}$ be the updated value of $v^{(t+\Delta t)}$ from the iterative solution, viz.

$$\hat{v}^{(t+\Delta t)} = v^t + g \cdot \Delta t - \left(\frac{\rho_f Fl}{2D_h M} v^{(t+\Delta t)} \left| v^{(t+\Delta t)} \right| \times A_c \times dt \right) - \left(\frac{\rho_f}{2M} v^t \left| v^t \right| \times A_c \times \Delta t \right) \tag{3.21}$$

Instead of taking $\hat{v}^{(t+\Delta t)}$ as the value of $v^{(t+\Delta t)}$ at the $(t+\Delta t)$ step, use

$$v^{(t+\Delta t)} = \omega \hat{v}^{(t+\Delta t)} + (1-\omega) v^{(t+\Delta t)} \tag{3.22}$$

$$\text{Until} \qquad error = \left| \frac{v^{(t+\Delta t)} - \hat{v}^{(t+\Delta t)}}{v^{(t+\Delta t)}} \right| < \in$$

where ω is a relaxation factor and $\in$ is the error order. The basic step in Eq. (3.21) is called relaxation.

$\omega < 1$ causes the iterations to more slowly move towards the solution.

This is called *under-relaxation*.

$\omega > 1$ causes the iterations to accelerate, i.e. to be more aggressive.

This is called *over-relaxation*.

The amount of over or under-relaxation used can be critical. Too much leads to numerical instabilities, while too little slows down convergence. In the present analysis, the under-relaxation technique is employed for stable convergence, forfeiting the computational time. But, it is noticed that the required computational time is small. The following criteria are implemented in the ongoing analysis:

$$\begin{cases} \textit{Relaxation factor}: & \omega = 0.1 \\ \textit{Error order}: & \in = 10^{-5} \end{cases} \tag{3.23}$$

The instantaneous penetration length of the melt (l) in the flow path is determined by:

$$l^{(t+\Delta t)} = l^{t} + v^{(t+\Delta t)} \cdot \Delta t \tag{3.24}$$

3.2.3.2 Heat transfer model discretization

The numerical methods for solving the phase change problems can be categorised into two types: Fixed grid and Variable grid methods (Sultana et al., 2018). These methods are briefly discussed in this section.

1. *Fixed grid method*

The fixed grid methods are those in which the space-time domain is subdivided into a finite number of equal grids for all times (Fig. 3.7). The numerical solution is carried out on a space grid that remains fixed throughout the computation.

2. *Variable grid method*

Under variable grid methods the space-time domain is subdivided into equal intervals in one direction only. So that the grid size changes as the calculations proceed. This method can be classified into two categories: *variable time steps method* (interface fitting method) and *variable space grids method* (dynamic methods).

- *Variable time steps method*

In this method the space-time domain consists of a uniform spatial grid but a non-uniform time step (Fig. 3.8). The time step is determined such that the boundary traverses exactly one space mesh during that interval. It has been repeatedly employed to solve two-phase and one-dimensional problems.

- *Dynamic grid method*

The dynamic grid method is such that the number of spatial intervals are kept constant and adjusted to ensure the moving boundary is on a particular grid point. Thus, in this method the spatial intervals are a function of time.

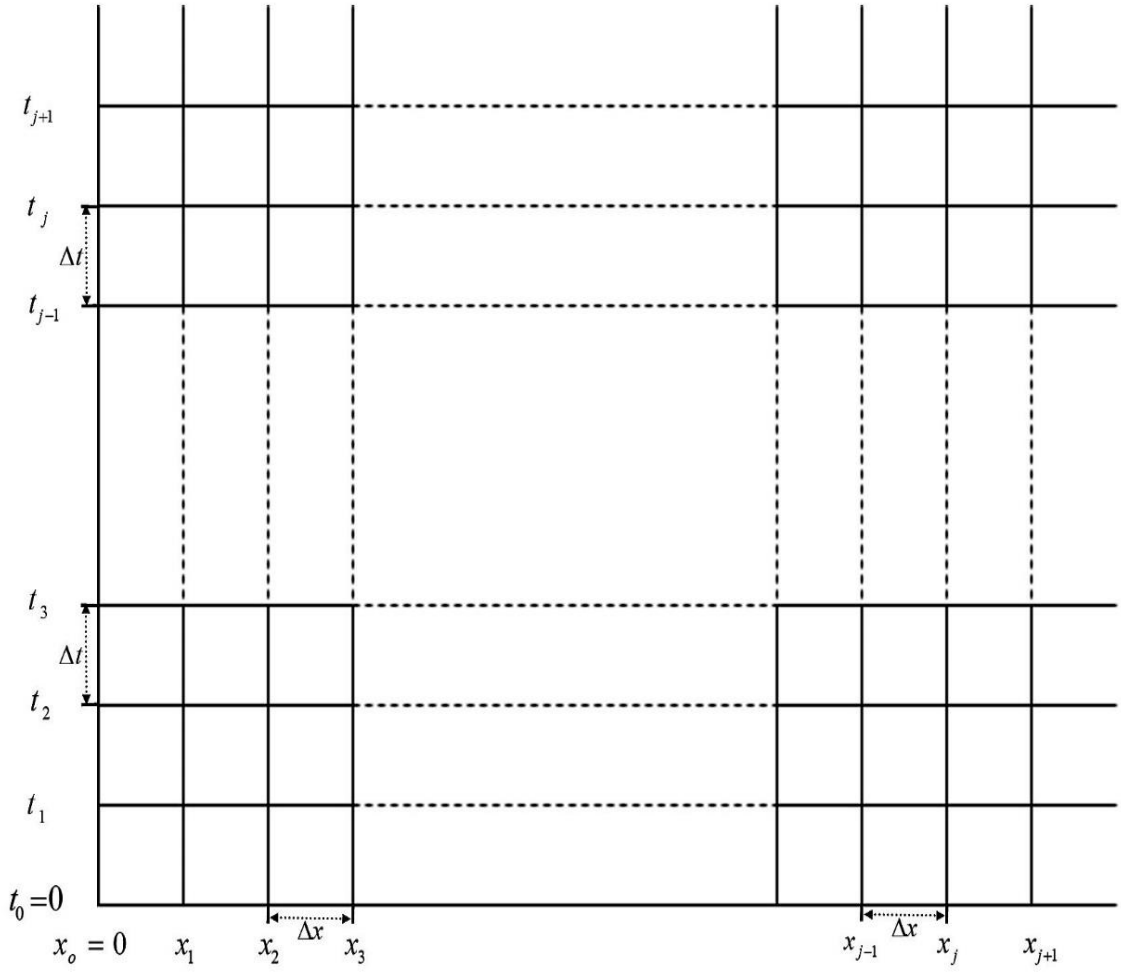

Fig. 3.7: Schematic of the fixed grid system.

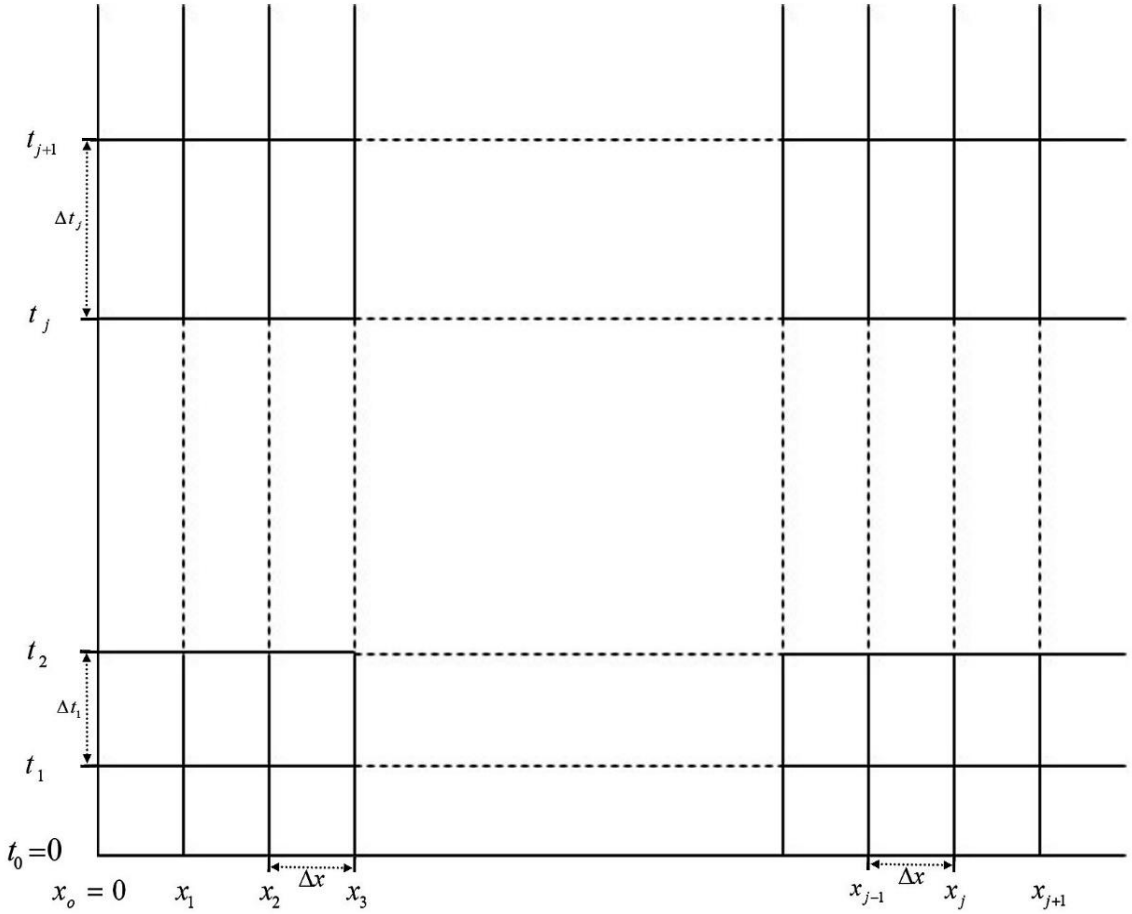

Fig. 3.8: Schematic of the variable time step grid system.

In the present work, we are concerned with variable time step methods only. The z - *t* domain of the present problem case is divided into a uniform spatial grid of size Δz = 1 mm and non-uniform time step (Δt_j) such that the boundary crosses exactly one space mesh during that time step. The time interval (Δt_j) is assessed from the output details of the fluid dynamic model. So, this demands interfacing between the models during the computational methodology. All the thermo-physical properties of the control volume (grid) of the structures and moving molten fuel are assigned at their nodal points (nodes) of the corresponding grids. Besides that, the enthalpy formulation for the control volumes is analysed at their corresponding nodal points.

The enthalpy formulations of the heat transfer model (Eq. (3.8) – (3.11)) are discretized employing the finite difference discretization technique of explicit type. The forward difference scheme is exercised for the discretization procedure.

***Melt pool*:**

The discretized form of energy equation of the melt pool (Eq. (3.8)) is given as follows:

$$H_{pool}^{t+\Delta t_j} = H_{pool}^{t} + \dot{Q}_g^{t}\,\Delta t_j - G_{p-c}^{t}\left(T_{pool}^{t} - T_{c[1]}^{t}\right)\left(\Delta t_j \Big/ M_{pool}^{t}\right) - G_{p-b}^{t}\left(T_{pool}^{t} - T_{b[1]}^{t}\right)\left(\Delta t_j \Big/ M_{pool}^{t}\right) \tag{3.25}$$

where Δt_j is the time step value to cross the j^{th} control volume, the integer j represents the node index of the control volume reached by the molten fuel, t is the penetration time and is updated after each time step; T_{pool}^{t}, $T_{c[1]}^{t}$ and $T_{b[1]}^{t}$ are the temperature values of the pool, and of the boundary control volumes of clad and blanket attached to the pool.

Molten fuel:

The discretized form of enthalpy equation of the molten fuel (Eq. (3.9)) is expressed as follows:

$$\begin{aligned} H_{f[p]}^{t+\Delta t_j} = H_{f[p]}^{t} &- G_{f-c}^{t}\left(T_{f[p]}^{t} - T_{c[p]}^{t}\right)\left(\Delta t_j \Big/ m_f + \dot{m}\,\Delta t_j\right) + \dot{Q}_g^{t}\left(m_f \Delta t_j \Big/ m_f + \dot{m}\,\Delta t_j\right) \\ &+ G_{f-f}^{t}\left(T_{f[p-1]}^{t} - T_{f[p]}^{t}\right)\left(\Delta t_j \Big/ m_f + \dot{m}\,\Delta t_j\right) - G_{f-f}^{t}\left(T_{f[p]}^{t} - T_{f[p+1]}^{t}\right)\left(\Delta t_j \Big/ m_f + \dot{m}\,\Delta t_j\right) \end{aligned} \tag{3.26}$$

and the index p = 2, 3,……, j-1.

The discretized equation of the boundary control volume (CV) located at the top (p = 1) yields:

$$H_{f[1]}^{t+\Delta t_j} = H_{f[1]}^{t} - G_{f-c}^{t}\left(T_{f[1]}^{t} - T_{c[1]}^{t}\right)\left(\Delta t_j \Big/ m_f + \dot{m}\Delta t_j\right) + \dot{Q}_g^{t}\left(m_f \Delta t_j \Big/ m_f + \dot{m}\Delta t_j\right) - G_{f-f}^{t}\left(T_{f[1]}^{t} - T_{f[2]}^{t}\right)\left(\Delta t_j \Big/ m_f + \dot{m}\Delta t_j\right) \tag{3.27}$$

Similarly, for boundary CV located at the bottom ($p = j$) is stated as:

$$H_{f[j]}^{t+\Delta t_j} = H_{f[j]}^{t} - G_{f-c}^{t}\left(T_{f[j]}^{t} - T_{c[j]}^{t}\right)\left(\Delta t_j \Big/ m_f + \dot{m}\Delta t_j\right) + \dot{Q}_g^{t}\left(m_f \Delta t_j \Big/ m_f + \dot{m}\Delta t_j\right) + G_{f-f}^{t}\left(T_{f[j-1]}^{t} - T_{f[j]}^{t}\right)\left(\Delta t_j \Big/ m_f + \dot{m}\Delta t_j\right) \tag{3.28}$$

Clad:

The discretized form of energy equation of the clad (Eq. (3.10)) is expressed as follows:

$$H_{c[p]}^{t+\Delta t_j} = H_{c[p]}^{t} + G_{f-c}^{t}\left(T_{f[p]}^{t} - T_{c[p]}^{t}\right)\left(\Delta t_j \Big/ m_c\right) - G_{c-b}^{t}\left(T_{c[p]}^{t} - T_{b[p]}^{t}\right)\left(\Delta t_j \Big/ m_c\right) + G_{c-c}^{t}\left(T_{c[p-1]}^{t} - T_{c[p]}^{t}\right)\left(\Delta t_j \Big/ m_c\right) - G_{c-c}^{t}\left(T_{c[p]}^{t} - T_{c[p+1]}^{t}\right)\left(\Delta t_j \Big/ m_c\right) \tag{3.29}$$

and the index p = 2, 3,……, j.

For the boundary CV located at the top adhering to the melt pool (p=1), the discretized equation yields:

$$H_{c[1]}^{t+\Delta t_j} = H_{c[1]}^{t} + G_{f-c}^{t}\left(T_{f[1]}^{t} - T_{c[1]}^{t}\right)\left(\Delta t_j \Big/ m_c\right) - G_{c-b}^{t}\left(T_{c[1]}^{t} - T_{b[1]}^{t}\right)\left(\Delta t_j \Big/ m_c\right) + G_{p-c}^{t}\left(T_{pool}^{t} - T_{c[1]}^{t}\right)\left(\Delta t_j \Big/ m_c\right) - G_{c-c}^{t}\left(T_{c[1]}^{t} - T_{c[2]}^{t}\right)\left(\Delta t_j \Big/ m_c\right) \tag{3.30}$$

Blanket:

The discretized form of heat equation of the blanket (Eq. (3.11)) is expressed as follows:

$$H_{b[p]}^{t+\Delta t_j} = H_{b[p]}^{t} + G_{c-b}^{t}\left(T_{c[p]}^{t} - T_{b[p]}^{t}\right)\left(\Delta t_j / m_b\right) + G_{b-b}^{t}\left(T_{b[p-1]}^{t} - T_{b[p]}^{t}\right)\left(\Delta t_j / m_b\right) - G_{b-b}^{t}\left(T_{b[p]}^{t} - T_{b[p+1]}^{t}\right)\left(\Delta t_j / m_b\right) \quad (3.31)$$

and the index p = 2, 3,……, j.

The discretized equation of the boundary CV located at the top adjoining the melt pool (p=1) is expressed as:

$$H_{b[1]}^{t+\Delta t_j} = H_{b[1]}^{t} + G_{c-b}^{t}\left(T_{c[1]}^{t} - T_{b[1]}^{t}\right)\left(\Delta t_j / m_b\right) + G_{p-b}^{t}\left(T_{pool}^{t} - T_{b[1]}^{t}\right)\left(\Delta t_j / m_b\right) - G_{b-b}^{t}\left(T_{b[1]}^{t} - T_{b[2]}^{t}\right)\left(\Delta t_j / m_b\right) \quad (3.32)$$

3.2.4 Solution Sequence

In the beginning, the discretized fluid dynamic equation (Eq. (3.20)) is solved in the flow domain for a time step Δt. By integrating the particle viscosity model and under-relaxation scheme during numerical computation, the solution of the discretized equation assuredly predicts the instantaneous velocity (v) of the molten fuel in the flow path at the end of time step. From this, the transient penetration length (l) of the melt in the subchannel is determined using Eq. (3.24). The obtained results are coupled to the heat transfer model.

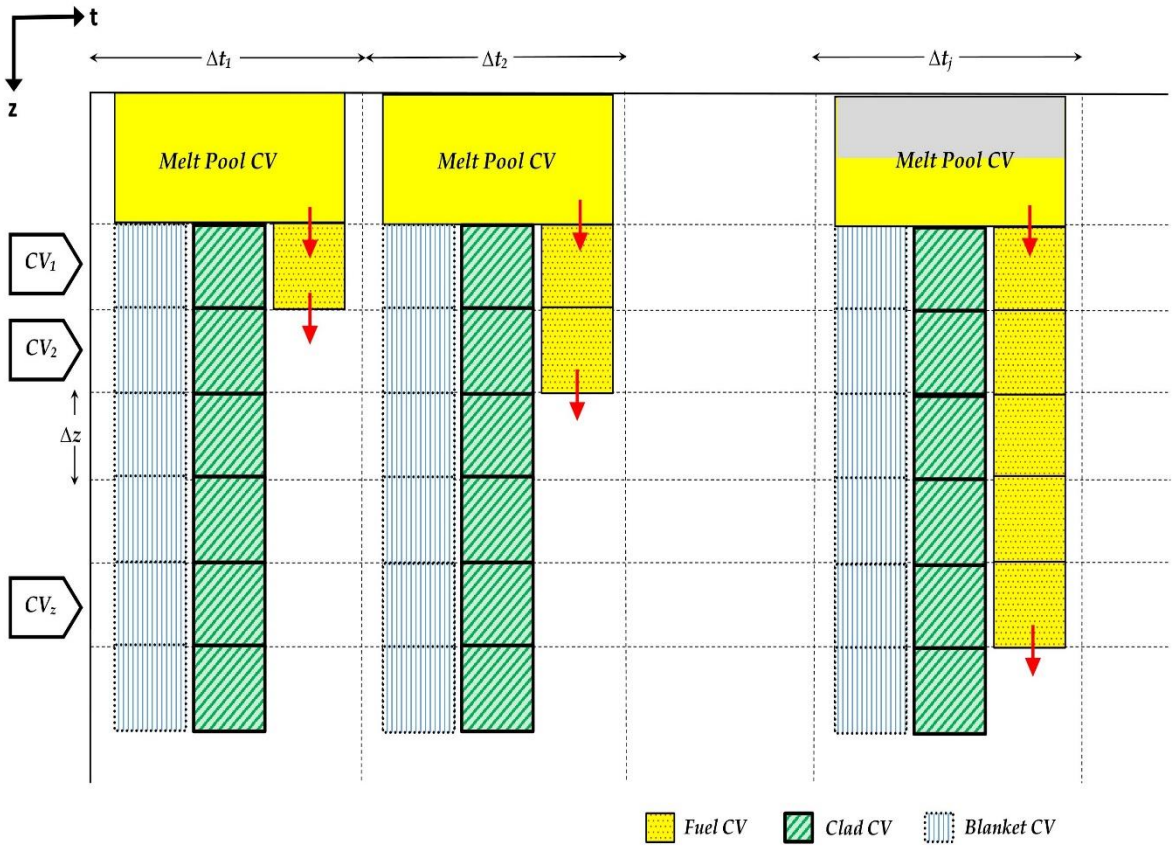

Fig. 3.9: General schematics of position of control volumes across the variable grid.

An interpretative diagram representing the positions of the control volumes of the molten fuel and structural elements after each time interval Δt_j is shown in Fig. 3.9. The movement of the molten fuel across the variable grid is shown by an arrow sign. It is derived that the molten fuel crosses exactly one CV in the time interval Δt_j .

The discretized enthalpy formulations (Eq. (3.25) - (3.32)) of the heat transfer model are solved throughout the heat transfer domain for the time interval (Δt_j) that is assessed from the output details of the fluid dynamic model. Therefore, these inter-linked equations are needed to be solved successively along with the discretized fluid dynamic equation. The solution yields the end of time interval enthalpies for the fuel,

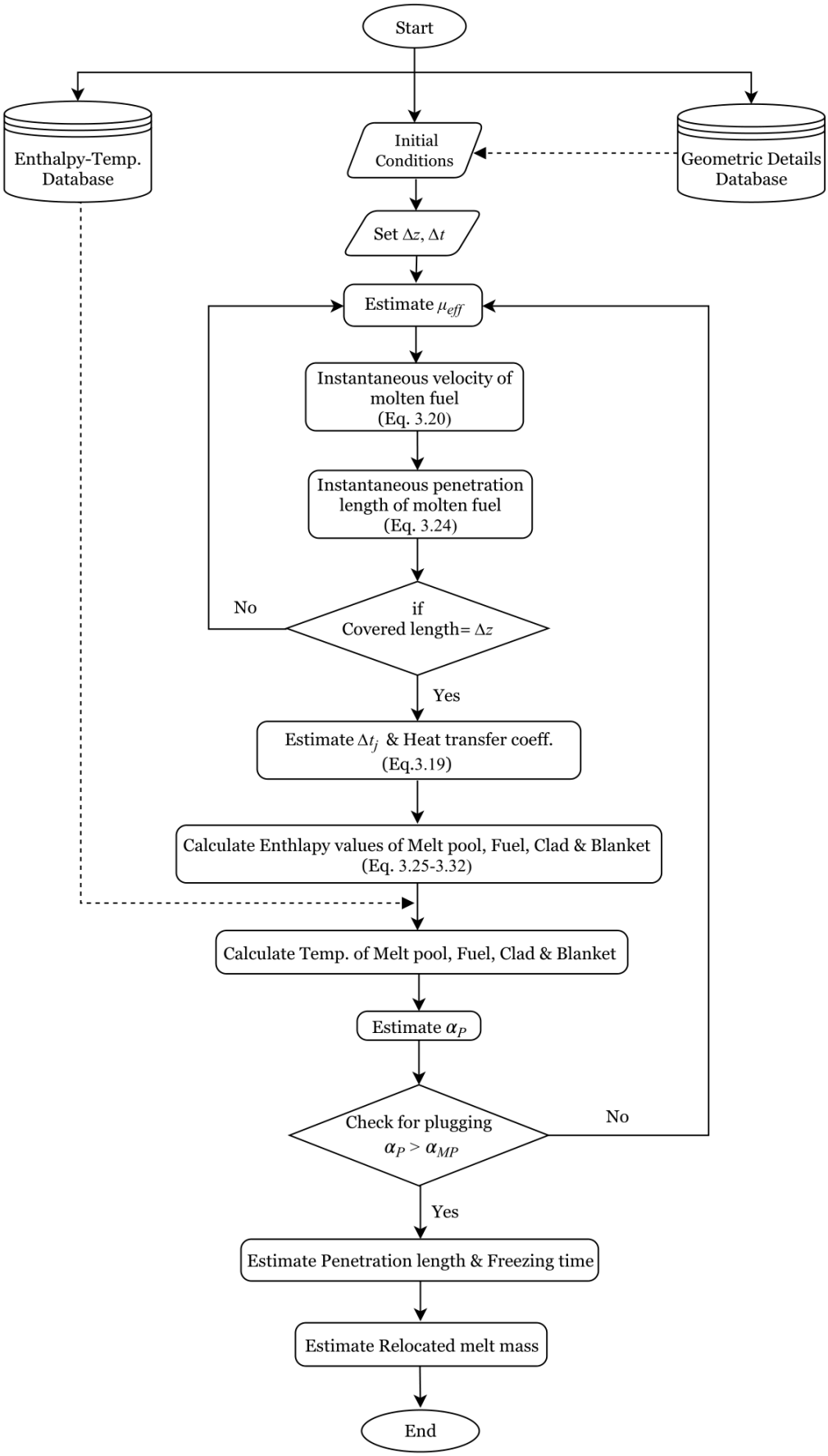

Fig. 3.10: Flow chart of solution procedure.

clad, and blanket domains. Once the enthalpy values of each node at a given time interval are available, the corresponding temperatures of melt pool, fuel, clad, and blanket are determined using an enthalpy-temperature database that has been prepared from the available enthalpy-temperature correlation presented in Appendix A. This reduces the computational time too. The temperature data predicts the physical states of molten fuel and structure. The obtained enthalpy data of fuel is utilized to estimate the particle volume fraction in molten fuel. Once the solid fraction in the melt exceeds 60%, the numerical simulation is terminated following the assumption of blockage formation in the available flow path due to solid particles. The above solution procedure is represented in a flow chart (Fig. 3.10) for better understanding.

Therefore the integrated model evidently evaluates the real-time physical behaviour of the melt and the structures in the flow path during a severe accident.

3.3 CLOSURE

The described mathematical model integrates the hydrodynamics of streaming down molten fuel with the freezing of the melt and/or the melting of the structural elements. The mathematical structure described here is implemented in a computer code and applied towards the analysis of streaming, freezing, and blocking characteristics of the molten fuel in a fuel SA under accident conditions in the subsequent chapter.

CHAPTER 4

Validation Study

4.1 INTRODUCTION

The developed mathematical model is used to analyse the penetration, freezing, and plugging phenomena of molten fuel in the coolant channels during the transition phase of a severe accident. In this context, the primary requisite of the developed model is its validation study to ascertain the applicability of the model in assessing the streaming and freezing behaviour of the streaming molten fuel.

4.2 VALIDATION

A good deal of (in-pile and out-of-pile) information on the dynamics of molten material relocation following severe accident is reported in open literature. Several reviews of this literature were earlier elucidated in the Chapter-2. Their studies investigate the fundamental freezing behaviour of the molten material during penetration into the relatively simple structures. However, understanding of the behaviour of the transition phase in severe accidents is still limited partly owing to difficulties in conducting related experiments to describe the accidents.

To address the limited experimental investigations, Hossain et al. (2009) conducted a series of simulant experiments using Wood's metal to study the fundamental mechanism underlying the penetration and freezing behaviour of the molten metal through a seven-pin channel, which is a more practical geometry representing the reactor case.

4.2.1 Seven-Pin Experiments

A schematic view of the seven-pin bundle apparatus is shown in Fig. 4.1. The experimental facility consists of a melt tank and a flow channel section. The melt tank is used to melt and inject the simulant material (Wood's metal) into the flow channel. The melt tank is made of Pyrex glass with a Teflon plug being attached at the base of the melt tank. The flow channel section of length 500 mm consists of seven pins made of stainless steel tubes, each closed off at the top, and encased by an outer glass tube for flow visualization. The whole set-up is placed on a stainless steel base and supported

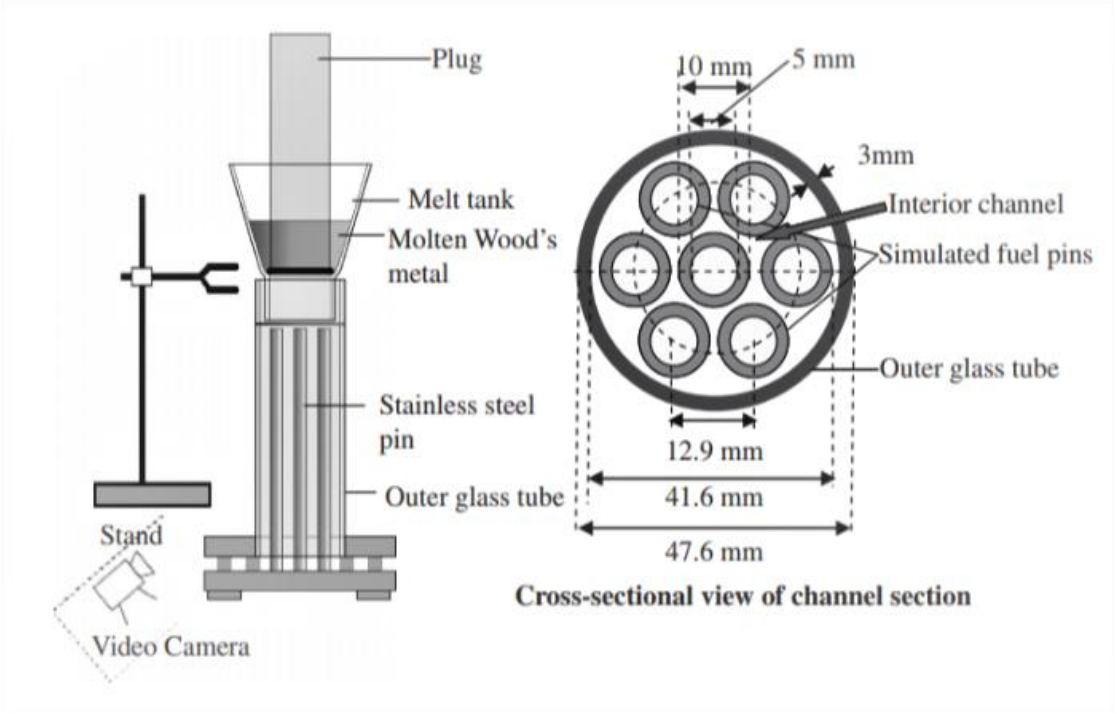

Fig. 4.1: Schematic diagram of seven-pin bundle experimental apparatus.

by a fixed stand. A total of 21 k-type thermocouples are attached to the pins and melt tank to measure the temperatures of the pins and streaming melt. A digital video camera is kept to record the melt streaming and freezing behaviour in the pin channel. The hydraulic parameters used in the series of experiments are summarized in Table 4.1.

Table 4.1
Hydraulic parameters for the seven-pin channel experiment.

Parameter	Value
Number of fuel pins	7
Outer pin diameter (mm)	10
Inner pin diameter (mm)	5
Pin pitch (mm)	12.9
Hydraulic diameter excluding outer gap (mm)	8.31
Inner diameter of the outer circular wall (mm)	41.6
Outer diameter of the outer circular wall (mm)	47.6
Thickness of the outer circular wall (mm)	3

A thin fusible (~1 mm thickness) solid plate of Wood's metal was initially placed at the melt tank base for smooth injection of melt into the pin channel. The pins inside the flow channel section were uniformly heated by blowing hot air and was monitored using a thermocouple to achieve a desired pin temperature. At the same time, a specified quantity of Wood's metal was heated using an electric heater; the temperature of the melt was monitored using a digital thermometer to achieve a desired melt temperature. A transient melt pool is formed at the base of the melt tank and upon melting of the thin fusible Wood's metal layer, the melt flowed into and down the pin channel under the action of gravity. The local penetration lengths of the streaming melt

at all six sub-channel positions were measured. Then their average value was used to represent the penetration length of the bulk melt flow. All the experiments were carried out at atmospheric pressure.

The physical properties of Wood's metal and stainless steel are listed in Table 4.2. The experimental conditions are summarized in Table 4.3.

Table 4.2

Physical properties of Wood's metal and stainless steel.

Properties	Wood's metal	Stainless steel (Grade 316L)
Melting point (ºC)	78.8	1430
Density (kg/m^3)	8400	8000
Thermal conductivity (W/m-K)	11.1	16.2
Specific heat (J/kg-K)	150	530
Kinematic viscosity (m^2/s)	2×10^{-7}	1.97×10^{-7}
Latent heat of fusion (J/kg)	2.53×10^4	3.39×10^5

Table 4.3

Experimental conditions.

Melt mass (g)	Pin temperature (°C)	Melt temperature (°C)
215/325	25	100
215	25	130

4.2.2 Seven-Pin Experiment Validation

Numerical simulation of the experiment using the present model is carried out for the verification and validation of the present mathematical model. The simulation results are compared with that of the experimental data. The experiment was also analysed using SIMMER III code. The details of validation results are discussed here.

The simulation results of all the experimental conditions (mentioned in Table 4.3) are compared with that of experimental and SIMMER-III values (Hossain et al., 2009).

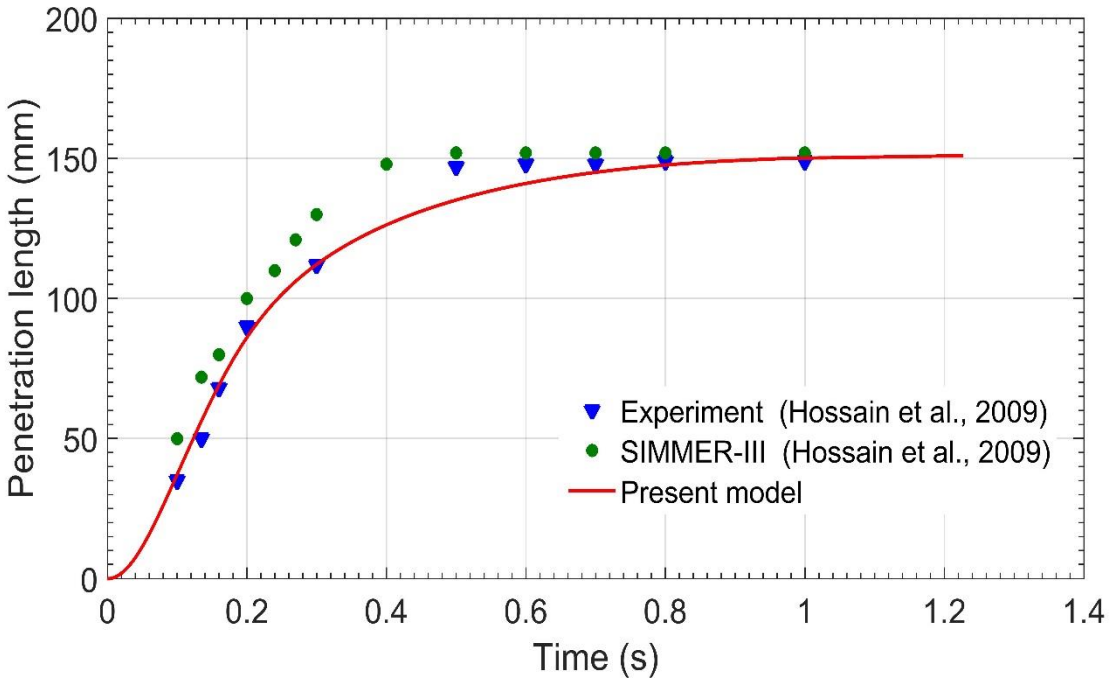

Fig. 4.2: Transient penetration length of molten metal (melt mass: 215g, melt temperature: 100°C, pin temperature: 25°C)

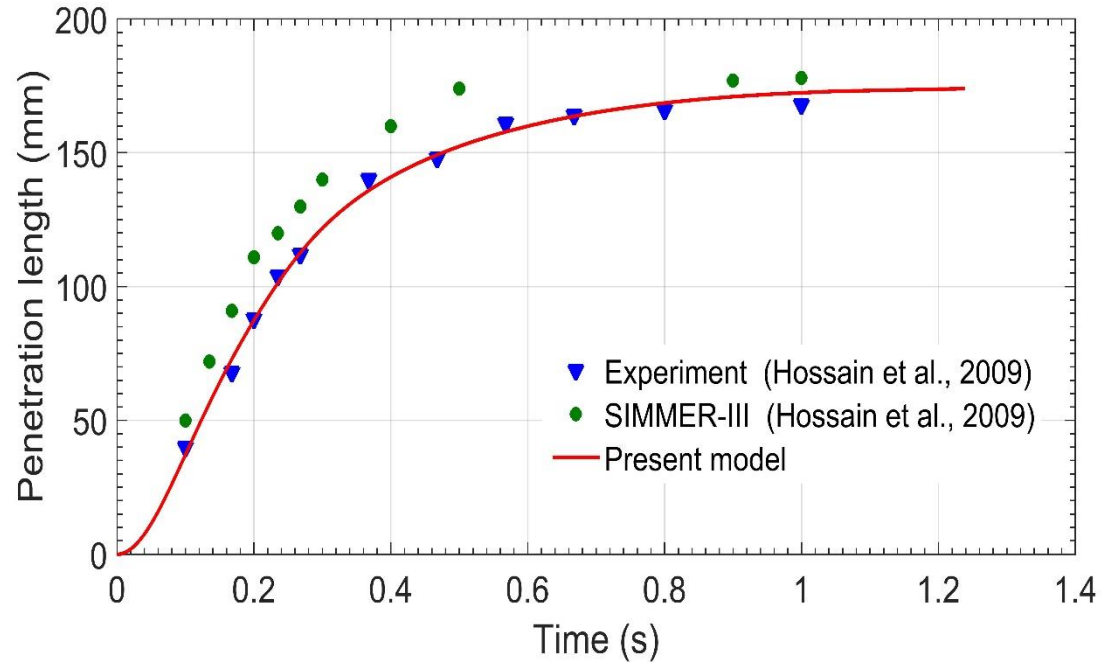

Fig. 4.3: Transient penetration length of molten metal (melt mass: 215g, melt temperature: 130°C, pin temperature: 25°C)

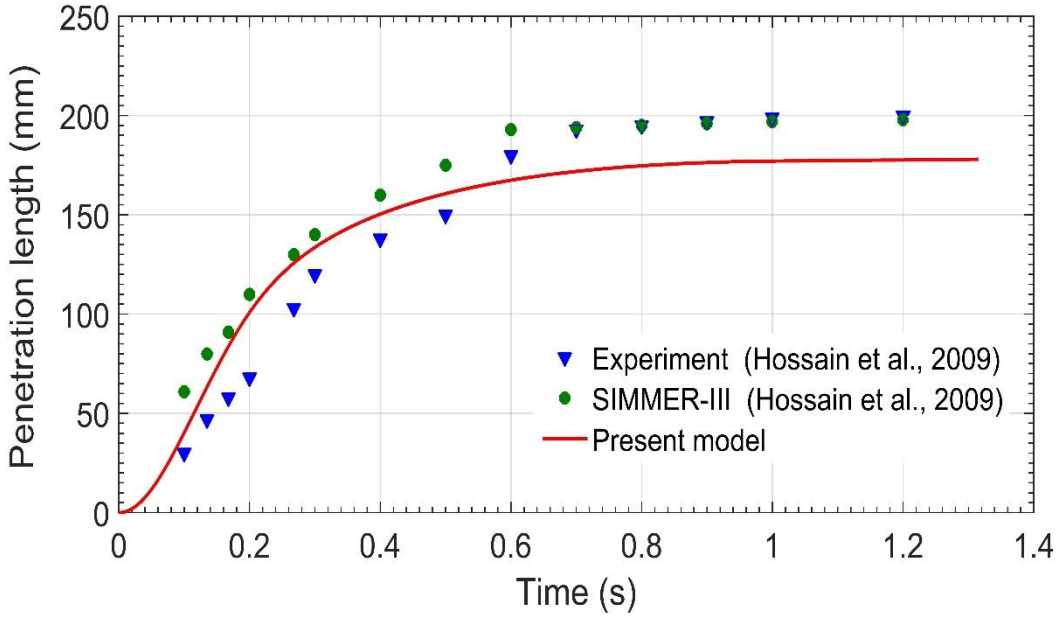

Fig. 4.4: Transient penetration length of molten metal (melt mass: 325g, melt temperature: 100°C, pin temperature: 25°C)

The predicted advancements of the molten metal in the pin bundle corresponding to the respective experimental condition are presented in Figs. 4.2 - 4.4. It is noticed that the molten metal freezes quickly owing to high heat transfer from molten metal to the colder pin channel. As a result, the enthalpy of the streaming melt decreases and a plug forms with the loss of latent heat of fusion. The movement is heavily ceased due to a marked increase in the effective viscosity of the molten metal under freezing. The present simulation results are similar to those observed in the experiment and reported results from SIMMER-III code with a relative error in the range of 3% - 18%, demonstrating the acceptability of the present model. The error was found to be low for low melt mass and high for the large melt mass. However, the simulation results are sensitive to the selection of parameters of the particle viscosity model (Ref. Eq. (3.5)) which, determines the effective viscosity of the melt owing to

particle formation. Towards this, a sensitivity analysis is performed to investigate the influence of parameters on the simulation results and discussed in the next section.

4.3 SENSITIVITY ANALYSIS

In order to consider the effect of solid particles on the melt flow, a particle viscosity model (Ref. Section 3.2.1) is incorporated in the present model. As per this model, the effective viscosity of molten metal owing to particle formation is calculated applying Eq. (3.5) as:

$$\mu_{eff} = \mu_l \left\{ \frac{\alpha_l}{\alpha_l + \alpha_p} + \frac{f\,\alpha_{MP}\,\alpha_p}{\alpha_{MP}\left(\alpha_l + \alpha_p\right) - \alpha_p} \right\}$$

where α_{MP} is the maximum volume fraction of solid particles and f is the model parameter. In the present modelling, we have considered parameter values: f = 8.0 and α_{MP} = 0.62 to realize the smooth change of effective viscosity over the wide range of particle volume fraction and gain a better approximation of present model with that of the experiment.

The selection of α_{MP} is derived from the shear viscosity formulation proposed by Russel (1983). Russel has made a comprehensive report related to the rheology of colloidal suspensions and suggested the maximum fraction of the suspended solid particles is ~ 62%.

The value of model parameter (f) was initially taken as 5 from the SIMMER-III code study. Later on, the influence of f on the simulation result is investigated w.r.t the experimental values. After successive refinements, the value of f is corrected and with f = 8, we have obtained a good match of the present model result

with that of experimental value, which is apparent from Figs. 4.5 - 4.7. These plots explicitly depict the influence of *f* on the simulation results and form the basis for the selection of the value of model parameter (*f*).

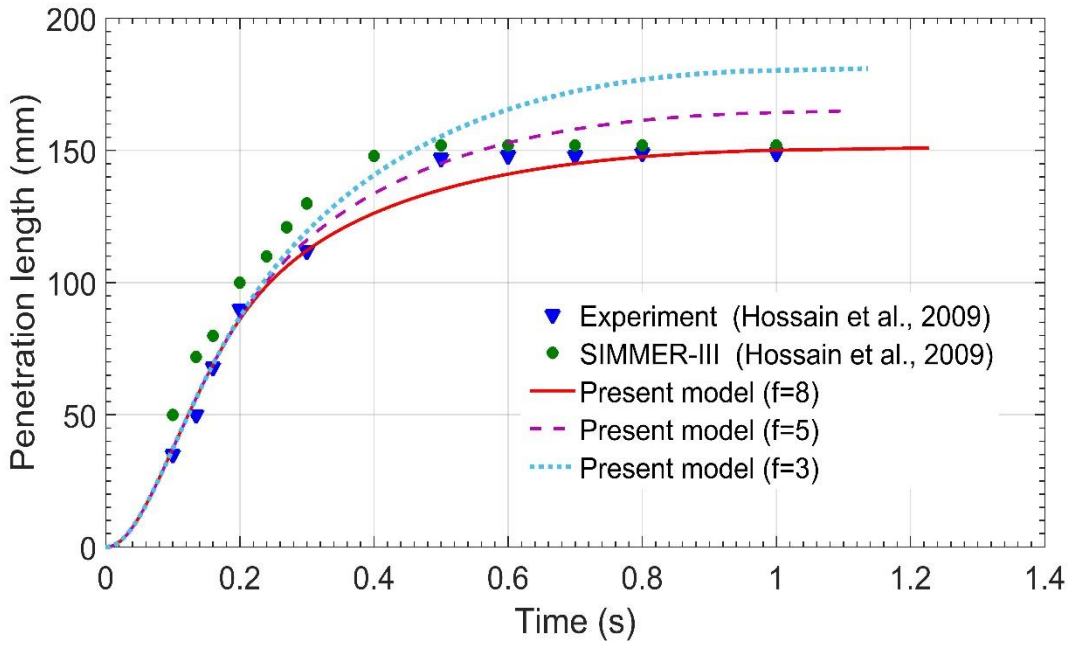

Fig. 4.5: Sensitivity analysis of model parameter (*f*) for experimental condition (melt mass: 215g, melt temperature: 100°C, pin temperature: 25°C) simulation

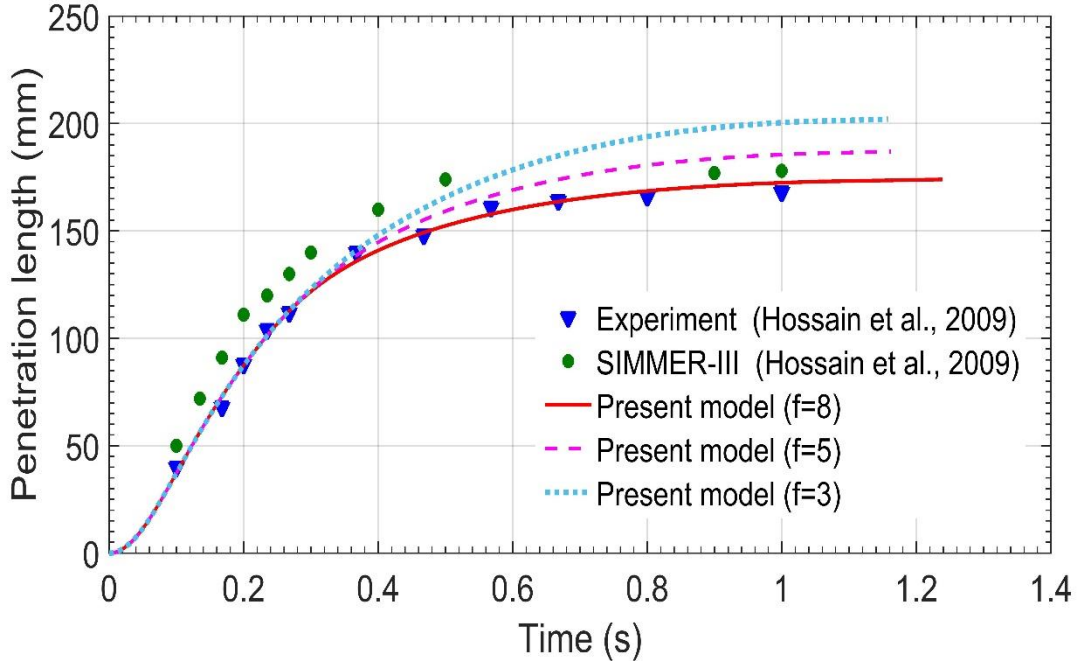

Fig. 4.6: Sensitivity analysis of model parameter (*f*) for experimental condition (melt mass: 215g, melt temperature: 130°C, pin temperature: 25°C) simulation

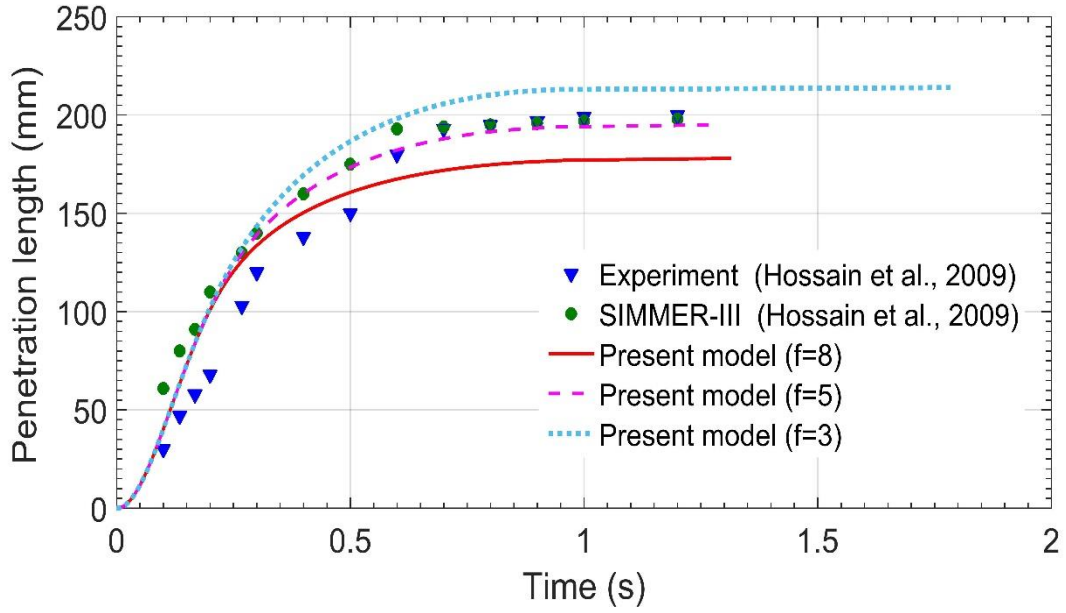

Fig. 4.7: Sensitivity analysis of model parameter (f) for experimental condition (melt mass: 325g, melt temperature: 100°C, pin temperature: 25°C) simulation

4.4 CLOSURE

Through the validation study, it is found that there is a good agreement between the results predicted by the model and the experimental data. Further, the simulation results produced similar trends of penetration length as those observed in SIMMER-III code. The validation study evidently demonstrates the acceptability of the present model.

CHAPTER 5

Simulation of Molten Fuel Drainage from a Prototype Fuel Subassembly

5.1 INTRODUCTION

Following the successful demonstration of acceptability of the present mathematical model, it is applied to analyze the streaming, freezing, and blocking phenomena of the molten fuel in the subchannels of a blocked fuel SA. The detailed simulation of molten fuel drainage in a prototype fuel SA is covered and reviewed in this chapter. Further, a parametric study is carried out to investigate the importance of core design, especially the length and diameter of the coolant subchannels below the core on the fuel drainage phenomena. The results of the parametric study are discussed in this chapter.

5.2 GEOMETRIC DETAILS OF FUEL SUBASSEMBLY

The dimensional details of a prototype SFR fuel SA considered for the present study are enlisted in Table 5.1.

Table 5.1

Geometric details of the prototype fuel subassembly.

Parameter		**Value**
Number of fuel pins		217
Pin pitch type		Triangular
Pin pitch (***P***)		8.28 mm
Fuel pellet	Inner diameter	1.8 mm
	Outer diameter	5.55 mm
Clad	Inner diameter (***d_{ic}***)	5.7 mm
	Outer diameter (***d_{oc}***)	6.6 mm
Blanket diameter (***d_b***)		5.55 mm
Wire diameter		1.65 mm
Wire helical pitch (***H***)		200 mm
Hexcan inner side face length		72 mm
Hexcan thickness		3.4 mm
Hydraulic diameter		3.686 mm
Active core height		1000 mm
Length of bottom blanket		300 mm
Distance from active core to bottom plug of pin		1050 mm

5.3 MOLTEN FUEL DRAINAGE SIMULATION

Initially, a heat generating melt pool is located at the top of the lower blanket region after the complete meltdown of fuel region of the blocked SA. The initial conditions taken for the investigation are summarized in Table 5.2. The control volume size (Δz) and time step size (Δt) considered for the investigation in the problem domain are 1mm and 0.0001s respectively.

Table 5.2

Initial conditions taken for simulation study.

Parameter	Value
Molten fuel mass (kg)	51.53
Molten fuel temperature (K)	3120
Clad temperature (K)	673
Blanket temperature (K)	673
Specific decay heat generation rate (MWt/kg)	0.16

From the simulation result, it is observed that the molten fuel slumps down under gravity from the melt pool. It has to pass the long narrow passages available in between the pins to reach the bottom of the fuel subassembly. Since the pins are tightly packed in a prototype subassembly (SA) with a hydraulic diameter of about 3.686 mm, the fuel descends slowly through the SA. The velocity profile of the molten fuel while moving along the subchannel is indicated in Fig. 5.1. It is observed that there is a gain in velocity by the penetrating molten fuel during its motion. During the travel, the molten fuel shares a bulk amount of its latent heat with the cold clad due to very high convective heat transfer coefficient (h) value of the order of ~12000 W/m^2-K. As a

result, the molten fuel starts freezing forming solid particles. These solid particles significantly influence the streaming behaviour of the molten fuel by effectively increasing the fluid viscosity, which is determined using the particle viscosity model (Eq. 3.5). The increment in fluid viscosity prompts the molten fuel to decelerate in the flow path, resulting in a decline in the rate of increase in velocity as represented in Fig. 5.2. Thus, by the time it reaches the lower section of the subchannel the molten fuel losses a significant amount of energy, resulting in a more rapid rate of solidification. Subsequently, the mobility of the molten fuel heavily ceases to freeze formation due to a sharp rise in fluid viscosity. It is observed that the melt front freezes in the flow channel after penetrating a distance of ~ 85 mm within ~ 0.134 s from Fig. 5.3.

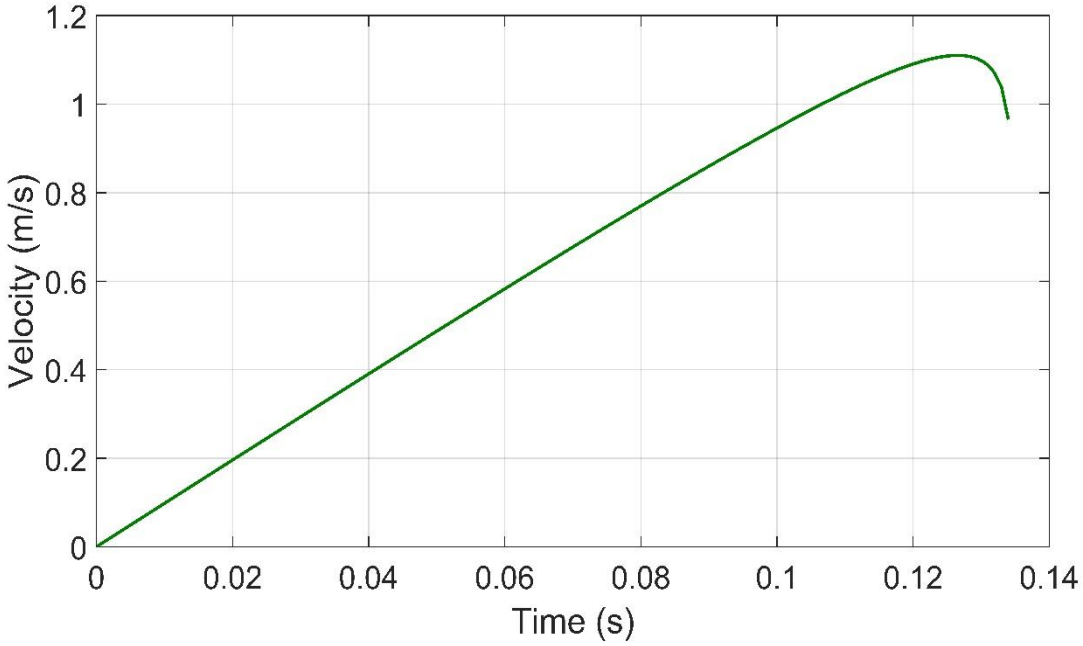

Fig. 5.1: Instantaneous velocity of the streaming molten fuel in subchannel.

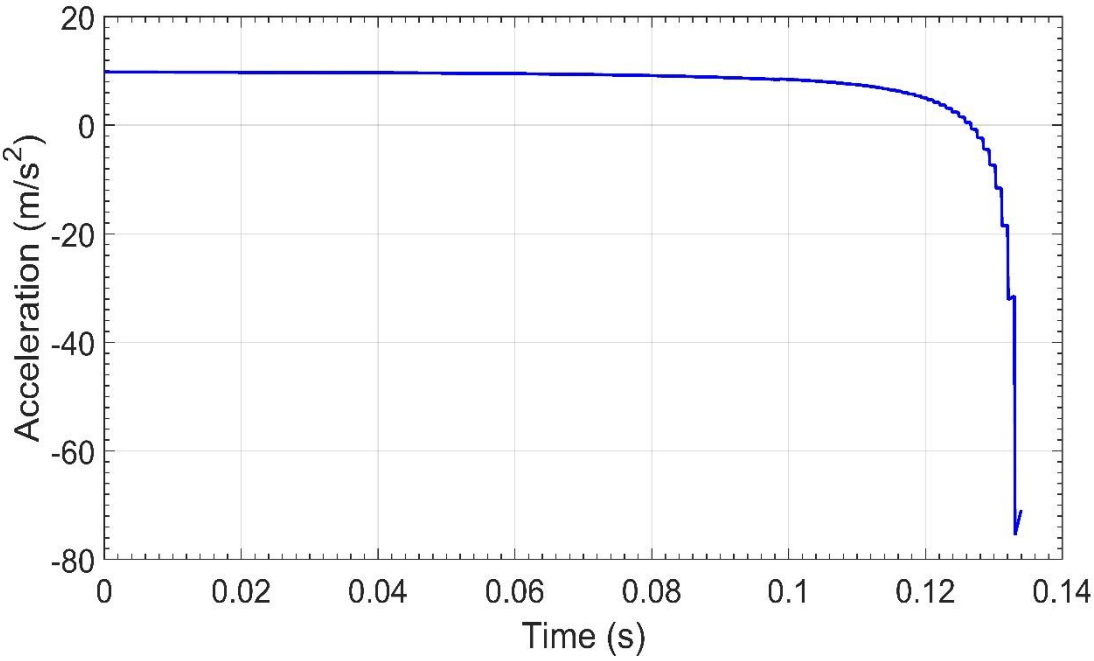

Fig. 5.2: Acceleration profile of the molten fuel.

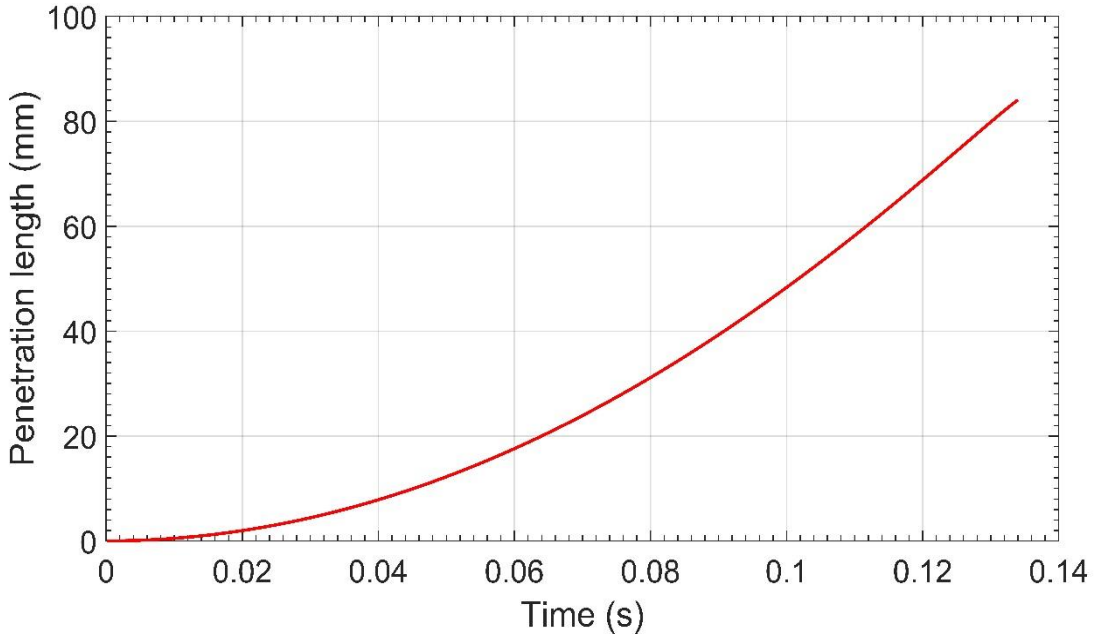

Fig. 5.3: Instantaneous position of draining melt front inside a SFR fuel SA during TIB.

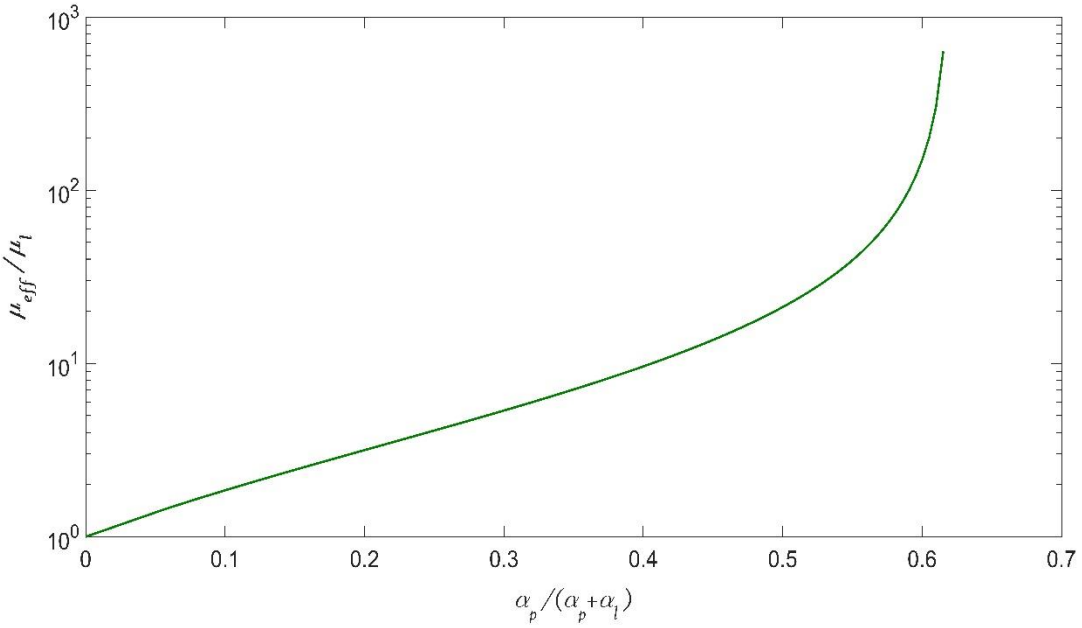

Fig. 5.4: Increase of molten fuel viscosity due to formation of solid particles.

Figure 5.4 illustrates the effective viscosity of the molten fuel in the flow path obtained from the simulation. The semi-log plot delineates the rise in the fluid viscosity due to the existence of solid particles. During penetration, the fuel dissipates a large amount of heat to the colder surrounding structure, increasing the solid fraction. When the solid volume fraction exceeds 62%, there is a sudden rise in the viscosity value. As a result, the movement of the fuel is completely arrested, it eventually freezes due to blockage formation at the leading edge. This particular characteristic of the molten fuel is attributed to the particle viscosity model adopted in the present work.

Figure 5.5 depicts the solidification of the streaming fuel, initially at the fusion temperature, in the fuel pin bundle as a function of time. The staircase shape profile appears due to the application of variable grid system to solve the phase change problem in the present work. The initial step size is a little larger since the molten fuel starts streaming down from rest and to achieve a velocity, it requires some fraction of seconds. The time step size is gradually decreasing later on as the molten fuel starts moving at

higher speed. The step size is proportional to the heat exchange between molten fuel and clad, subsequently related to the solidification rate. Therefore, a higher jump in solidification is observed at the beginning (~ 6 %). Since the melt front always encounters the fresh clad which are at a lower temperature (~ 673 K) during the motion, the melt front freezes first, thus blocking the fuel escape path. The blockage is formed when the solid fraction exceeds roughly 62%. Therefore, it is essential to keep a record of solidification behaviour of the melt front.

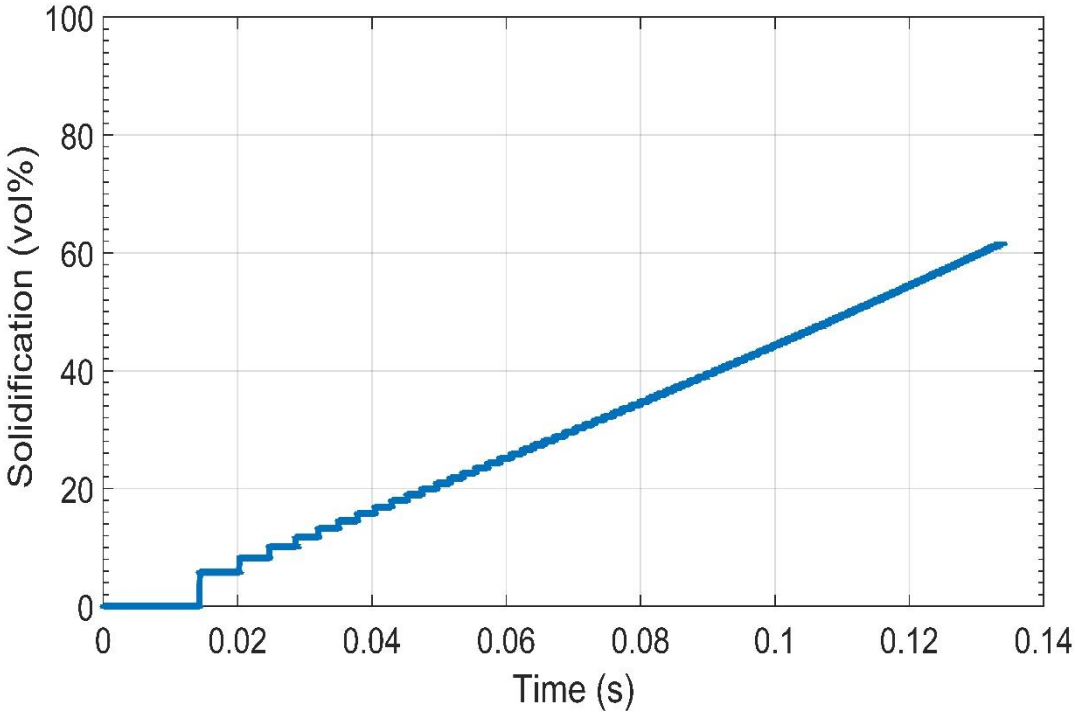

Fig. 5.5: Solidification of the melt front.

The neutronics behaviour of an SFR core following TIB accident mainly depends on the amount of molten material that gets relocated out of the core region. From the simulation result, it is noticed that ~ 8% (amounting to 4 kg) of the total molten fuel mass is migrated from the active core. The molten mass relocated as a function of

time is represented in Figure 5.6. The assessment of remaining fuel inventory in the core assists in determining the reactor kinetic characteristics and reactivity of the core.

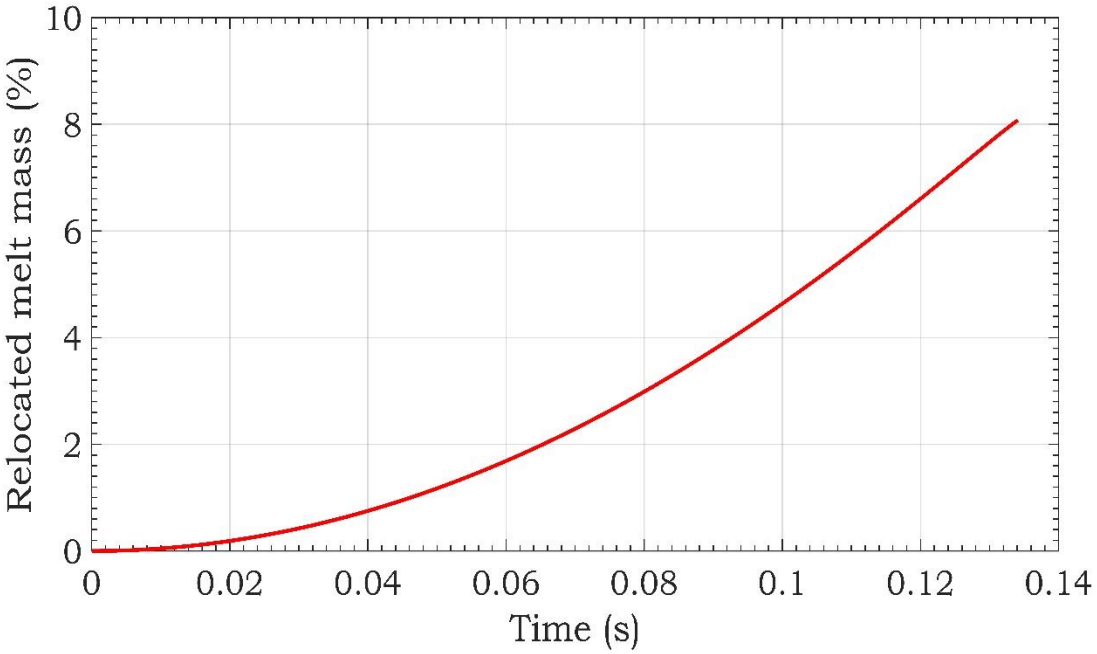

Fig 5.6: Molten fuel mass relocated out of active core.

5.3.1 Thermal Behaviour of Associated Structural Elements

Another important aspect of material motion is to assess the physical states of the surrounding structures. During steaming down, the molten fuel comes across several structural elements viz. clad and blanket in the flow path. In the preceding section, we have discussed the access timing and capacity of the escape path (subchannels). It is observed that the molten fuel is in a position to cover a distance of ~ 85 mm within ~ 0.134 s in the subchannels before freezing. The melt was unable to pass through the lower blanket zone, having a length of 300 mm. During motion, the melt exchanges heat with the clad, subsequently, energy exchange takes place between clad and blanket through the Helium-filled gap. The temperature profile of the molten fuel after freezing in the flow path is indicated in Figure 5.7. Since the molten fuel losses its latent heat

during migration, a significant amount of molten fuel remains in the two-phase region (mushy state) while rest (lying ~18 mm from the bottom of the pool) became superheated liquid due to the heat carried away by it from the melt pool. The peak temperature of the molten fuel recorded is ~ 3150 K, and that fuel control volume lies just next to the pool.

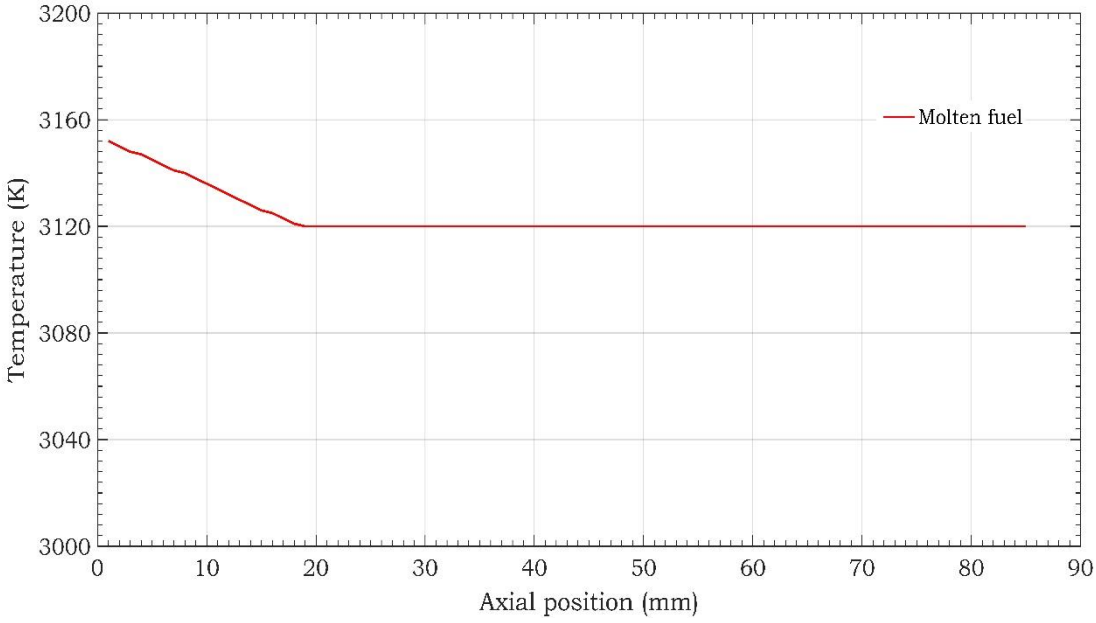

Fig. 5.7: Temperature profile of molten fuel (Axial position is from bottom of pool)

The temperature evolution of the clad during migration is depicted in Figure 5.8. It is found that the clad control volume adjacent to the melt pool gets melted, but the clad away from the pool remains in its physical state with temperature decreasing along the downstream direction. Since molten fuel and cladding steel are immiscible and due to unavailability of space, the molten clad will remain at its location.

Similarly, the temperature evolution of the blanket during penetration is displayed in Figure 5.9. The peak temperature of blanket is ~ 1085 K and it occurs at the blanket portion adjoining the pool. The temperature of the blanket is decreasing

along the flow direction, like cladding. All the parts of the blanket remain in the solid state.

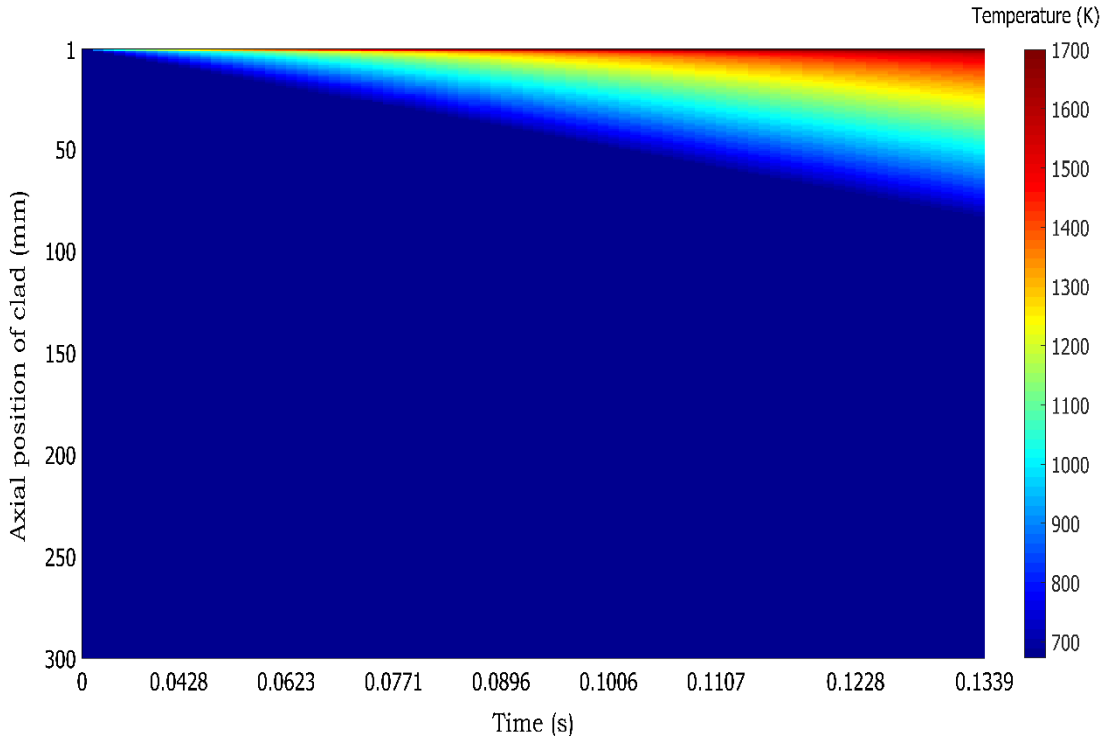

Fig. 5.8: Temperature evolution of clad during relocation (Axial position measured from bottom of pool).

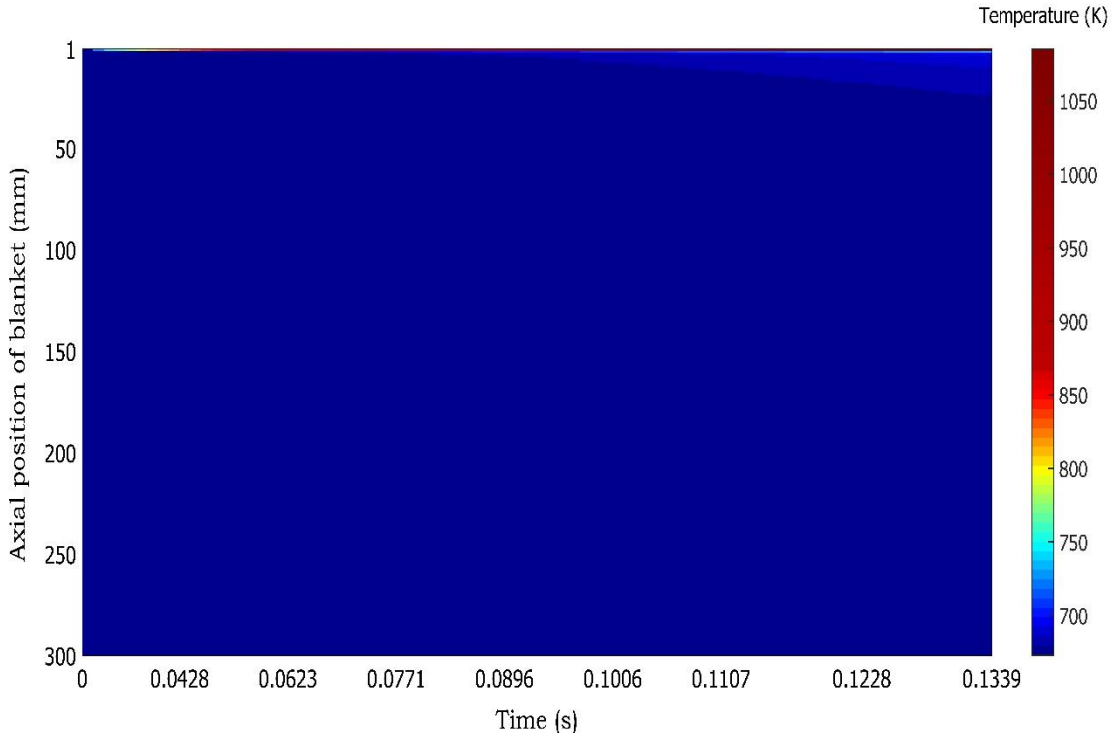

Fig. 5.9: Temperature evolution of blanket during relocation (Axial position measured from bottom of pool).

5.3.2 Rest Position Analysis

During relocation, the molten fuel freezes rapidly and subsequently forms a blockage at the melt front. The leading edge of the melt is a frozen crest. Therefore, the molten fuel is trapped in the subchannels by the strong mechanical surroundings and blockage formed by frozen fuel (Fig. 5.10). For the detailed investigation of this scenario, a rest position analysis is carried out employing the heat transfer model with suitable modifications. The rest position analysis is performed for a transient time up to 2 minutes with a step size of 0.001s.

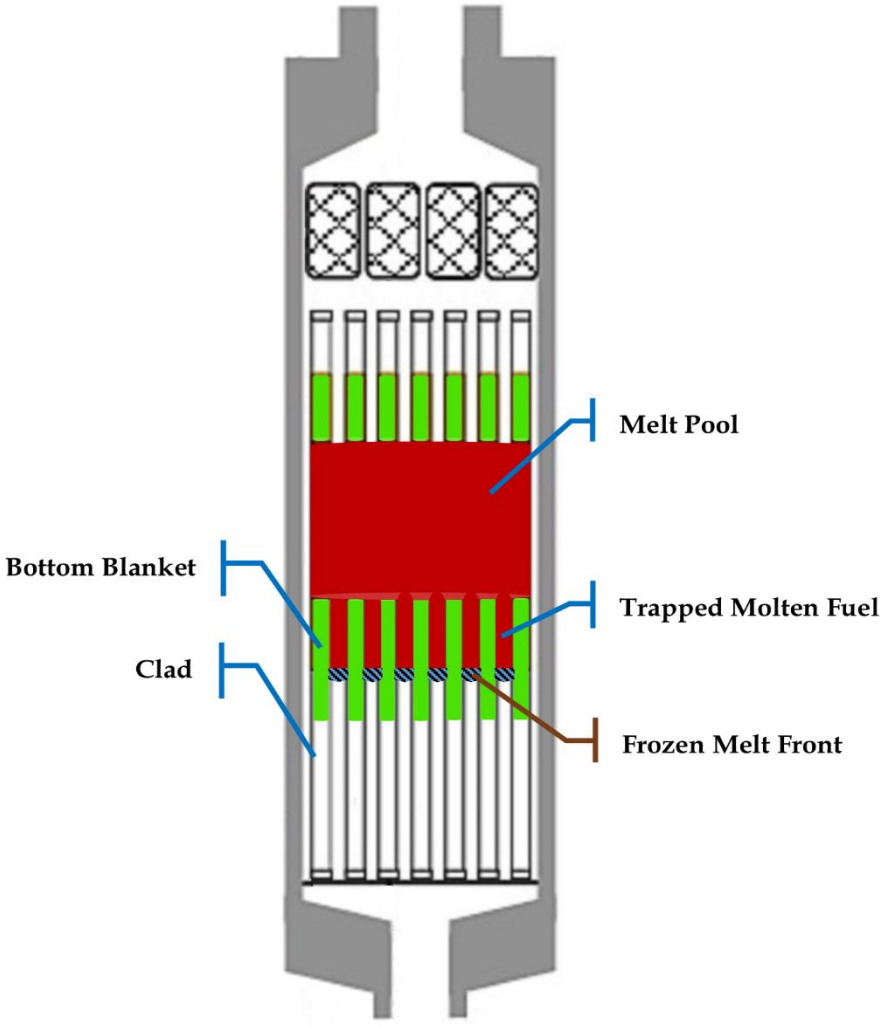

Fig. 5.10: Schematic of trapped molten fuel in pin channel.

Axial position: 10 mm

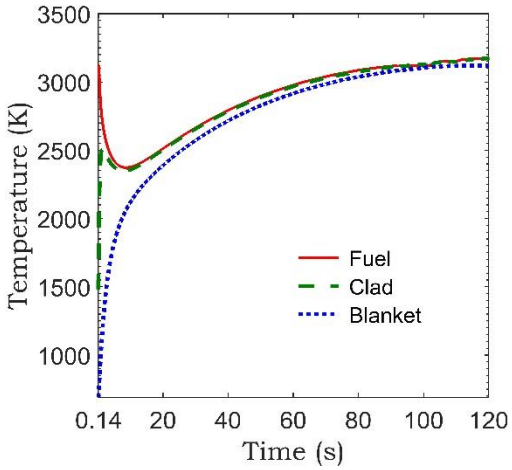

Axial position: 20 mm

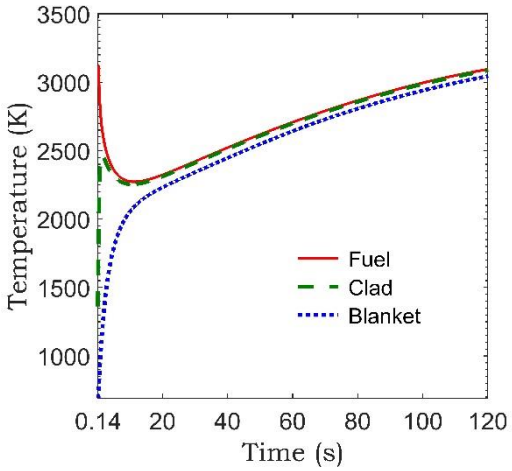

Axial position: 40 mm

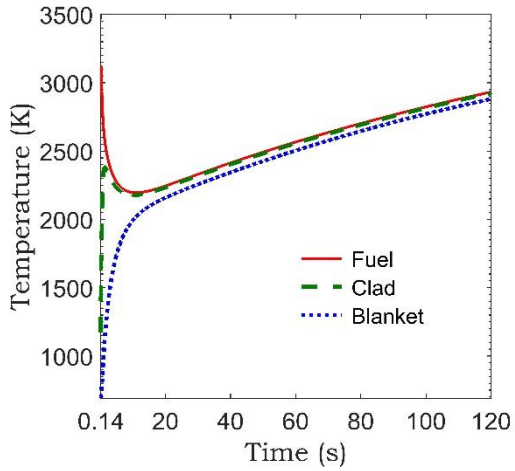

Axial position: 60 mm

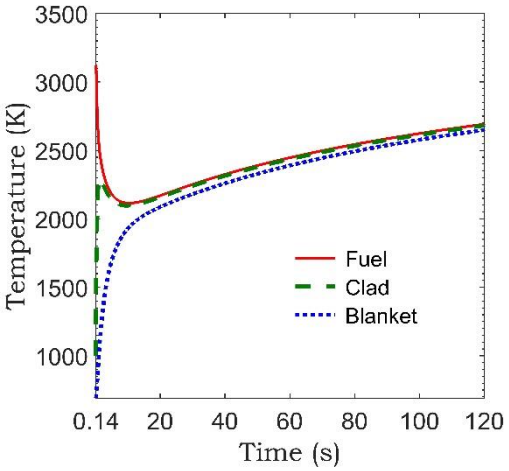

Axial position: 75 mm

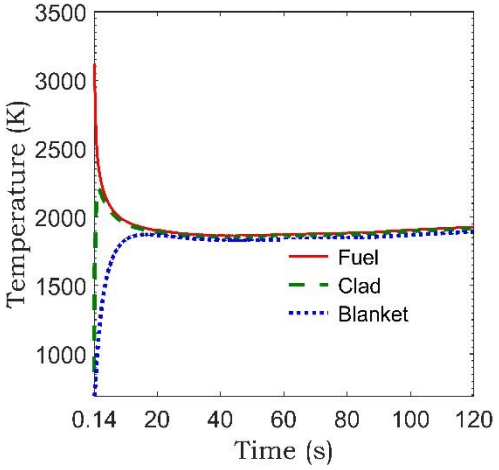

Axial position: 85 mm

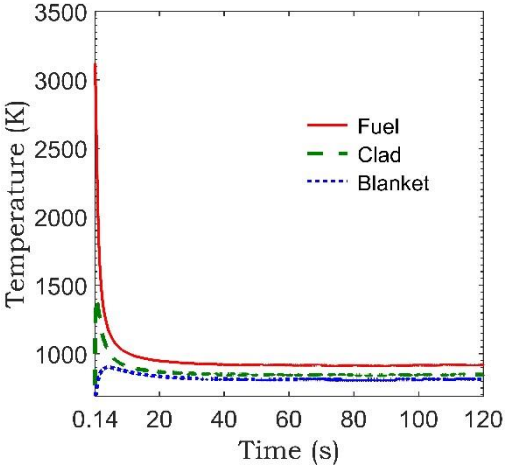

Fig. 5.11: Temperature distributions of fuel, clad, and blanket at various axial positions from bottom of pool.

It is strongly perceived from the simulation results plotted in Fig. 5.11 that after the fuel being trapped in the subchannels due to blockage, the confined molten fuel comes into thermal equilibrium with the surrounding structures within 20 s. Besides that, there is a gradual rise in temperatures of fuel, clad, and blanket control volumes located in between 3/4 th portion of the total penetrating length, i.e. ~ 65 mm from the bottom of pool after achieving the thermal equilibrium. The possible reasons for the gradual rise in temperature are decay heat generated in the molten fuel and axial heat conducted from the pool and other higher temperature sections to colder sections. But, a quite distinct characteristic is noticed at the bottom portion. The frozen melt front is unable to remelt again; instead it forms a firm blockage towards the bottom end, leaving no available space for molten fuel and structural material to escape out in the axial direction. Subsequently, these molten materials find other available path attacking the structures radially, resulting in rupture of wrapper wall.

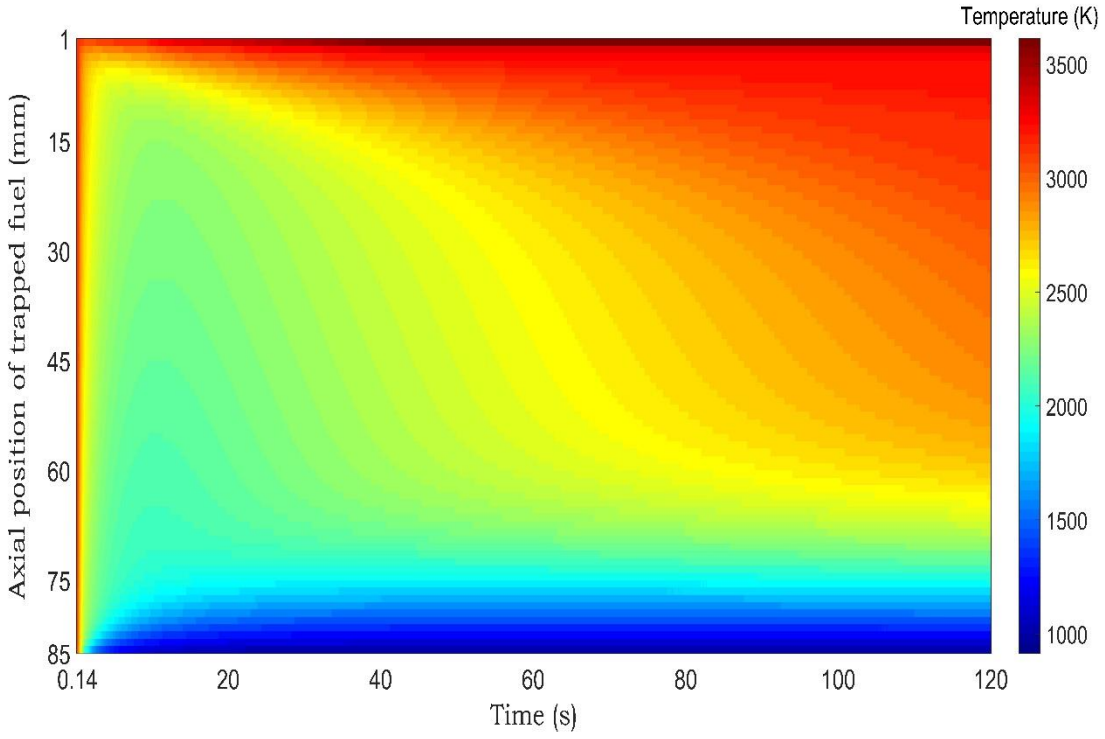

Fig. 5.12: Temperature evolution of molten fuel at rest.

The temperature evolution of fuel column located in between the melt pool and frozen plug is shown in Fig. 5.12. Initially, there is a drop in temperature value for the entire fuel column except those adjacent to the pool. This is because of the imbalance between heat generation and heat removal. Since the pool is at a higher temperature, there is a rise in temperature of fuel control volumes adjoining it. The thermal equilibrium prevails within ~20s. Due to the volumetric heat generation, a continuous increase in temperature is noticed after achieving the thermal equilibrium. A tight blockage appears to build up towards the bottom end. The possible reason can be stated as: the energy content of the molten fuel at the bottom portion is significantly lower than that of the top part owing to continual interactions of the leading edge of the molten fuel with the colder structures on the way during streaming. As a result, the thermal equilibrium attained in this portion is at a much lower temperature than that of top portion. Subsequently, the successive heat addition due to heat generation is not adequate to remelt the frozen plug, resulting in augmentation of blockage at the bottom end.

The temperature evolution of clad follows a similar trend as that of molten fuel and represented in Fig. 5.13. The temperature of the cladding continuously increases during the event progression. Most portions of the cladding got melted in the course of event progression. However, the bottom portion of the cladding remains in its physical state, imparting a strong mechanical surrounding to the frozen plug. This facilitates favourable aid for the tight blockage of the relocation path in the axial direction.

Figure 5.14 describes the temperature evolution history of the blanket during the event progression. The temperature rise in the blanket component is moderate unlike cladding owing to the presence of a Helium gas layer in between the clad and blanket.

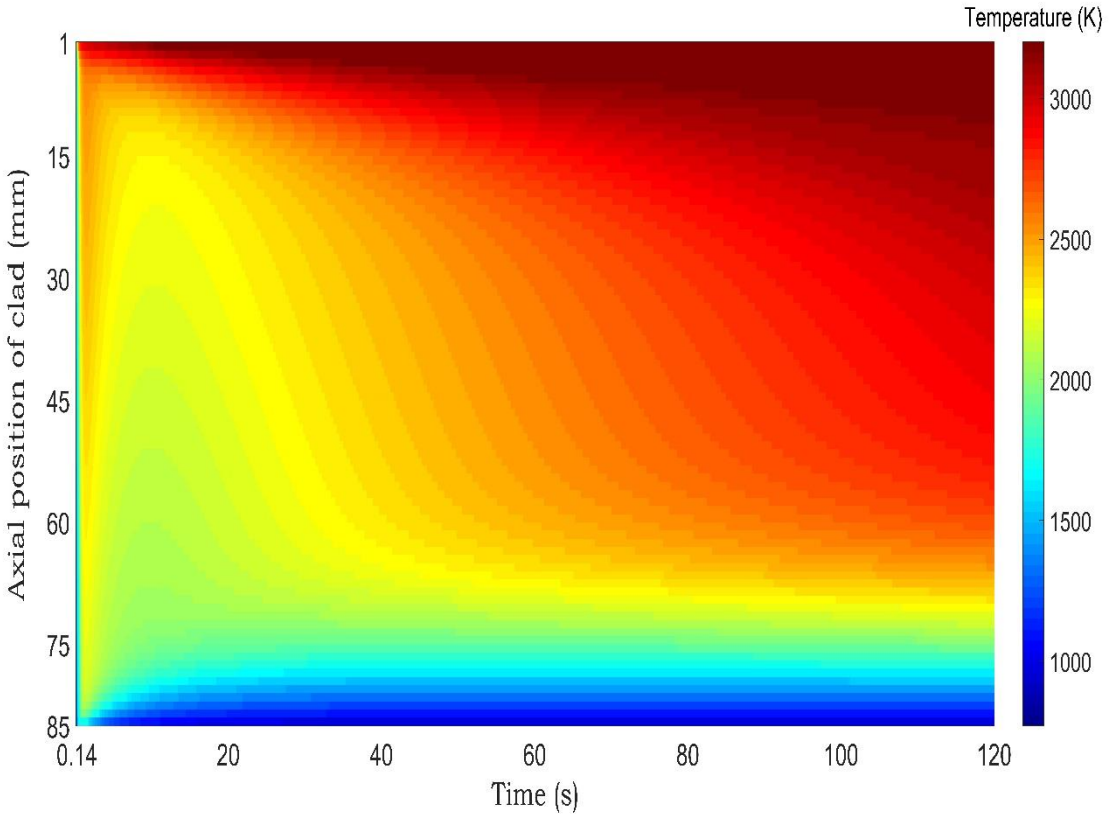

Fig. 5.13: Temperature evolution of clad.

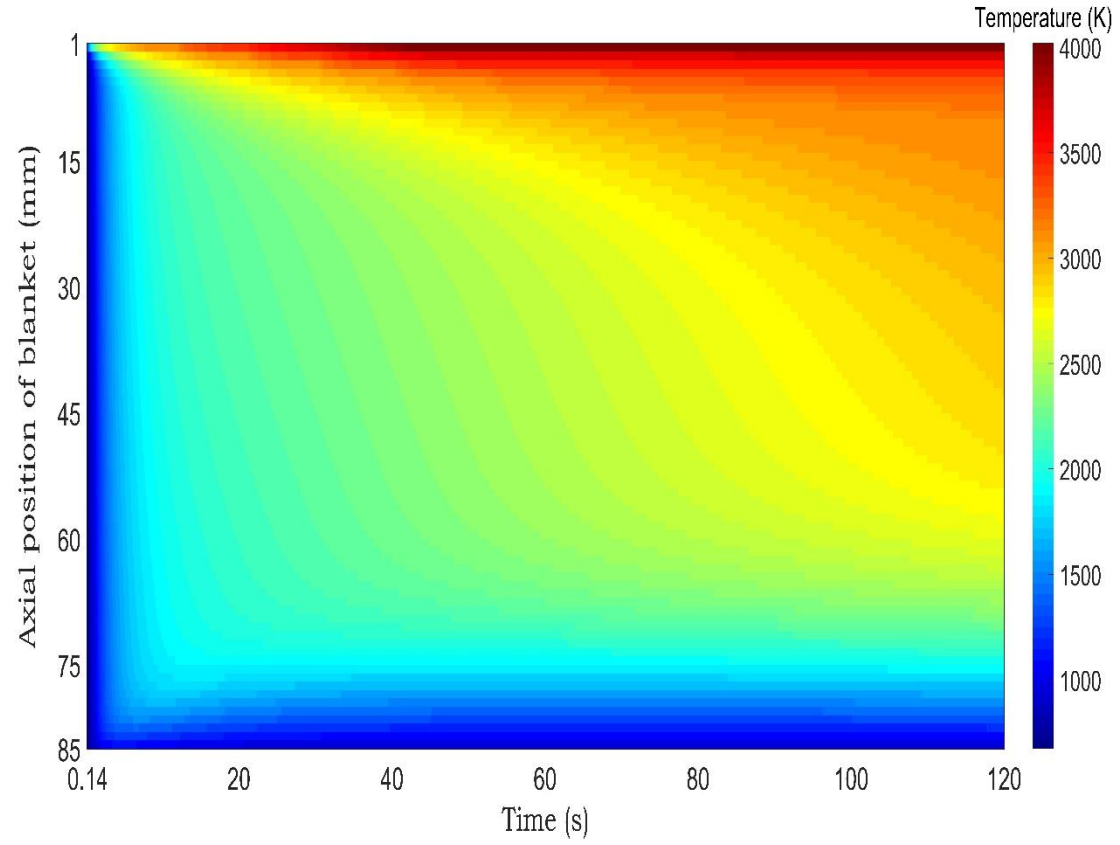

Fig. 5.14: Temperature evolution of blanket.

Hence, only a small portion of the blanket near to pool got melted, but the rest parts remain in its physical state, which is evident from the Fig. 5.14.

5.4 PARAMETRIC ANALYSIS

The simulation result describes that the molten fuel is unable to cross the lower blanket zone (~300 mm) of the blocked fuel SA following a severe accident. From the rest position analysis, it is obtained that the frozen melt front is unable to remelt, instead forms a firm blockage. Consequently, the trapped molten fuel attacks structures in the radial direction, resulting ablation of the hexcan wall and release of fissile inventory. To prevent the release of molten fuel out of the wrapper and to retain the integrity of SA, it is essential to relocate the molten fuel to the core catcher before it freezes. Towards this, it is necessary to investigate the influence of critical parameters on the melt relocation and freezing characteristics. The parameters chosen for the study are the number of pins, the decay heat power, blanket pellets, and the pin dimensions.

5.4.1 Effect of Number of Fuel Pins

The influence of number of fuel pins in a SA on the melt streaming is discussed in this section. Simulation of melt penetration and freezing is carried out for different pin bundles by varying the number of pins in a pin bundle while retaining the dimensions and geometry of the fuel pins as that of the reactor case study (Ref. Table 5.1). The predicted advancement of the molten fuel in all the cases are approximately identical. This is because the flow parameters viz. hydraulic diameter, Reynolds number etc. of the pin bundles remain preserved even after altering the number of pins in a SA. The results of the parametric study are briefly summarized in Table 5.3.

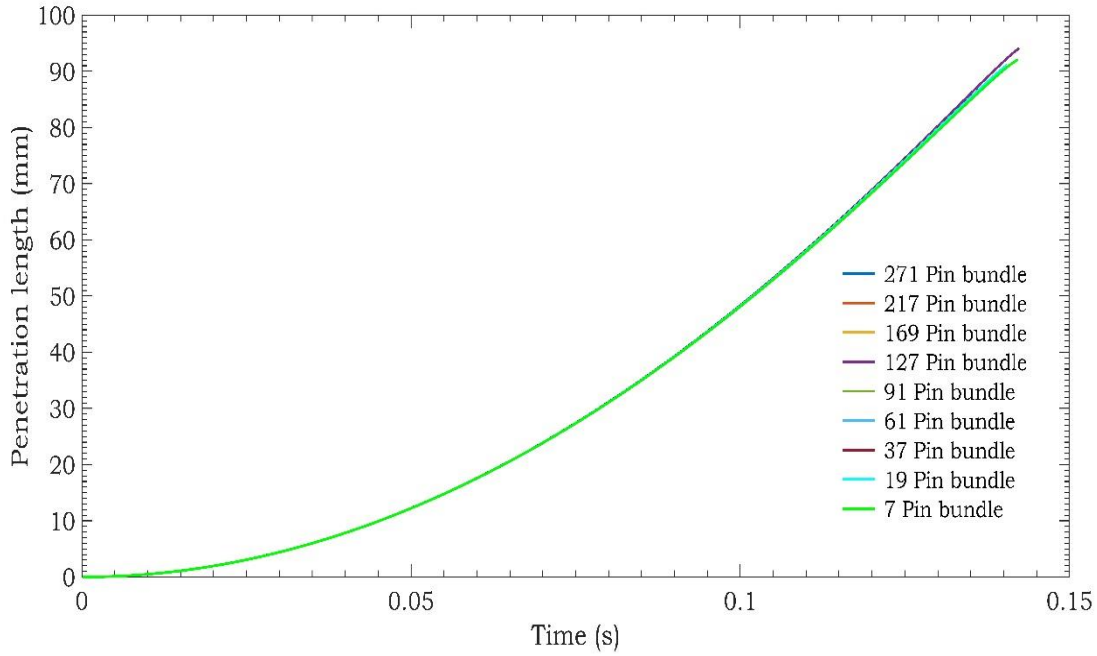

Fig. 5.15: Melt advancement in different pin bundles.

Table 5.3

Comparison of results of pin bundle parametric study.

Total no. of pins	Hydraulic diameter (mm)	Penetration length (mm)	Plugging time (s)
7	3.88	92.09	0.1422
19	3.85	91.10	0.1405
`37	3.80	89.11	0.1386
61	3.70	88.11	0.1378
91	3.74	87.09	0.1370
127	3.89	94.13	0.1424
169	3.67	85.15	0.1351
217	3.69	84.19	0.1341
271	3.67	84.10	0.1342

In general, it is derived from the present investigation that the molten fuel relocation and freezing are roughly independent of the number of pins in a fuel SA.

5.4.2 Effect of Decay Heat Power

The molten fuel relocates through the subchannels carrying the latent heat and decay power solely. During streaming, it exchanges a maximum portion of its energy with the surrounding structures, resulting in the freezing of the melt. The point of interest particularly lies with the share of decay heat in that energy exchange during relocation. Therefore, the analysis of the effect of decay heat power on the molten fuel freezing is quite relevant in this aspect. Figure 5.16 illustrates the significance of decay power on the melt streaming behaviour. The obtained freezing length at different decay power level is detailed in Table 5.4. It is understood from the results that the share of transient decay power in energy exchanged between fuel and surrounding structures is

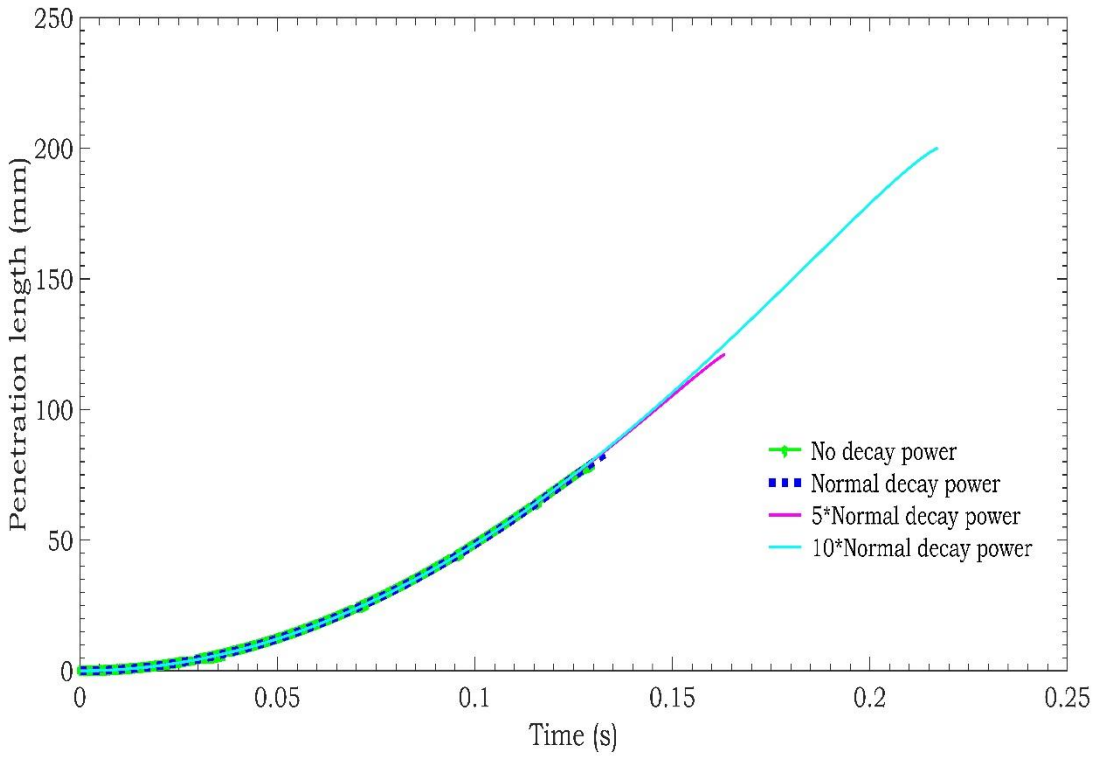

Fig. 5.16: Melt penetration for various decay power level.

small. So, the influence of decay power in melt penetration is minor until the decay power is raised tenfold. But, the tenfold increment or further rise in decay power level seems to be vague in the present reactor condition, and if possible, the desired penetration length (~1050 mm) may not be reached by the molten fuel before freezing. The probable reason for the minimal share of decay heat is due to the rapid freezing of the molten fuel with the loss of its latent heat. The heat generated during the transient period is much lower than that of heat exchanged to the surroundings, resulting in rapid freezing of melt. Therefore, the role of decay power in melt streaming is not that much influential. However, the influence of decay power holds significant during the transient analysis of trapped fuel following the formation of blockage.

Table 5.4

Transient study at various decay power level.

Parameter	Penetration length (mm)	Plugging time (s)
No decay power	78.04	0.1296
0.5 x Normal decay power	81.09	0.1316
0.8 x Normal decay power	83.11	0.1333
Normal decay power	84.19	0.1341
1.2 x Normal decay power	86.12	0.1359
1.5 x Normal decay power	88.15	0.1375
2 x Normal decay power	92.13	0.1408
3 x Normal decay power	101.1	0.1484
5 x Normal decay power	121.2	0.1633
8 x Normal decay power	163.1	0.1931
10 x Normal decay power	200.2	0.2172

5.4.3 Effect of Blanket Pellet

Fertile blanket pellets are kept inside cladding to yield fissile inventory. The molten fuel crosses the lower blanket zone of the SA during relocation. So, the presence of blanket may influence the freezing behaviour of the penetrating fuel and this needs to be investigated. This forms the basis of the present parametric study. The analysis result is depicted in Fig. 5.17. It is apprehended that the presence of blanket is not at all influencing the freezing characteristics of the molten fuel on account of existence of Helium gap existing between clad and blanket sections and very less available freezing time. Therefore, the blanket pellets are irrelevant particularly in the context of melt freezing behaviour.

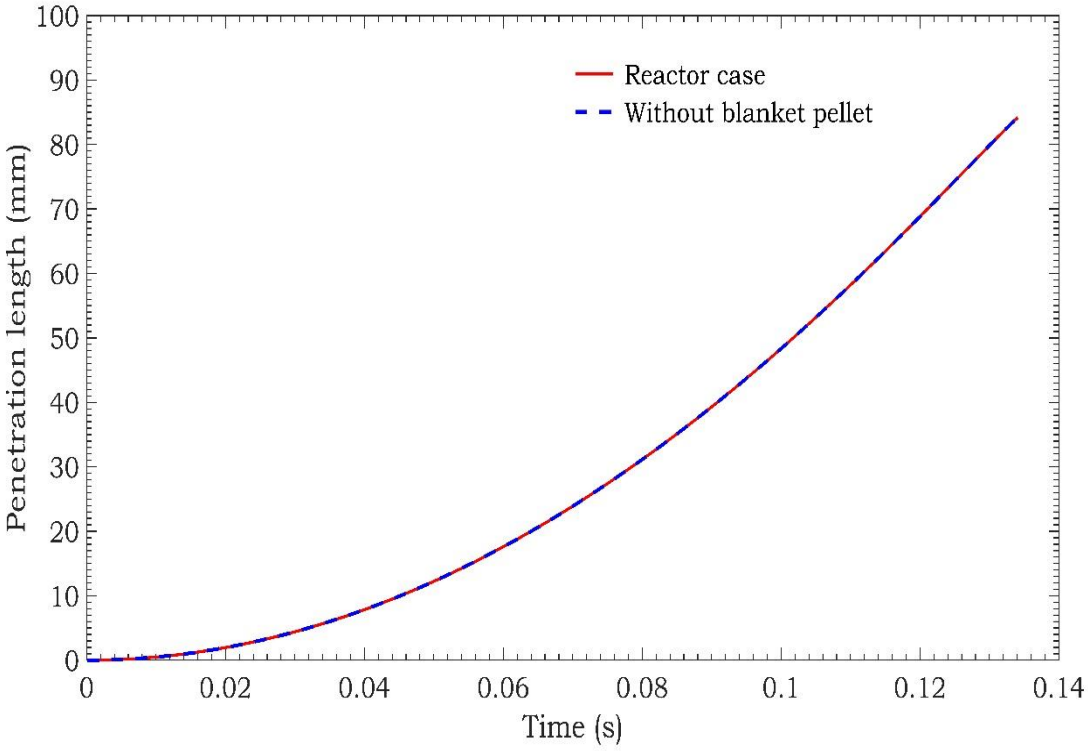

Fig. 5.17: Influence of blanket pellet on melt progression.

5.4.4 Effect of Pin Dimensions

A detailed study has been carried out to investigate the effect of fuel pin dimensions on the freezing characteristics. This is presumed to be one of the most important outlooks of the present work. Several cases have been investigated in this study by varying the dimensions of the pin. Some critical cases are highlighted, and the transient analysis results of a few specific cases are depicted in Fig. 5.18. The dimensional details of various cases are enlisted in Table 5.5. It is annotated that the structures dwindle in size retaining the thickness to prevent any irradiation exposure. The estimated melt progression in axial direction for the mentioned cases are indicated in Table 5.6. There is a pronounced enhancement in fuel relocation and delayed freezing by dwindling the size of the surrounding structures. The desired penetration length of melt (~1050 mm) is noticed from Case 3 afterwards.

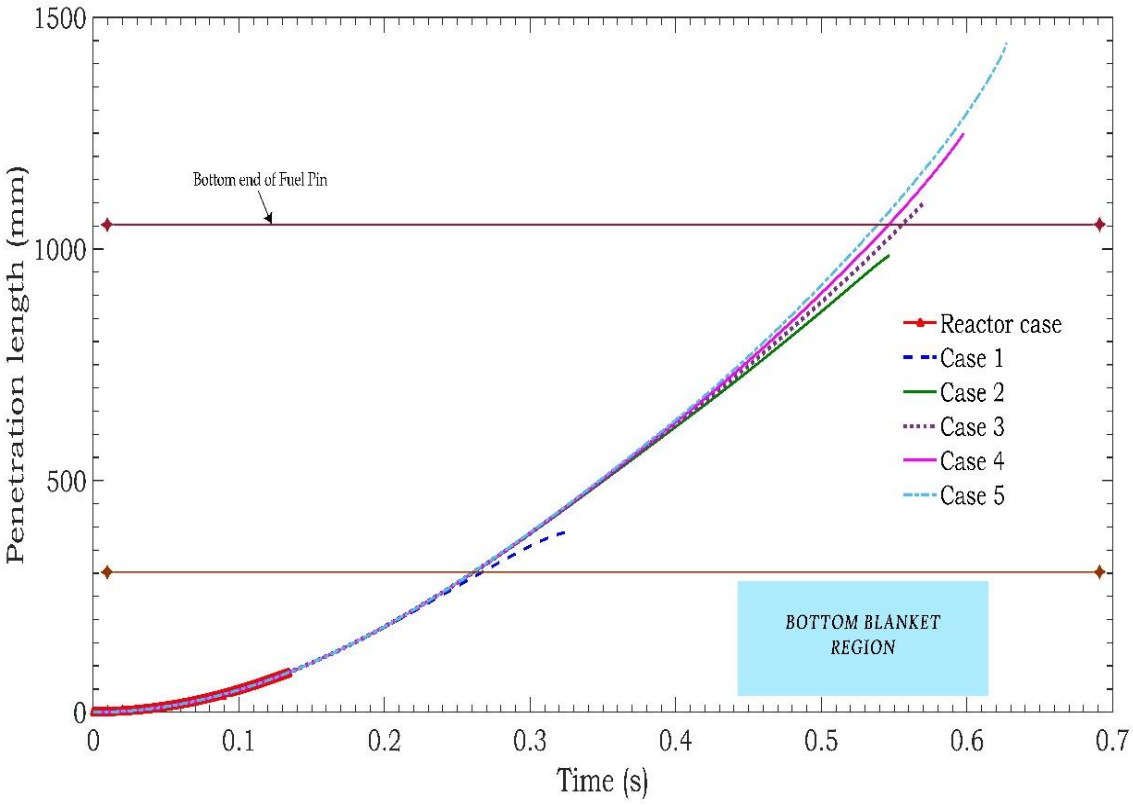

Fig. 5.18: Comparative analysis of melt progression for different pin dimensions.

Table 5.5

Geometrical details of pin for various case study.

Case No. / Characteristic		Reactor Case	Case 1	Case 2	Case 3	Case 4	Case 5
Clad	*Inner Diameter (mm)*	5.7	4.8	3.9	3.8	**3.7**	3.6
	Outer Diameter (mm)	6.6	5.7	4.8	4.7	**4.6**	4.5
Blanket Diameter (mm)		5.55	4.65	3.75	3.65	**3.55**	3.45
% Reduction from Reference Dimension		0	13	27	28	**30**	32

Table 5.6

Transient simulation results for various case study.

Case No.	Freezing length (mm)	Plugging time (s)
Reactor case	84.19	0.1341
Case 1	389	0.3203
Case 2	986	0.5461
Case 3	1102	0.5708
Case 4	**1250**	**0.5975**
Case 5	1444	0.6271

But, **Case 4** is considered as the **limiting case** since the melt is capable enough to traverse the entire length and arrive at the foot of the SA. In this case, whole molten fuel mass got penetrated out of the active core zone. Therefore, a reduction of 30% or above from the reference dimensions of surrounding structures will be favourable for the complete relocation of the molten fuel. Hence, it is strongly perceived that the blockage formation during relocation is dependent on the core design, especially the length and diameter of the pin channel below the core. However, the design modification ramifies the structural, hydraulic and neutronic behaviour of the core and requires further investigations.

5.5 MELT THROUGH OF SUBASSEMBLY FOOT

Parametric investigations have brought out the potential relation between melt relocation and core design. Further research of the limiting case (Case 4) in the foot section of the SA is carried out and briefly discussed in this section. The foot section of the SA is depicted in Fig. 5.19 (a). After crossing the entire length of pin, melt arrives at the foot. Finally, the melt extends throughout the foot and occupies the whole section as shown in Fig. 5.19 (b). From the geometric details of foot, the minimum thickness section is precisely located at the coolant entry slots and eventually evolved to be the weak section due to ease in melt out of this section. In the previous section, it is calculated that the melt took ~ 0.6 s to reach at the bottom of the SA, following the severe accident. Subsequently, the melt pool comes in contact with the entry slot section, which is the region of analysis in the present investigation. This leads to the onset of melt-foot interaction due to energy exchange between them. As a result, there is a sudden rise in temperature of the foot section (specifically the analysis region).

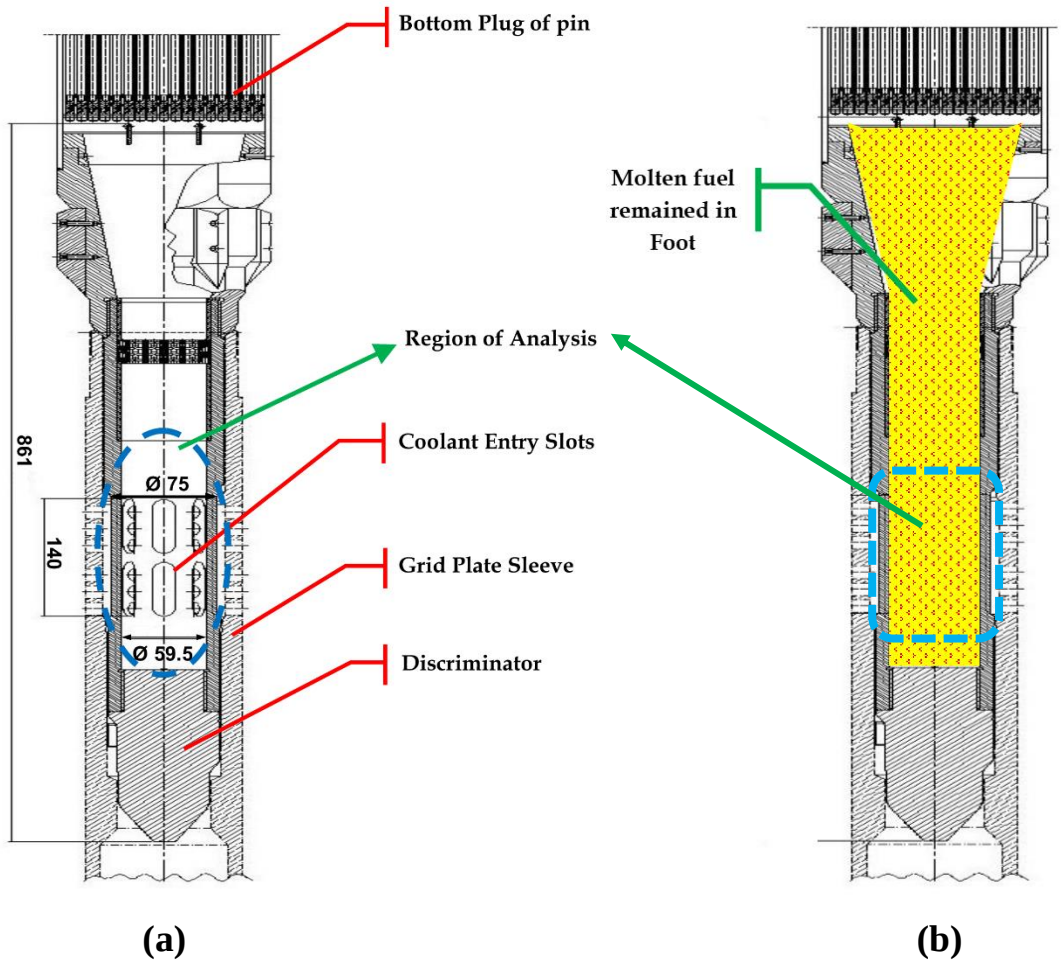

Fig. 5.19: (a) Details of foot zone and (b) Melt remained in the foot section.

At ~10s, the meltdown of foot section begins together with freezing of the melt-adhering to the inner side of foot as shown in Fig. 5.20a. Later on, there is progression in the melting of the foot section layer by layer from the inner side. In addition, there is solidification of molten fuel layer by layer co-occurring with the foot melt out. The complete meltdown of the foot section takes place within ~ 69s (see Fig. 5.20b). After melt out, the molten foot section drains away through the open passages. Meanwhile, a tough crust of frozen solid fuel is formed surrounding to the interior super-heated molten fuel. So, the molten fuel is confined inside the solid crust and unable to relocate for some time.

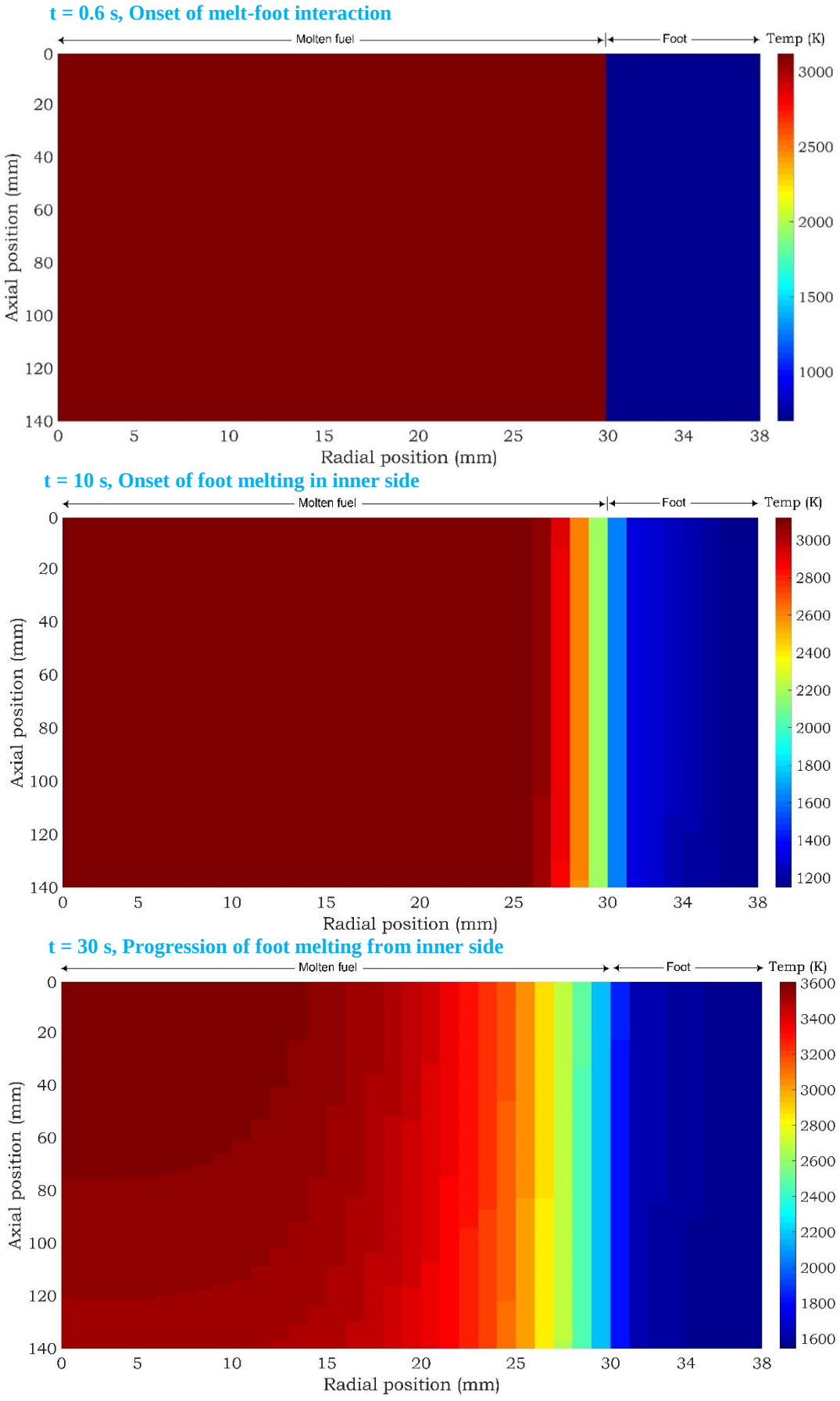

Fig. 5.20a: Temperature evolution during melt-foot interaction (Axial position is from top entry slot; Radial position is from the central line)

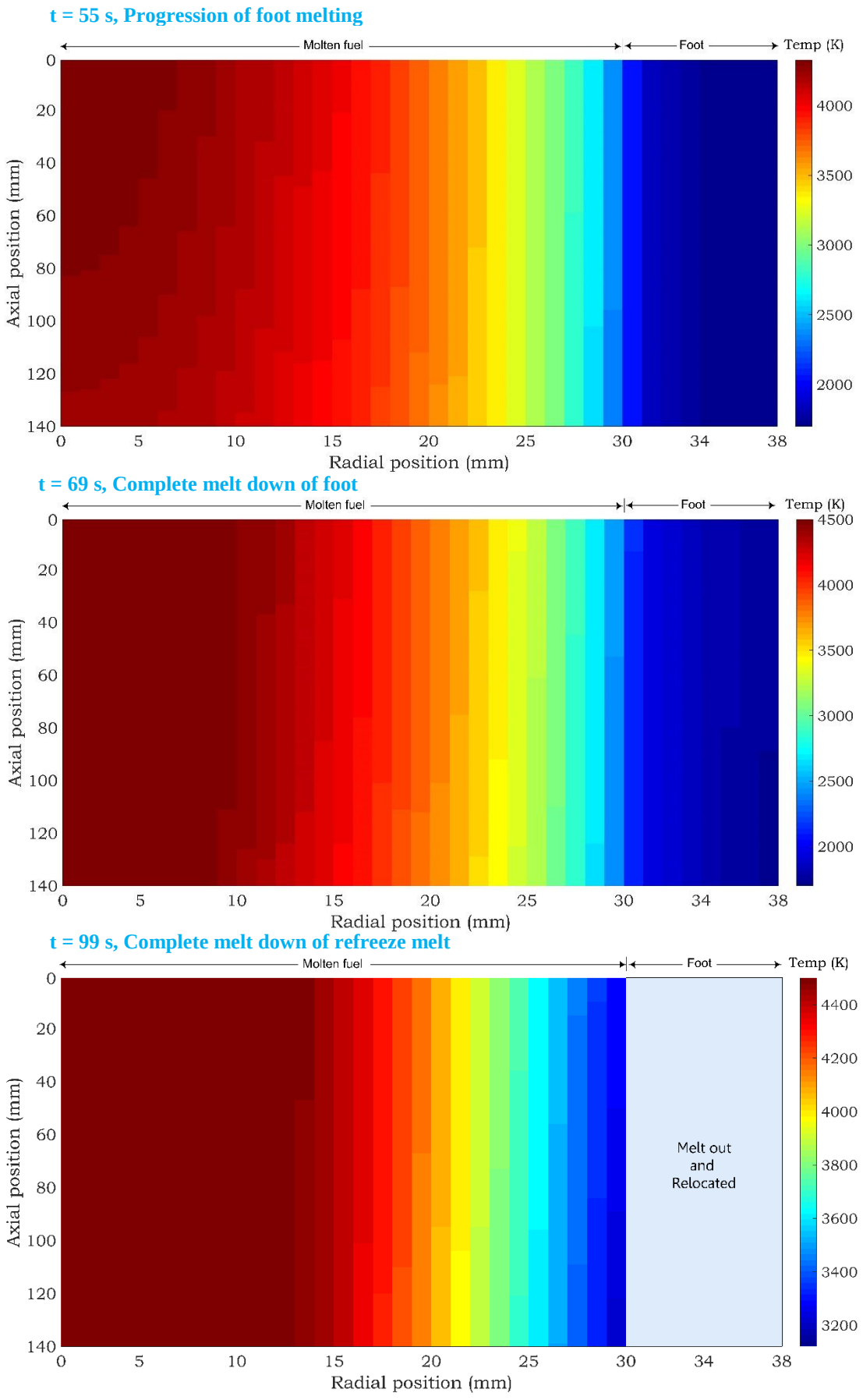

Fig. 5.20b: Temperature evolution during melt-foot interaction (Axial position is from top entry slot; Radial position is from the central line)

Later on, due to the decay heat generation inside the molten fuel, there is a gradual rise in its temperature. This leads to meltdown of solid crust layer by layer within ~99s. Finally, the molten fuel escapes out through the available spaces and reaches the bottom plate of the grid plate.

5.6 CLOSURE

Towards understanding the streaming and freezing characteristics of molten fuel in a prototype SFR fuel SA, a numerical simulation is carried out in the present work. It was found that the molten fuel is unable to cross the blanket zone, resulting in damage propagation to the neighbouring SAs. Apart from this the influence of critical parameters viz. number of pins, the decay heat power, blanket pellets, and the pin dimensions on the melt relocation and freezing characteristics are investigated. The parametric study reveals that the modified fuel SA design, in particular length and diameter of fuel pin, dramatically enhances the material relocation characteristics of molten fuel and prevents the progression of the accident to the neighbouring SAs. However, the influence of other critical parameters on relocation characteristics is either meagre or unsubstantial.

CHAPTER 6

Conclusions and Scope for Future Research

6.1 INTRODUCTION

The present work is devoted in particular to the modelling of relocation and freezing characteristics of molten fuel following a severe accident in a blocked SFR fuel subassembly. In this context, a robust computational model is developed based on the presently available scientific knowledge and fundamental understanding of the phenomena. Validation studies of the model were carried out against the available experimental data in the literature demonstrating the applicability of the model. Further, parametric studies are undertaken to investigate the influence of crucial parameter on the relocation behaviour. Prime results and conclusions emerging out from the present work are summarized in the succeeding section.

6.2 CONCLUSIONS

i. The simulation results of the present model are in good agreement with that of the seven-pin channel experiment and SIMMER III code results, implying its predictability in the analysis of molten relocation and freezing during accident.

ii. The molten fuel is unable to cross the blanket zone of the prototype SFR fuel subassembly owing to rapid freezing.

iii. The frozen melt front forms a firm blockage at the leading edge, obstructing the available space for melt progression in the axial direction. As a result, the trapped melt attacks the surrounding structures radially, resulting in melting of the structures and finally release of fissile inventories after breach out of the protective hexcan wall.

iv. The number of pins in a pin bundle has no significant influence on the streaming behaviour of the melt.

v. Due to rapid freezing, the share of decay power generated is substantially lower than that of convective heat released out. As a result, the influential effect of decay power on melt streaming is not significant. However, the decay power boosts further progression of accident radially in case the molten fuel remains in rest position.

vi. The provision of blanket pellets does not influence the penetration characteristics of the molten fuel mainly due to rapid freezing.

vii. Varying the dimensions of fuel pin, especially the length and diameter of the pin channel below the core, has a significant contribution towards the enhancement of fuel relocation. However, the design modification ramifies the structural, hydraulic and neutronic behaviour of the core and requires further investigations.

viii. The molten fuel, if reached the foot of the blocked SA, requires ~ 99s to melt the foot and disperses out to the bottom plate of grid plate.

6.3 RECOMMENDATIONS FOR FUTURE WORK

- The present model does not account for the reactivity changes owing to the melt relocation. Hence, the present computational model can be coupled with neutronics model.
- The present model is a single component (molten fuel) based computational model. But, in realistic phenomena the molten pool consists of churns of clad and/or fuel, molten fuel and/or clad materials. The presence of multi-materials influences the streaming behaviour. This requires further investigations and recommended development in the present model.
- The present model needs further extension to integrated 2-D model for a more accurate look and better understanding of the modelled phenomena.

Appendix A

Thermo-physical Properties

The various thermo-physical properties describing various thermal states of fuel, clad, and blanket materials are enlisted in this appendix. These correlations, suggested by Chawla et al. (1984), Kothandaraman et al. (2003), and Fink (2000), are considered in the present work. All the thermo-physical properties are in the SI unit scale.

Materials of components

Component	Material
Fuel	UO_2
Clad	Stainless steel type 316
Blanket	UO_2
Hexcan	Stainless steel type 316

Thermo-physical properties of UO_2

Phase	Physical Property	Property Equation/Value
Solid	Density (ρ), kg/m^3	$\rho = 10.97\times10^3(1.0056 - 1.6324\times10^{-5}T - 8.3281\times10^{-9}T^2 + 2.0176\times10^{-13}T^3)$
	Enthalpy (H), J/kg	$For\ 298K \le T \le 3120K,$ $H(T) - H(298) = C_1 + C_2t + C_3t^2 + C_4t^3 + C_5t^4 + C_6t^5 + C_7t^{-1}$ $where\ t = T/1000, C_1 = -78.4303, C_2 = 193.238, C_3 = 162.8647,$ $C_4 = -104.0014, C_5 = 29.2056, C_6 = -1.9507, C_7 = 2.6441$

	Thermal conductivity (K), W/m-K	$For\ 298K \le T \le 2670K,$ $K = \frac{1}{a+bT+cT^2} + dT\exp^{-e/kT}$ $For\ 2670K \le T \le 3120K,$ $K = 4.1486 - 2.2673\times10^{-4}T$ $where\ a = 6.8337\times10^{-2}, b = 1.6693\times10^{-4}, c = 3.1886\times10^{-8},$ $d = 1.2783\times10^{-1}, e = 1.1608, k = 8.6144\times10^{-5}$
	Melting point (T_{mp}), K	T_{mp} = 3120 K
	Latent heat of fusion (L), J/kg	$L = 2.77\times10^5$
Liquid	Density (ρ), kg/m^3	$\rho = 8.86\times10^3 - 0.916(T - 3120)$
	Enthalpy (H), J/kg	$For\ 3120\,K \le T \le 4500\,K,$ $H(T) - H(298) = 2.977\times10^6 + 0.931T - 4.9215\times10^9 T^{-1}$
	Specific heat (C_p), J/kg-K	$For\ 3120\,K \le T \le 4500\,K,$ $C_p = 484.95$
	Thermal conductivity (K), W/m-K	K = 5.5
	Viscosity (μ), kg/s-m	$\mu = 0.988\times10^{-3}\, e^{4620/T}$
	Boiling point (T_{bp}), K	T_{bp} = 4500 K

Thermo-physical properties of Stainless steel type 316

Phase	Physical Property	Property Equation/Value
Solid	Density (ρ), kg/m^3	$\rho = 8.084\times10^3 - 4.209\times10^{-1}T - 3.894\times10^{-5}T^2$
	Specific heat (C_p), J/kg-K	$For\ T \le 1700K,$ $C_p = 462.656 + 0.1338T$
	Thermal conductivity (K), W/m-K	$For\ T \le 1700K,$ $K = 9.248 + 1.571\times10^2 T$
	Melting point (T_{mp}), K	T_{mp} = 1700 K

	Latent heat of fusion (L), J/kg	$L = 2.7033\times10^{5}$
Liquid	Density (ρ), kg/m^3	$\rho = 7.433\times10^{3} + 3.934\times10^{-2}T - 1.801\times10^{-4}T^{2}$
	Specific heat (C_p), J/kg-K	$C_p = 776.2$
	Thermal conductivity (K), W/m-K	$K = 12.41 + 3.279\times10^{-3}T$
	Boiling point (T_{bp}), K	$T_{bp} = 3200\ K$

Thermo-physical property of Helium gas (*He*)

Helium gas is filled in the gap available between clad and blanket. The presence of Helium gas significantly affects the heat exchange rate between clad and blanket. From heat transfer point of view, it is essential to consider the thermal resistance offered by Helium. This heat transfer evaluation prerequisites thermal conductivity value (K_{He}) of Helium. The thermal conductivity of helium is determined using the following equation (Tallackson, 1976).

$$K_{He} = 1.0221\times10^{-3}\times T^{0.710} \quad W/m-K \tag{A.1}$$

Appendix B

Bundle Average Friction Factor

The value of Darcy friction factor (*F*) for wire-wrapped rod bundle is evaluated using the upgraded Cheng and Todreas correlation (Chen et al., 2018).

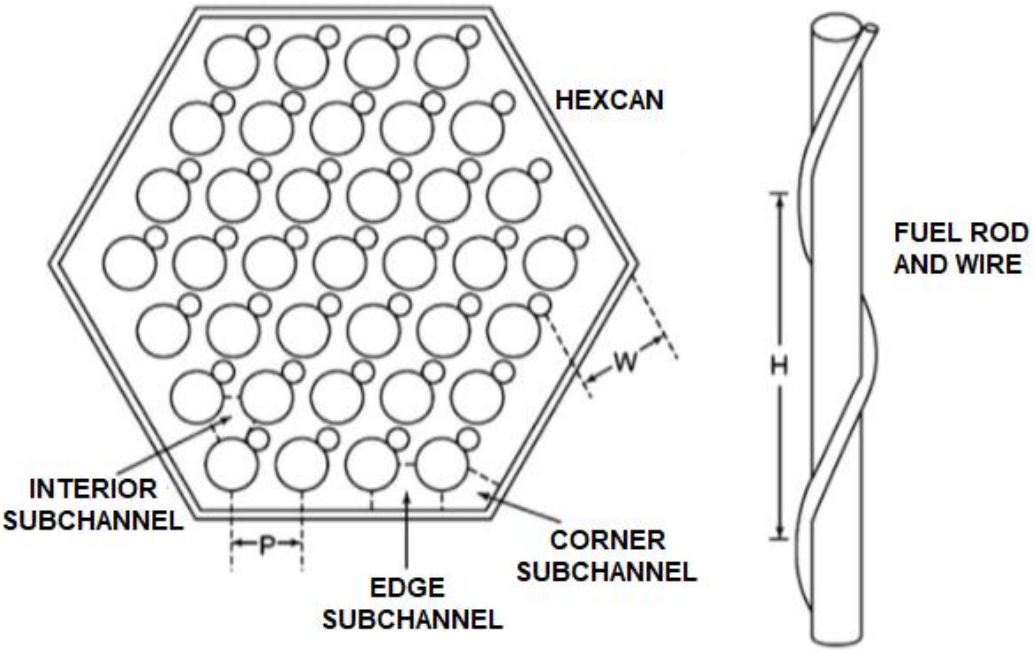

Fig. B.1: Cross-section of a typical SFR wire-wrapped subassembly

Upgraded Cheng and Todreas correlation:

Laminar region ($\mathrm{Re} < \mathrm{Re}_L$):

$$F_L = \frac{C_{fL}}{\mathrm{Re}} \tag{B.1}$$

Turbulent region ($\mathrm{Re} > \mathrm{Re}_T$):

$$F_T = \frac{C_{fT}}{\mathrm{Re}^{0.18}} \tag{B.2}$$

Transition region ($\mathrm{Re}_L \le \mathrm{Re} \le \mathrm{Re}_T$):

$$F_{TR} = F_L \left(1-\psi\right)^{1/3} \left(1-\psi^7\right) + F_T \psi^{1/3} \tag{B.3}$$

Where

$$\Psi = \text{Intermittency factor} = \frac{\log\left(\mathrm{Re}/\mathrm{Re}_L\right)}{\log\left(\mathrm{Re}_T/\mathrm{Re}_L\right)}$$

$$C_{fL} = \left\{-974.6 + 1612.0\left(\frac{P}{D}\right) - 598.5\left(\frac{P}{D}\right)^2\right\}\left(\frac{H}{D}\right)^{0.06-0.085\left(\frac{P}{D}\right)}$$

$$C_{fT} = \left\{0.8063 - 0.9022\log\left(\frac{H}{D}\right) + 0.3526\left(\log\left(\frac{H}{D}\right)\right)^2\right\}\left(\frac{P}{D}\right)^{9.7}\left(\frac{H}{D}\right)^{1.78-2.0\left(\frac{P}{D}\right)}$$

The range of applicability of the correlation is:

$19 \leqq N_r \leqq 217$

$1.025 \leqq \frac{P}{D} \leqq 1.42$

$8.0 \leqq \frac{H}{D} \leqq 50.0$

The flow region boundary definitions are:

$$\text{Laminar } (\mathrm{Re}_L) = 320\left\{10^{\left(\frac{P}{D}-1\right)}\right\}$$

$$\text{Turbulent } (\mathrm{Re}_T) = 10000\left\{10^{0.7\left(\frac{P}{D}-1\right)}\right\}$$

Bibliography

Alexanderson, E.P., 1979. Fermi-I: New age for nuclear power. LaGrange Park, IL: American Nuclear Society.

Berthoud, G., Duret, B., 1989, The Freezing of Molten Fuel: Reflections and New Results, Proceedings of the 4th Topical Meeting on Nuclear reactor Thermal Hydraulics (NURETH-4), Karlsruhe, Germany, 675-681.

Bertrand, F., Marie, N., Bachrata, A., Brun-Magaud, V., Droin, J.B., Manchon, X., Herbreteau, K., Farges, B., Carluec, B., Poumerouly, S., Lemasson, D., 2018. Status of severe accident studies at the end of the conceptual design of ASTRID: Feedback on mitigation features. Nuclear Engineering and Design 326, 55–64.

Cadiou, T., Louvet, J., 2006. Evaluation of the Accident Scenario Initiated by a Total Instantaneous Blockage in a Phénix Subassembly. Nuclear Technology 153, 256–263.

Central Electricity Authority, 2017. Growth of electricity sector in India from 1947-2017.

Chawla, T.C., Chasanov, M.G., Pedersen, D.R., Baker, L., Bingle, J.D., 1984. Thermophysical properties of MgO, UO2, their eutectic solution and slurry of liquid-solid mixtures, concrete, sodium, stainless steel and debris beds for use in molten pool penetration of MgO substrate. Nuclear Engineering and Design 80, 65–77.

Chen, S.K., Chen, Y.M., Todreas, N.E., 2018. The upgraded Cheng and Todreas correlation for pressure drop in hexagonal wire-wrapped rod bundles. Nuclear Engineering and Design 335, 356–373.

Chetal, S.C., Balasubramaniyan, V., Chellapandi, P., Mohanakrishnan, P., Puthiyavinayagam, P., Pillai, C.P., Raghupathy, S., Shanmugham, T.K., Pillai, C.S., 2006. The design of the Prototype Fast Breeder Reactor. Nuclear Engineering and Design 236, 852–860.

Cheung, F.B., Baker, L., 1976. Transient Freezing of Liquids in Tube Flow. Nuclear Science and Engineering 60, 1–9.

Chun, M.H., 1980. Investigation of Molten Fuel Relocation Dynamics with Applications to LMFBR Post-Accident Fuel Relocation. Nuclear Engineering and Technology 12, 88-98.

Dadillon, J., Chaudat, J.P., Schwaz, M., Tategrain, A., Heusener, G., Kuczera, B.,Kussmaul, G., Wolff, J., 1979. The CABRI test facility experimental fuel pin programme. Its objectives and present results. In: Proc. Int. Mtg. Fast Reactor Safety Technology, Seattle, Washington, vol. II.

Dadillon, J., Kussmaul, G., Agaisse, R., Augier, G., Bensoussan, P., Butement, A.W.,Fabrega, S., Haessler, M., Hoppe, P., Mitsuki, S., Philipponneau, Y., Rongier, P., Steinbock, L., Wolff, J., 1982. The CABRI project-recent progress and present status. In: Proc. LMFBR Safety Topl. Mtg, Lyon, France, vol.II. European Nuclear Society/American Nuclear Society, 177-188.

DOENE (USDOE Office of Nuclear Energy, Science and Technology (NE)), 2002. A Technology Roadmap for Generation IV Nuclear Energy Systems (No. GIF-002-00, 859029).

Doerner, R.C., Bauer, T.H., Morman, J.A., Holland, J.W., 1992. Features of Post failure Fuel Behavior in Transient Overpower and Transient Undercooled/Overpower Tests in the Transient Reactor Test Facility. Nuclear Technology 98, 124–136.

Duret, B., Bonnard, J.C., 1988, Crust Instability Criteria during Transient Freezing on a Liquid Film, Proceedings of the ASME Winter Annual Meeting, Chicago, Illinois.

Edwards, A.J., Bird, M.J., Denham, M.K., 1992. Molten Fuel Propagation in Sodium-Filled Fast Reactor Subassembly Geometries. Nuclear Technology 98, 70–78.

El-Genk, M., CRONENBERG, A.W., 1978. An Assessment of Fuel Freezing and Drainage Phenomena in a Reactor Shield Plug following a Core Disruptive Accident. Nuclear Engineering and Design 47, 195-225.

Epstein, M., Grolmes, M.A., Henry, R.E., Fauske, H.K., 1976. Transient Freezing of a Flowing Ceramic Fuel in a Steel Channel. Nuclear Science and Engineering 61, 310–323.

Fanning, T.H., Brunett, A.J., Sumner, T., 2017. The SAS4A/SASSYS-1 Safety Analysis Code System, Version 5. (No. ANL/NE-16/19, 1352187), Argonne National Laboratory, United States.

Fauske, H.K., Koyama, K., Kubo, S., 2002. Assessment of the FBR Core Disruptive Accident (CDA): The Role and Application of General Behavior Principles (GBPs). Journal of Nuclear Science and Technology 39, 615–627.

Fieg, G., Möschke, M., Werle, H., 1992. Freezing Phenomena of Ceramic Alumina Melts Flowing in Pin Bundles. Nuclear Technology 99, 309–317.

Fink, J.K., 2000. Thermophysical properties of uranium dioxide. Journal of Nuclear Materials 18.

Gasser, R.D., Kazimi, M.S., 1977. A Study of Post-Accident Molten Fuel Downward Streaming through the Axial Shield Structure in the Liquid-Metal Fast Breeder Reactor. Nuclear Technology 33, 248–259.

Gauntt, R.O., Pickard, P.S., Berthier, J., Furutani, A., Royl, P., 1987. In-Pile Fuel Freezing and Penetration Experiments – the ACRR TRAN Experiments. British Nuclear Energy Society, United Kingdom.

Hossain, M.K., Himuro, Y., Morita, K., Nakagawa, K., Matsumoto, T., Fukuda, K., Maschek, W., 2009. Simulation of Molten Metal Penetration and Freezing Behavior in a Seven-Pin Bundle Experiment. Journal of Nuclear Science and Technology 46, 799–808.

IEA, 2017. Key world energy statistics. https://www.iea.org/publications/freepublications/publication/KeyWorld2017.pdf

Kaiser, A., Peppler, W., Will, H., 1994, SIMBATH 1976- 1992, Seventeen Years of Experimental Investigation of Key Issues Concerned with Severe Reactor Accidents, Proceedings of the IAEA/IWGFR Technical Committee Meeting on Material-Coolant Interactions and Material Movement and Relocation in Liquid Metal Fast Reactors, O-arai, Japan, 349-383.

Kamiyama, K., Brear, D.J., Tobita, Y., Kondo, S., 2006. Establishment of Freezing Model for Reactor Safety Analysis. Journal of Nuclear Science and Technology 43, 1206–1217.

Kayser, G., Charpenel, J., Jamond, C., 1998. Summary of the SCARABEE-N Subassembly Melting and Propagation Tests with an Application to a Hypothetical Total Instantaneous Blockage in a Reactor. Nuclear Science and Engineering 128, 144–185.

Kondo, S., 1994. Current R&D status on material motion and interactions relevant to core disruptive accidents. In: Proc. of IAEA/IWGFR Technical Committee Meeting on Evaluation of Material Coolant Interaction and Material Movement and

Relocation in Liquid Metal Reactors, O-arai Engineering Center, Japan, June 10, 1994

Konishi, K., Kubo, S., Konomura, M., Sato, I., Koyama, K., Toyooka, J., Kamiyama, K., Kotake, S., Vurim, A. D., Gaidaichuk, V. A., Pakhnits, A. V., and Vassiliev, Y. S., 2006. The Eagle Project to Eliminate the Recriticality issue of Fast Reactors: Progress and Results of In-Pile Tests. Proceedings of the 5th Korea–Japan Symposium on Nuclear Thermal Hydraulics and Safety (NTHAS5), Jeju, Korea, 465–471.

Kothandaraman, A.L., Puthiyavinayagam, P., Jalaldeen, S., Ravi Prasan, G.R., Ravichandar, S.C., 2003. Material properties for Design (No. PFBR/01000/DN/1000/R-E), Indira Gandhi Centre for Atomic Research, India.

Le Rigoleur, C., Hofmann, F., Stansfield, R., 1994. Review of European out-of-pile tests and analyses of molten material movement and relocation and of molten material - sodium interaction (IWGFR--89). International Atomic Energy Agency (IAEA).

Livolant, M., Dadillon, J., Kayser, G., Moxon, D., 1990. SCARABEE: a test reactor and programme to study fuel melting and propagation in connexion with local faults, objectives, and results. In: Proc. Int. Fast Reactor Safety Meeting 1990, Snowbird, Utah, vol. II, 177-186.

Ma, Z., Wu, Y., Qiu, Z., Tian, W., Su, G., Qiu, S., 2012. An innovative method for prediction of liquid metal heat transfer rate for rod bundles based on annuli. Annals of Nuclear Energy 47, 91–97.

Morita, K., Liu, P., Matsumoto, T., Fukuda, K., Tobita, Y., Yamano, H., Sato, I., 2009. Fundamental study on flow characteristics of disrupted core pool at a low energy

level (Joint research). (No. JAEA-Research 2009-018), Japan Atomic Energy Agency, Japan.

Onoda, Y., Fukano, Y., Sato, I., Marquie, C., Duc, B., 2011. Three-Pin Cluster CABRI Tests Simulating the Unprotected Loss-of-Flow Accident in Sodium-Cooled Fast Reactors. Journal of Nuclear Science and Technology 48, 188–204.

Ostensen, R. W., Henry, R. E., Jackson, J. F., Goldfuss, G. T., Gunther, W. H., and Parker, N. E., 1974. Fuel Flow and Freezing in the Upper Subassembly Structure Following an LMFBR Disassembly. Transactions of American Nuclear Society 18, 214.

Peppler, W., Kaiser, A., Will, H., 1988. Freezing of a thermite melt injected into an annular channel experiments and recalculations. Experimental Thermal and Fluid Science 1, 335–346.

Ravi, L., Velusamy, K., Chellapandi, P., 2013. A robust thermal model to investigate radial propagation of core damage due to total instantaneous blockage in SFR fuel subassembly. Annals of Nuclear Energy 62, 342–356.

Rehme, K., 1972. Pressure drop performance of rod bundles in hexagonal arrangements. International Journal of Heat and Mass Transfer 15, 2499–2517.

Roychowdhury, D.G., Govindarajan, S., Chetal, S.C., Bhoje, S.B., 1998. Design Approach to Local Blockages. IAEA-TECDOC-1157, 289–300.

Russel, W.B., 1983. Effects of Interactions between Particles on the Rheology of Dispersions, in: MEYER, R.E. (Ed.), Theory of Dispersed Multiphase Flow. Academic Press, 1–34.

Schleisiek, K., Aberle, J., Homann, C., Schmuck, I., Maschek, W., Rahn, A., Romer, O., Schmidt, L., Borms, L., Verwimp, A., 1998. The Mol-7C In-Pile Local Blockage

Experiments: Main Results, Conclusions, and Extrapolation to Reactor Conditions. Nuclear Science and Engineering 128, 93–143.

Scott, R.L., 1971. Fuel-melting incident at the Fermi reactor on Oct. 5, 1966. Nuclear Safety. 12 (2).

Soner, M.A.M., Hasegawa, Y., Seo, S., Himuro, Y., Morita, K., Matsumoto, T., Fukuda, K., Maschek, W., 2011. Experimental investigation of solid–liquid mixtures freezing behaviour in flow channels. Nuclear Engineering and Design 241, 4223–4235.

Spencer, B.W., Wilson, R.J., Vetter, D.L., Erickson, E.G., Dewey, G., 1985, Results of Recent Reactor-Material Tests on Dispersal of Oxide Fuel from a Disrupted Core, Proceedings of the Int. Top. Mtg. on Fast Reactor Safety, Knoxville, Tennessee, 877-882.

Shah, R.K., London, A.L., 1978. Laminar flow forced convection in ducts: a source book for compact heat exchanger analytical data, Advances in heat transfer Supplement. Academic Press, New York.

Sultana, K.R., Dehghani, S.R., Pope, K., Muzychka, Y.S., 2018. Numerical techniques for solving solidification and melting phase change problems. Numerical Heat Transfer, Part B: Fundamentals 73, 129–145.

Tallackson, J.R., 1976. Thermal transport properties of helium, helium-air mixtures, water, and tubing steel used in the CACHE program to compute HTGR auxiliary heat exchanger performance (No. ORNL-TM-4931). Oak Ridge National Lab, United States.

Tobita, Y., Morita, K., Kawada, K., Niwa, H., Nonaka, N., 1999. Evaluation of CDA energetics in the prototype LMFBR with latest knowledge and tools. Proceedings of

the 7th international conference on nuclear engineering, Japan Society of Mechanical Engineers, 4252.

Todreas, N.E., 2009. Thermal-Hydraulic Challenges in Fast Reactor Design. Nuclear Technology 167, 127–144.

Tentner, A.M., Parma, E., Wei, T., Wigeland, R., 2010. Severe accident approach - Final Report. Evaluation of design measures for severe accident prevention and consequence mitigation. (No. ANL-GENIV-128, 973483), Argonne National Laboratory, United States.

Venkataraman, G., 1994. Bhabha and his magnificent obsessions. University press, India Limited.

Voller, V.R., 1990. Fast Implicit Finite-Difference Method for the Analysis of Phase Change Problems. Numerical Heat Transfer, Part B: Fundamentals 17, 155–169.

Wang, Z., Cao, X.W., 2007. Preliminary thermal-hydraulic phenomena investigation during total instantaneous blockage accident for CEFR. Nuclear Engineering and Design 237, 1550–1559.

Yamano, H., Fujita, S., Tobita, Y., Kondo, S., Morita, K., Sugaya, M., Mizuno, M., Hosono, S., Kondo, T., 2003. SIMMER-IV: A Three-Dimensional Computer Program for LMFR Core Disruptive Accident Analysis; Version 2.A Model Summary and Program Description. (No. JNC-TN9400-2003-070), O-arai Engineering Center, Japan Nuclear Cycle Development Institute, Japan.

Yang, Z.M., 1998. Thermal Hydraulic Behaviour of Subassembly Local Blockage in China Experimental Fast Reactor. IAEA-TECDOC-1157, 281–288.

Nomenclature

English Symbols

a	Effective heat transfer area, m^2
A_c	Available subchannel cross sectional area, m^2
CV	Control volume
D_h	Hydraulic diameter, m
f	Model parameter
F	Darcy friction factor
g	Acceleration due to gravity, m/s^2
G	Effective thermal conductance, W/K
h	Heat transfer coefficient, W/m^2-K
H	Enthalpy, J/kg
K	Thermal conductivity, W/m-K
K_e	Entrance loss coefficient
l	Instantaneous penetration length, m
m	Control volume mass, kg
M	Total mass of molten fuel, kg
M_{pool}	Remaining melt mass in pool, kg

Nu	Nusselt number
P	Rod bundle pitch, m
$\dot{Q}_g$	Specific heat generation rate, W/kg
r	Control volume radius, m
r_{eq}	Equivalent annulus radius, m
Re	Reynolds number
t	Time, s
T	Temperature, K
v	Velocity of molten fuel, m/s

Greek Symbols

α	Volume fraction
α_{MP}	Maximum volume fraction of solid particle
ΔP	Pressure loss, N/m^2
Δt, dt	Time step, s
Δz	Control volume size, m
$\in$	Error order
μ_l	Liquid viscosity, Ns/m^2
μ_{eff}	Effective viscosity, Ns/m^2
ω	Relaxation factor
ρ	Density, kg/m^3

Subscripts

b	Blanket
c	Clad
d	Downstream control volume
drag	Frictional drag
entry loss	Entrance loss
f	Molten fuel
He	Helium
l	Liquid phase
p	Solid phase
pool	Molten fuel pool
u	Upstream control volume

Abbreviations

ASTRID	Advanced Sodium Technological Reactor for Industrial Demonstration
BDBE	Beyond Design Basis Event
CDA	Core Disruptive Accident
CEA	Central Electricity Authority
CEFR	Chinese Experimental Fast Reactor
CMR	Controlled Material Relocation
CRBR	Clinch River Breeder Reactor

DCS-M-TT	Mitigation Tube
DND	Delayed Neutron Detector
FAIDUS	Fuel Assembly Inner Duct System
IEA	International Energy Agency
JAEA	Japan Atomic Energy Agency
LBR	Limited Blanket Removal
MFCI	Molten Fuel Coolant Interaction
PHWR	Pressurized Heavy Water Reactor
SA	Subassembly
SFR	Sodium Cooled Fast Reactor
TIB	Total Instantaneous Blockage
ULOFA	Unprotected Loss of Flow Accident
UTOPA	Unprotected Transient Overpower Accident